正电子技术及其发展

叶邦角

核固体物理研究室

Laboratory of Nuclear Solid State Physics, USTC

二、其它正电子技术

- 正电子衍射
- 正电子俄歇谱
- 正电子微束技术
- 正电子极化技术
- 正电子显微镜

正电子表面研究技术

- 正电子衍射（低能和高能）
- PAES技术

四十多年以来，科学家们致力于寻找最合适的研究固体表面的探针，电子、正电子、光子、原子和离子都可作为研究表面的探针，然而，一个理想的表面结构探针应该具有以下的2个基本特性：

- 粒子必须要有小的平均自由程(<30A°)，即要对表面灵敏；
- 粒子与表面的相互作用应该较弱，以使测量结构可以被精确地模拟计算。

正电子最合适作为表面探针的理想粒子：

- 因为它在固体中的平均自由程很短，事实上，对能量低于200eV的正电子，其平均自由程比电子平均自由程要短；对能量大于200eV的正电子，平均自由程与电子类似。因此正电子对最初的3-4层原子层特别灵敏。
- 正电子的散射因子与X-射线和电子基本类似。而电子的散射因子有尖锐的各向异性角分布，而正电子的角分布圆滑变化，如图为微分角分布。

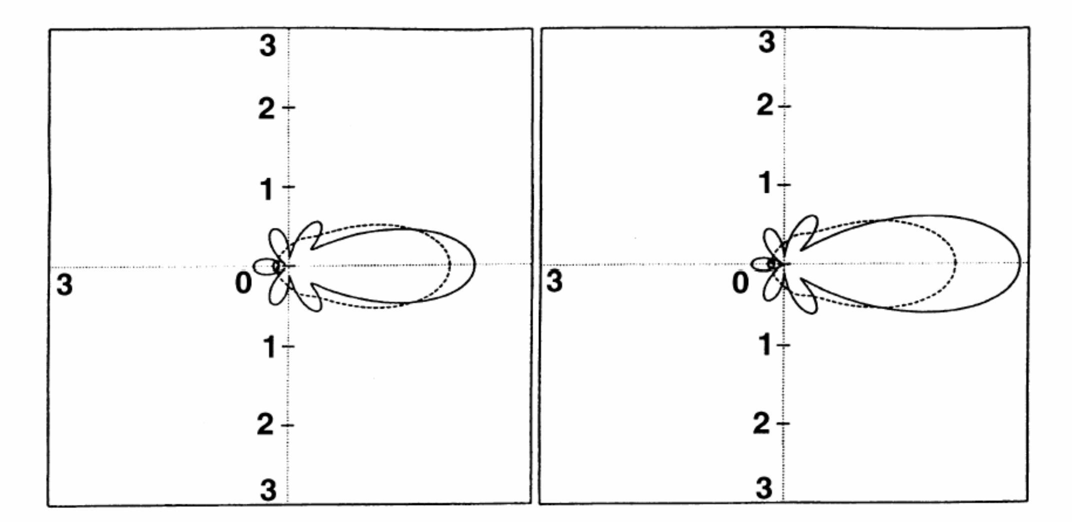

Messenger	Spectroscopy
Positron	LEPD RHEPD Positron work function measurement Positron re-emission spectroscopy and microscopy Re-emitted positron energy loss spectroscopy (REPELS) Positron tunnelling spectroscopy Positron backscattering
Ps	Ps emission/formation spectroscopies Inverse Ps formation spectroscopy* Ps diffraction*
Gamma photon	Surface ACAR Positron-annihilation microscopy
Electron	PAES Positron-induced secondary electron emission

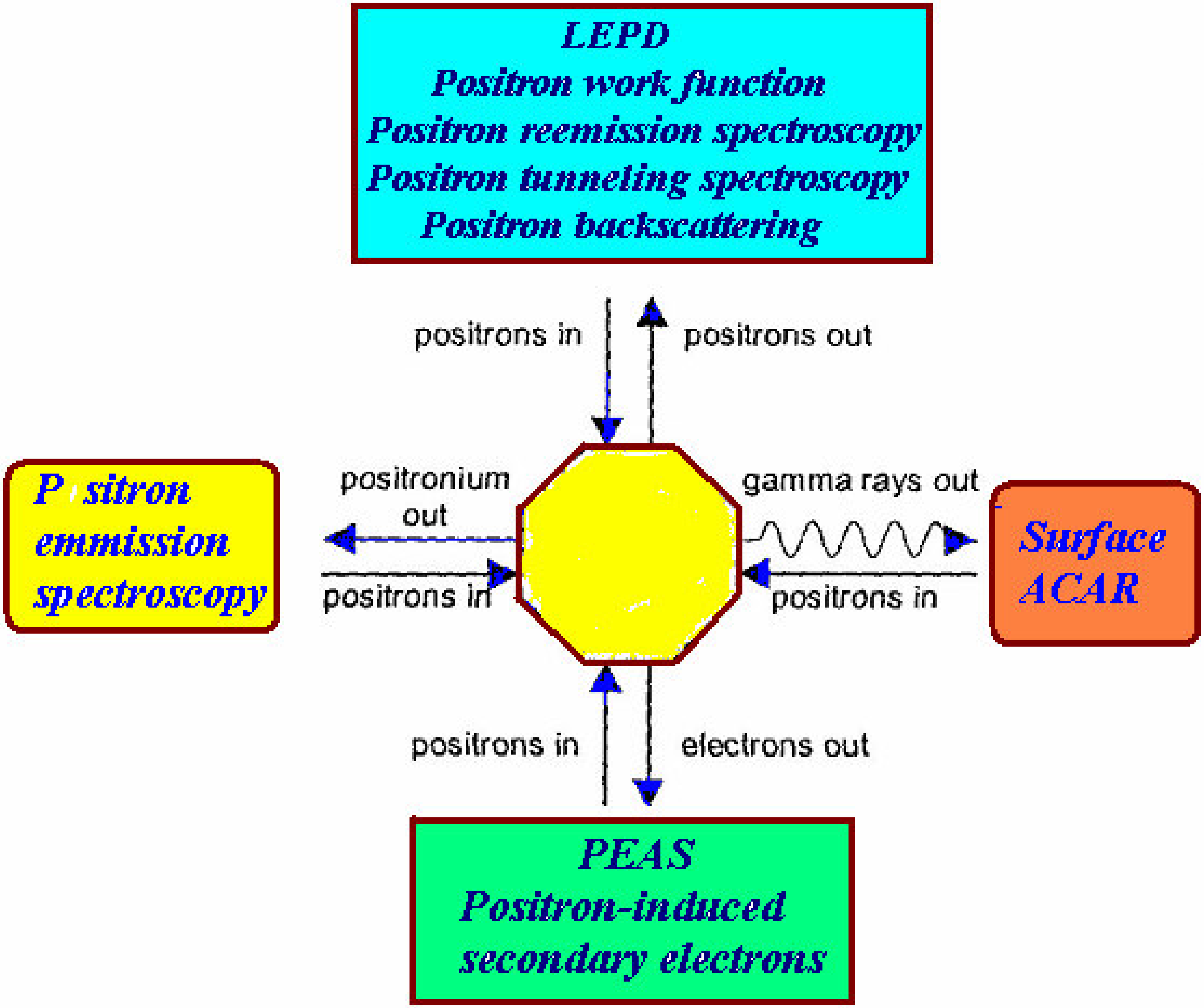
LEPD
Positron work function
Positron reemission spectroscopy
Positron tunneling spectroscopy
Positron backscattering
positrons in
positrons out
P sitron
emmission
spectroscopy
positronium
out
positrons in
gamma rays out
positrons in
Surface
ACAR
positrons in
electrons out
PEAS
Positron-induced
secondary electrons

7. 正电子衍射

■低能正电子衍射LEPD

正电子在表面上最成功的应用就是由美国**Brandeis** 大学的**Canter**和他的合作者在**1980**年开创的低能正电子衍射（**Low-Energy Positron Diffraction, LEPD**），该研究组经过**20**多年的发展，他们已经表明**LEPD**技术可以获得高质量的结果，并与理论结果相符合。由于正电子有较大的非弹截面，因而这使得该技术比之传统的低能电子衍射（**Low-Energy Electron Diffraction, LEED**）技术在研究表面结构上更加灵敏。

Positron Diffraction Experiments

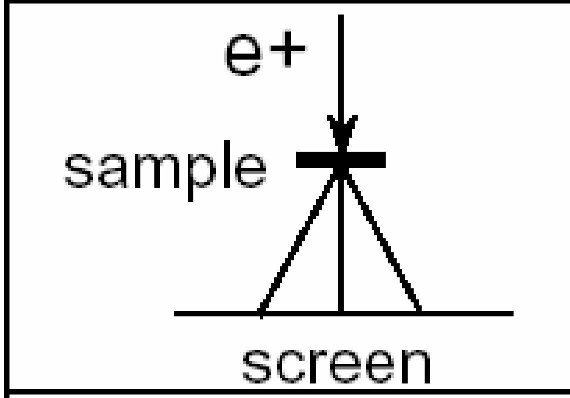

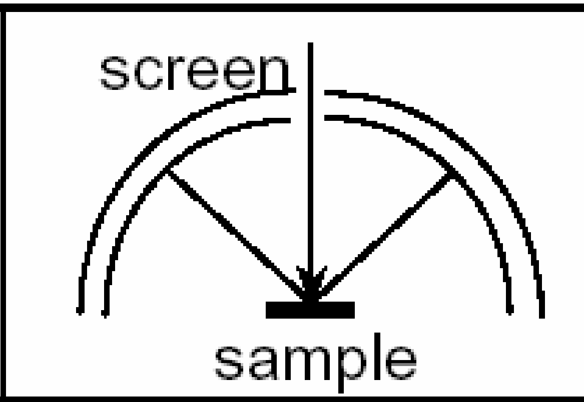

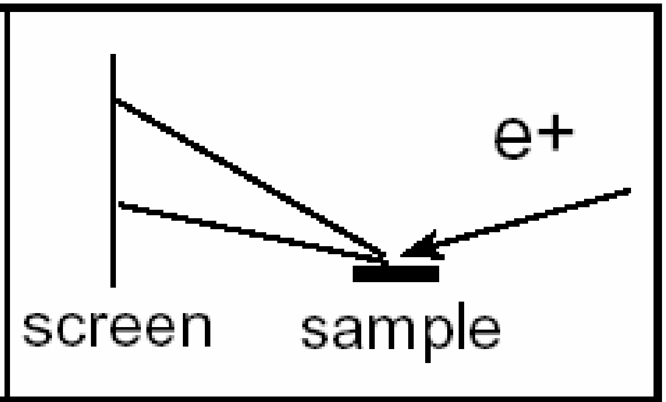

TPD **T**ransmission **P**ositron **D**iffraction	LEPD **L**ow **E**nergy **P**ositron **D**iffraction	RHEPD **R**eflection **H**igh **E**nergy **P**ositron **D**iffraction
100keV ▪ 1MeV	10 ▪ 500eV	10 ▪ 100keV
Bulk ▪ Study	**▪ Surface ▪ Study ▪**	

LEPD

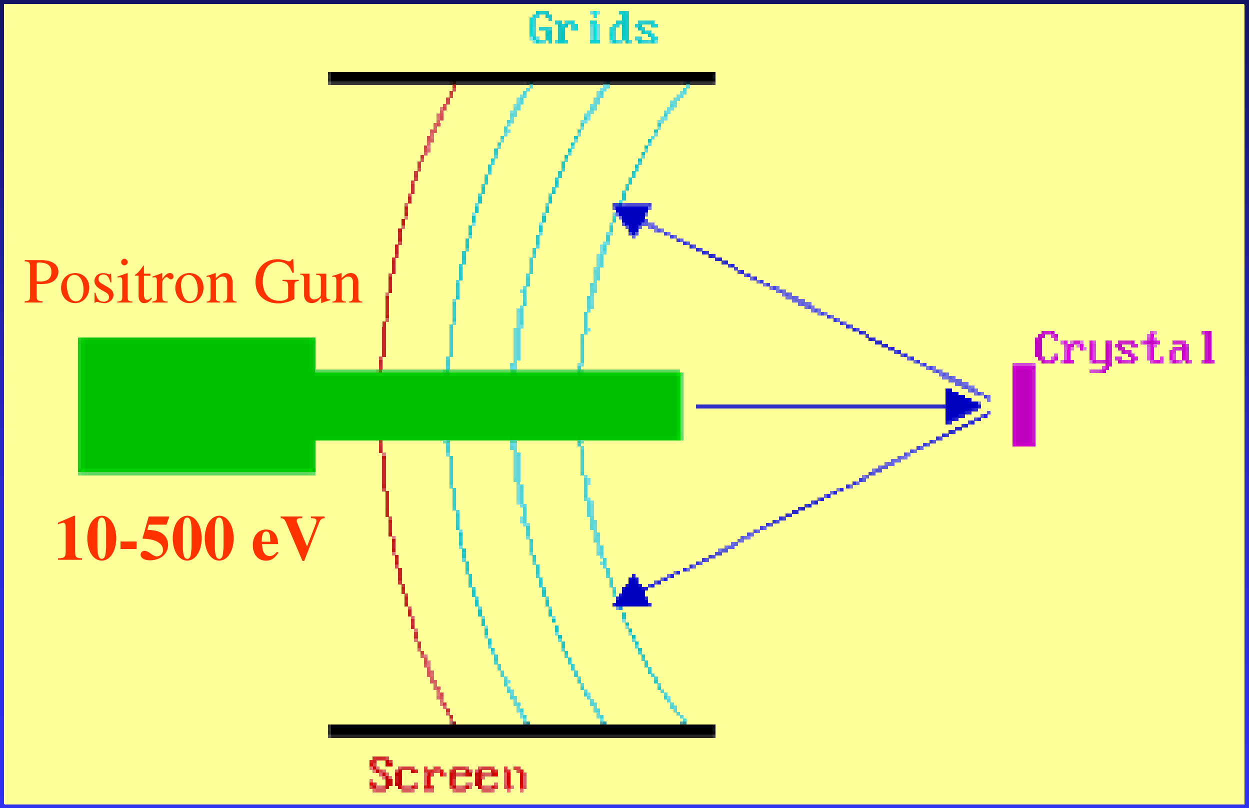

LEED

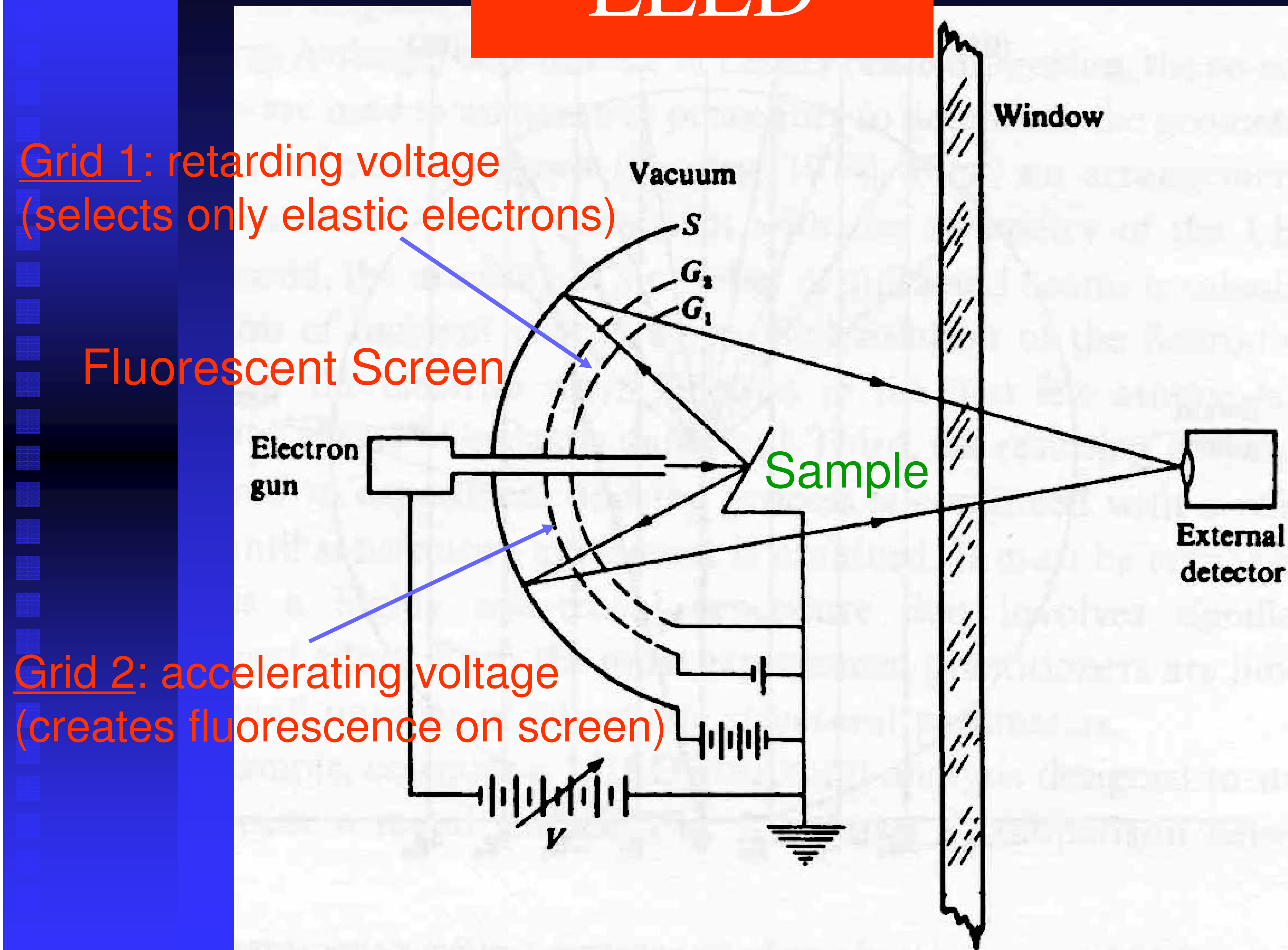
Grid 1: retarding voltage
(selects only elastic electrons)
Fluorescent Screen
Grid 2: accelerating voltage
(creates fluorescence on screen)
Window
Vacuum
S
G_2
G_1
Electron gun
Sample
External detector
V

Derive LEED equation using Bragg's Law for X-ray diffraction, where appropriate angles are substituted and λ is for the electron wavelength.

X-ray Diffraction

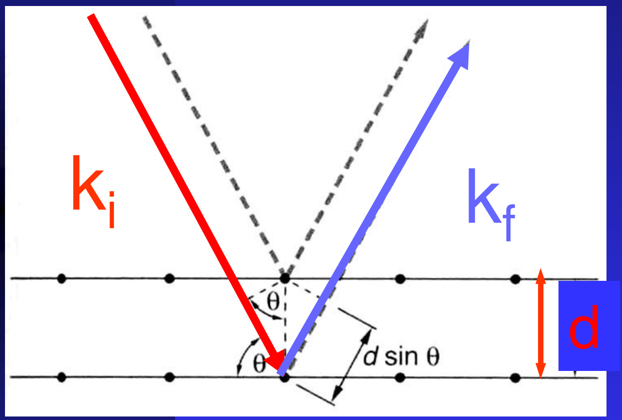

$$n\lambda_{\mathrm{xray}} = 2d\sin\theta$$

$$n\lambda = 2(D\sin\alpha)(\cos\alpha)$$

$$n\lambda = D\sin 2\alpha$$

Electron Diffraction

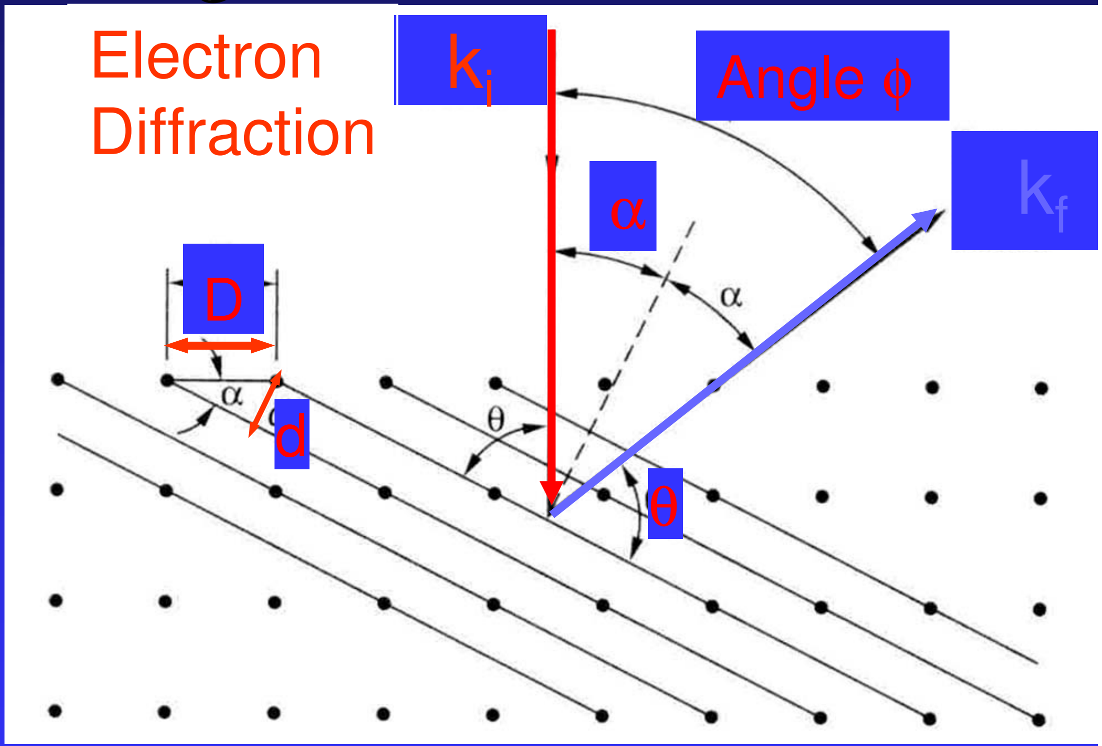

$$n\lambda_{\mathrm{elec}} = D\sin\phi$$

k-Space: Ewald Sphere for LEED

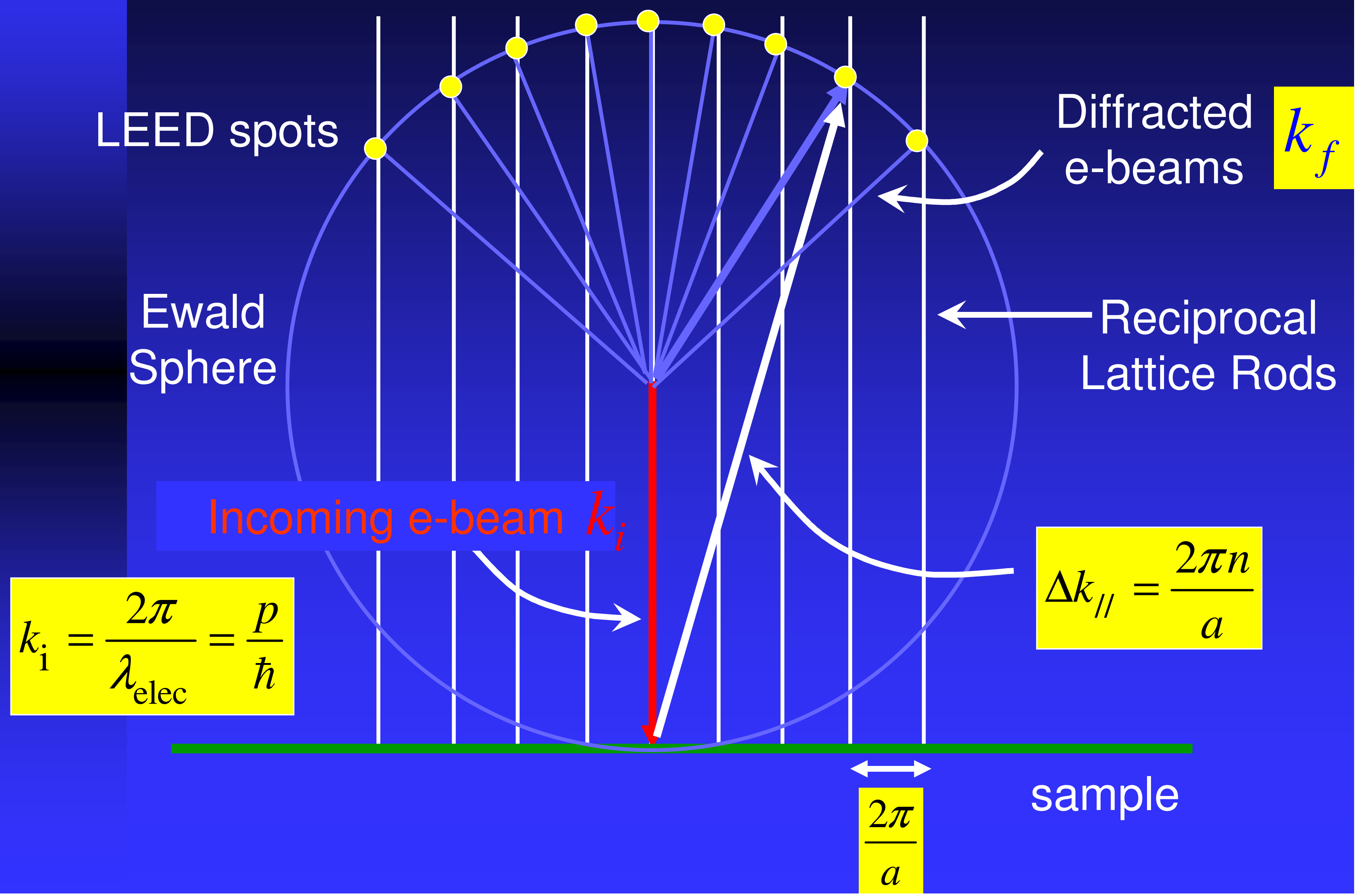

LEED: Si(111)7x7

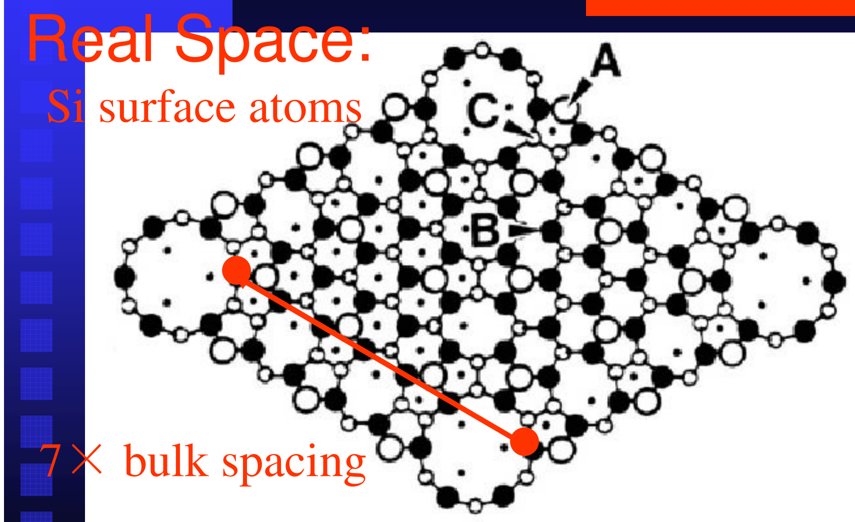

$$n\lambda = D \sin \phi$$

- Larger *D* spacings give closer LEED spots (smaller ϕ).
- Higher energy electrons give closer spots.

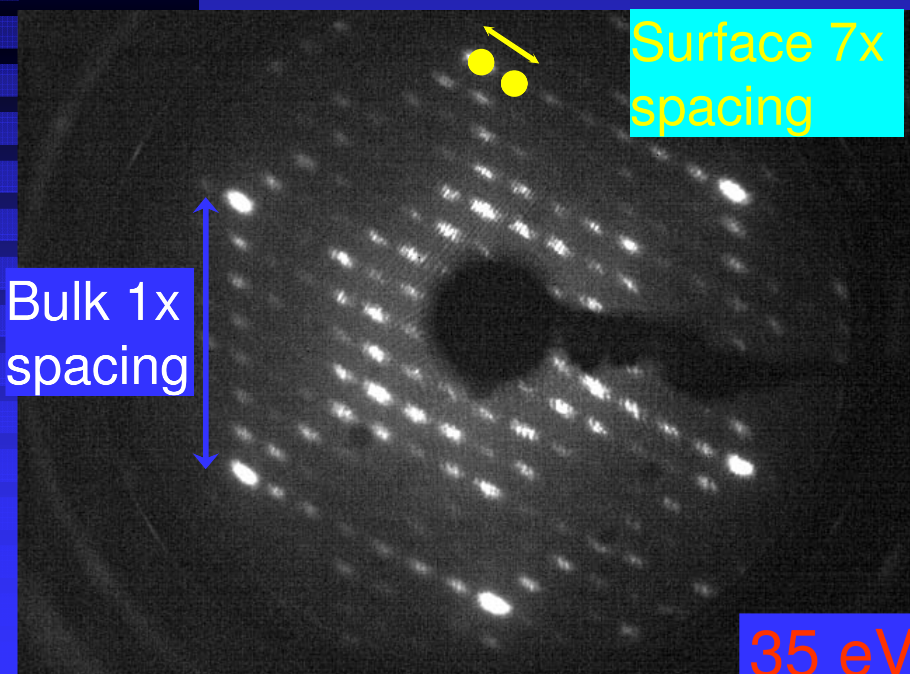

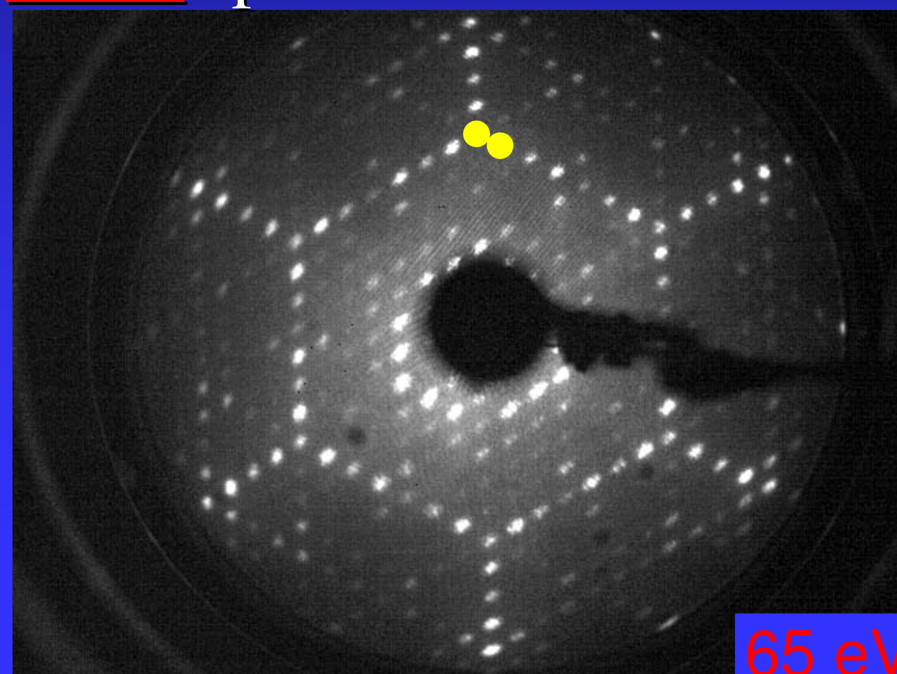

LEPD的优点

- 正电子散射的相移与原子序数 Z的依赖不如电子散射灵敏；因而LEPD在多成分系统对结构参数更加灵敏。
- LEPD的非弹截面大，意味着LEPD的平均自由程比LEED短，而平均自由程与扩散深度直接有关，因而，LEPD比LEED在表面有更大的灵敏度。
- 使用在LEPD I-V轮郭理论计算中的正电子–电子相互作用关联项的不确定比之在 LEED中等价的项要弱。
- 由于正电子接近离子芯时减速，因而对从高Z材料表面的散射电子其相对论效应如自旋 –轨道耦合将减少。

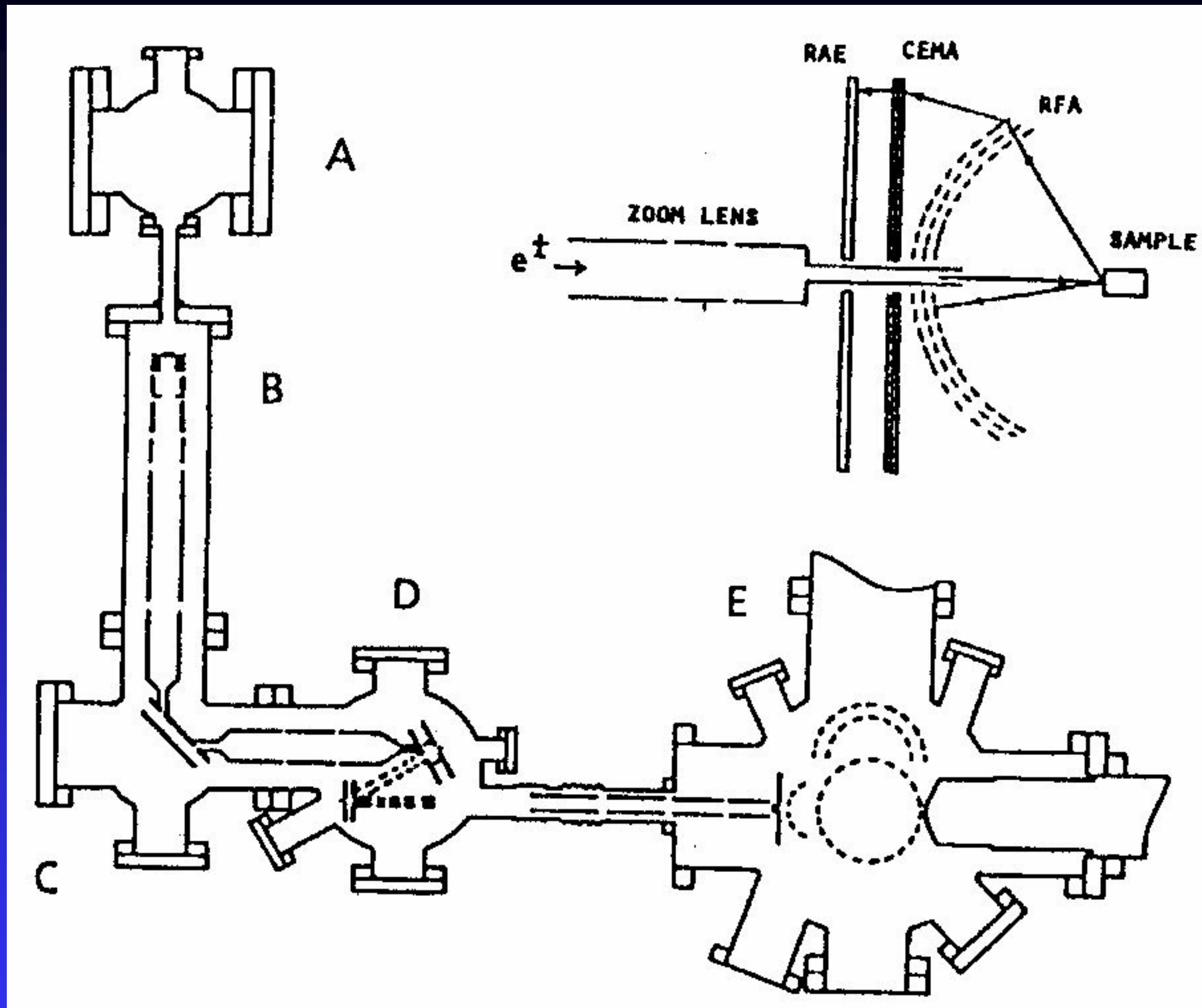

美国 Brandeis 大学慢正电子谱仪和球形 LEED-LEPD谱仪。B-正电子源， C-90园柱形镜，D-慢化和加亮，E-样品和衍射谱仪。

除了Brandeis 大学的工作外，最近美国Brookhaven实验室和 Bell实验室及其它研究中心也已经开始发展LEPD测量技术。

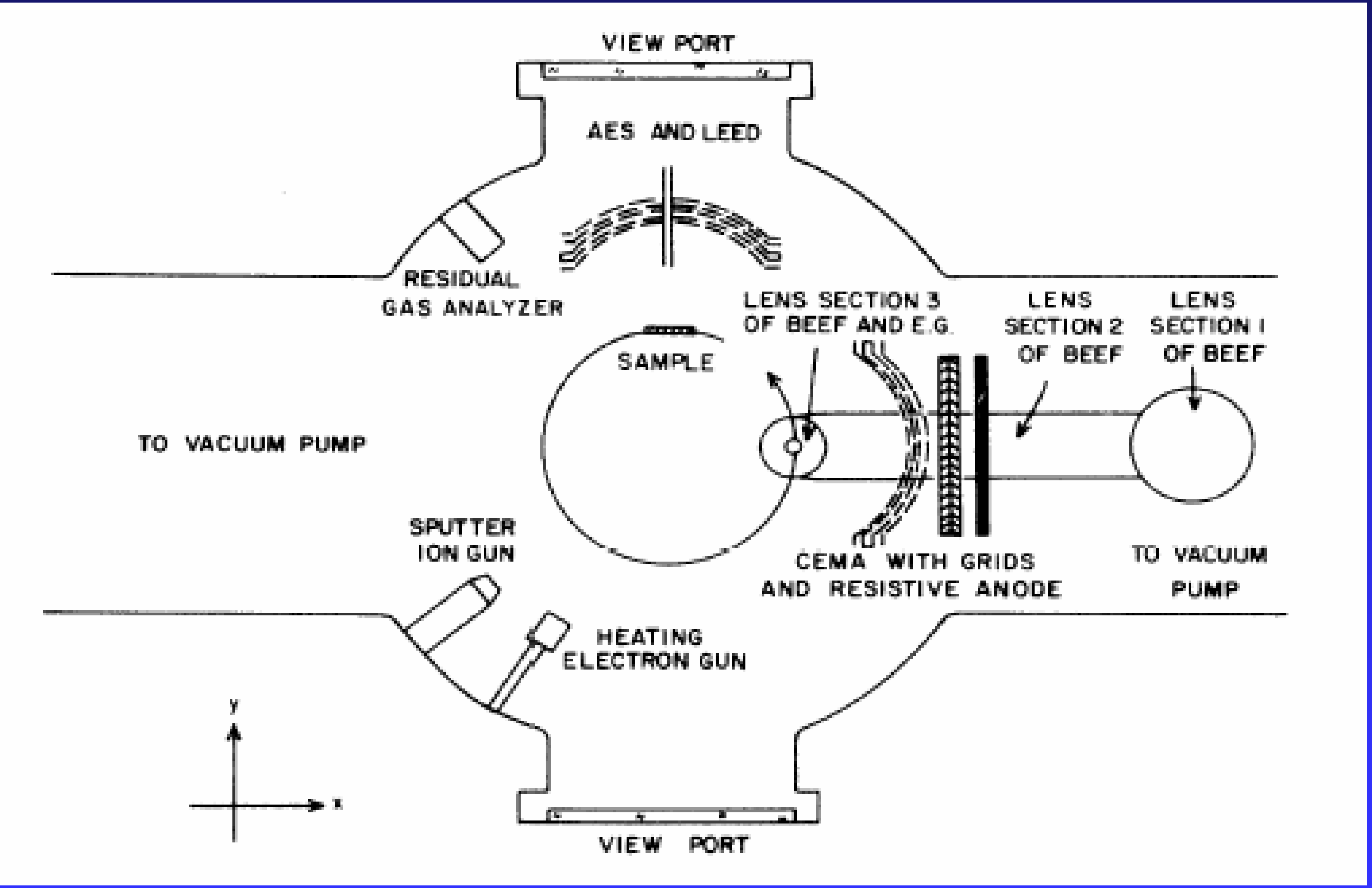

Brightness-enhanced

- A type intensity 1-3×10^6/s positrons is obtained by using 0.5Ci source.
- This beam still is low optical brightness:

$$R = \frac{I}{\theta^2 D^2 E}$$

Because a large D (10mm). The θD product of a typical beam is at least 20 times too large for the LEPD experiment.

对大部分的慢化体, 研究表明, 正电子发射动能近似等于正电子负功函数**ϕ_+**, 对一些特别的晶体和表面条件,其能量半高宽为**70meV**, 与ϕ_+无关. 对一个平板型的慢化体,其发射角为:

$$\theta_e = 2\left[\frac{0.035}{\phi_+}\right]^{1/2} \text{rad} = \frac{20}{\phi_+^{1/2}} \text{deg} .$$

Ni: $\phi_+ = 1.5\text{eV}$, 17°

W: $\phi_+ = 3\ \text{eV}$, 12°

Brightness-enhanced electrostatically focused (BEEF)

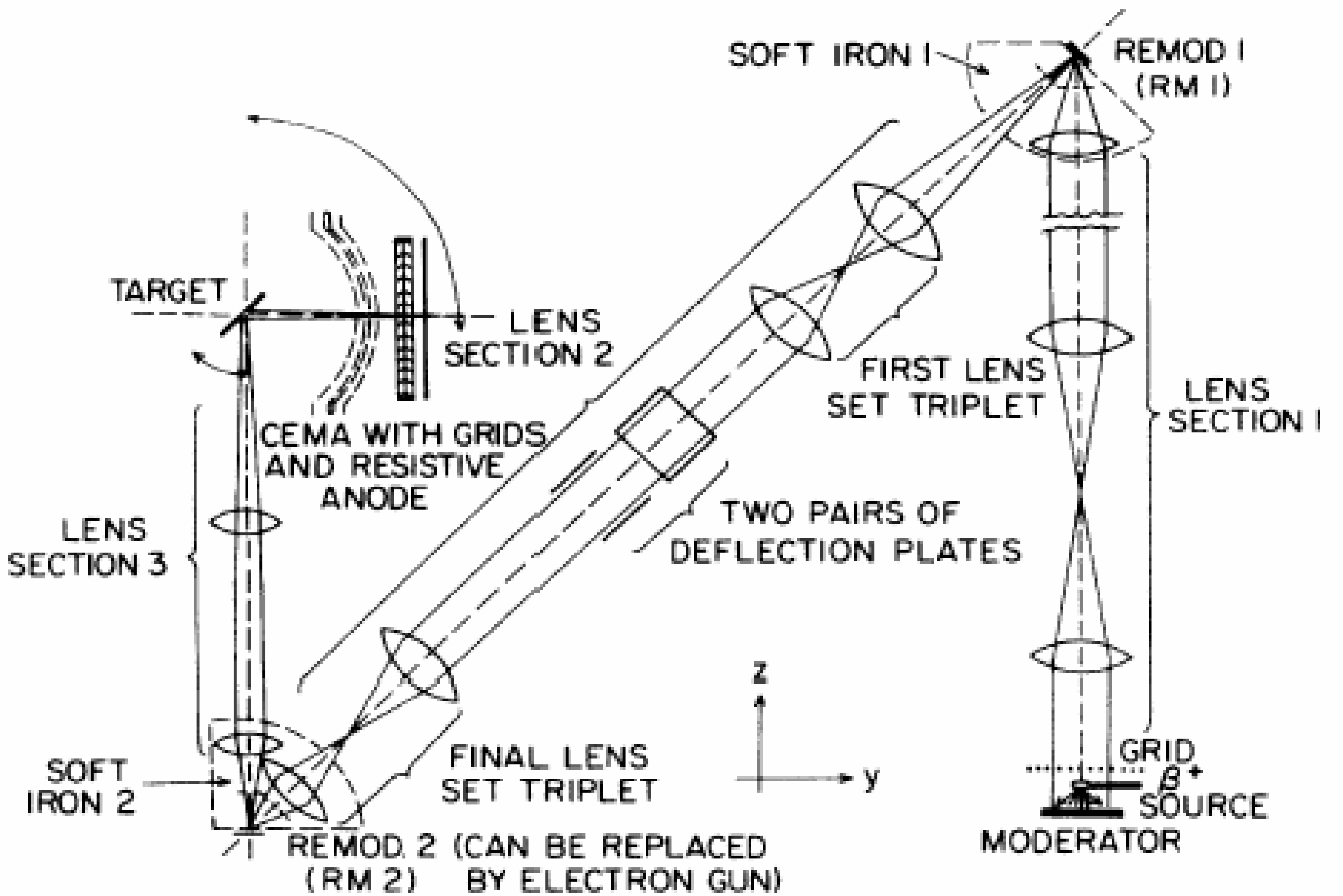

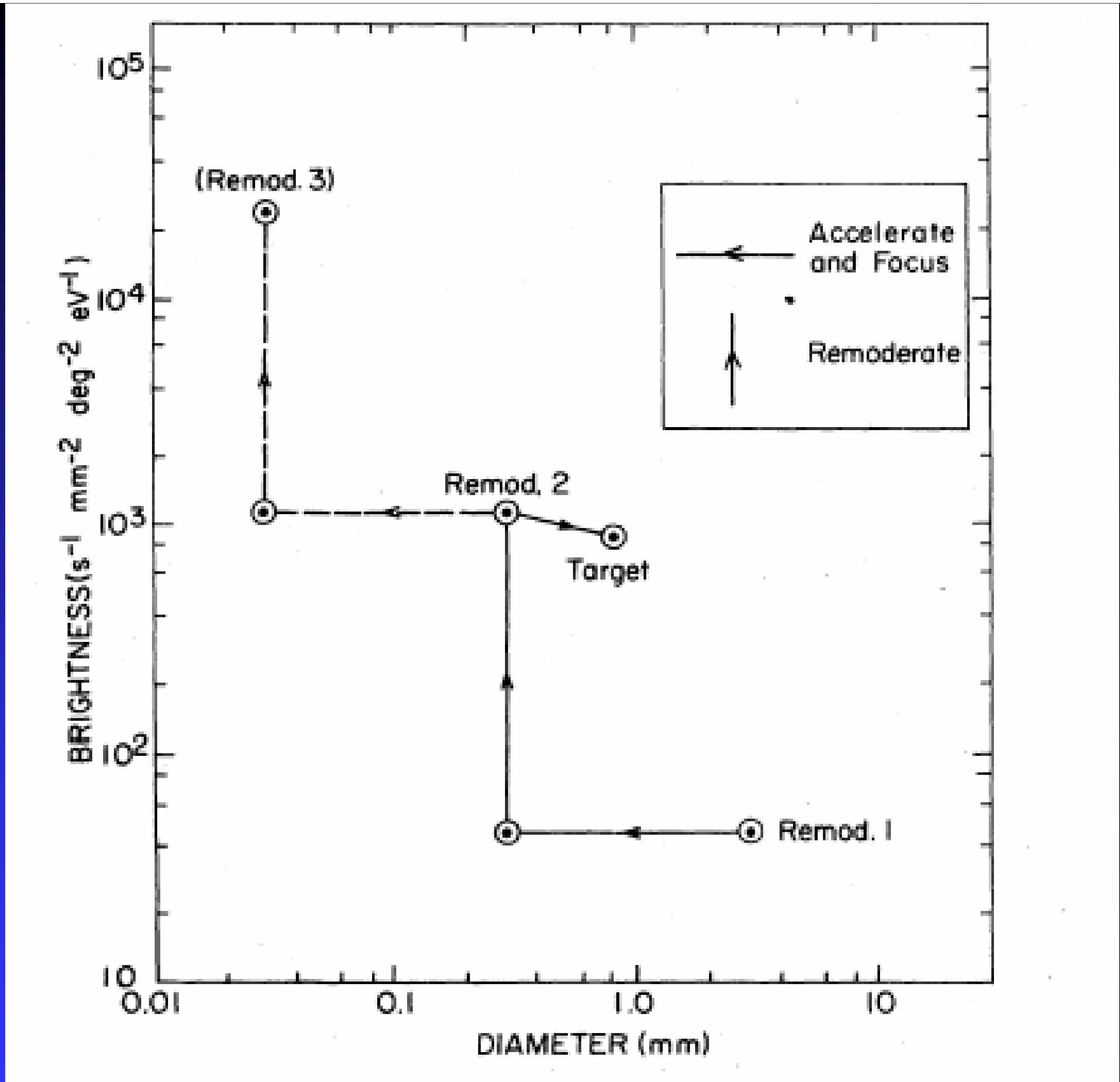

Brightness vs. Beam diameter

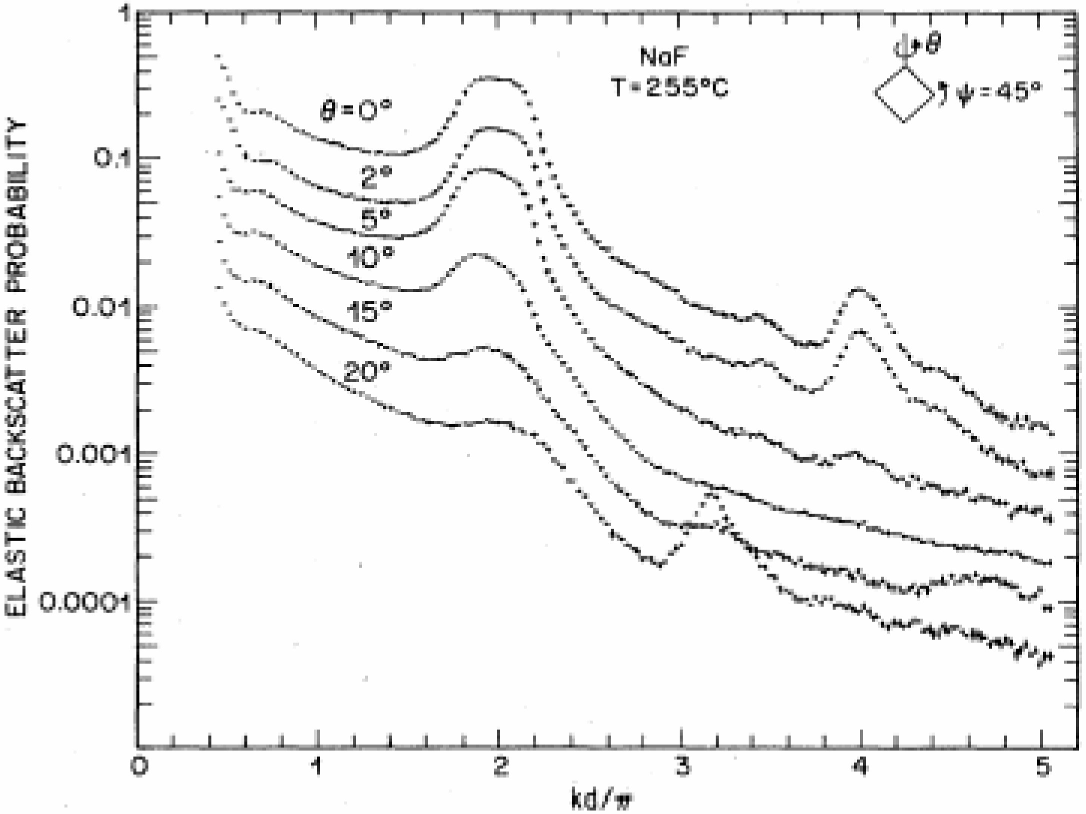

FIG. 3. Positron-diffraction intensities for a freshly air-cleaved (100) NaF crystal ro
(110) axis. The curves have
semilog plot by dividing succ
of 2.

If positrons have a mean free path λ in a crystal, the full width at half maximum of the simple Bragg peaks in Fig. 3 should be

$$\Delta = d/\pi\lambda.$$

From the width of the peak at $kd/\pi = 4$ we infer that the positron mean free path (see Table I) in NaF is about 7 Å at 27 eV.

低能正电子衍射(LEPD)在半导体表面可获得比电子衍射(LEED)更好的效果。早期工作的LEPD分辨较差， 典型的角分辨为~20 mm deg 。应用二次慢化正电子束，Frieze等人获得了角分辨为~1mm deg的LEPD，这已同商用的LEED相媲美，在他们测量的LEPD谱中的(01)和(10)束上强度改变表明了作用势的不同。

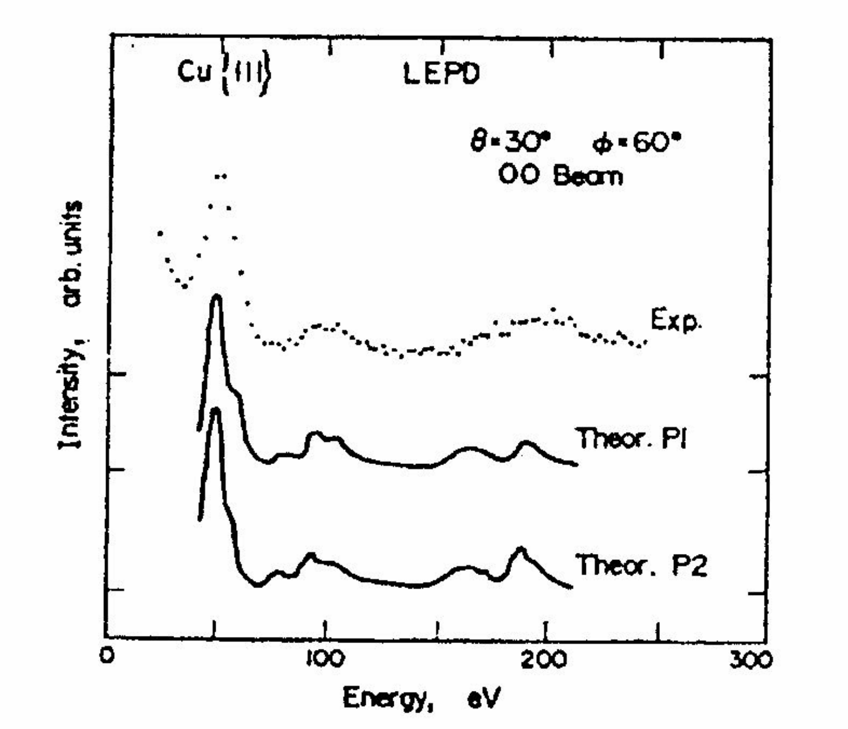

Brandeis LEPD在Cu（111）上的测量结果，图中的计算结果由Jona等人给出

低能电子和正电子在W（110）衍射的三维图， 束流能量为250eV平行注入[110]块体方向在ϕ=20的方向。

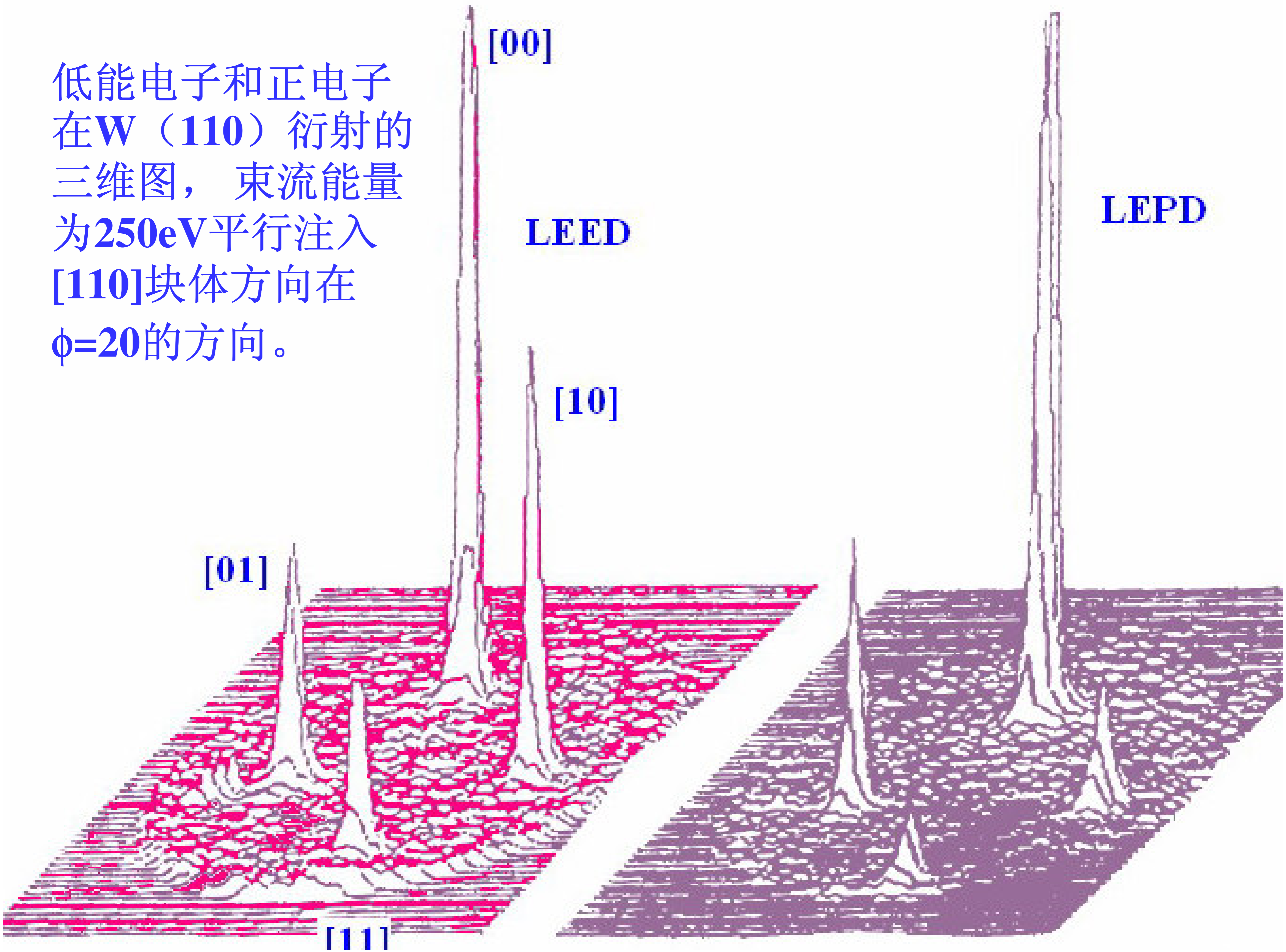

■高能正电子衍射(RHEPD)

Reflection high-energy positron diffraction

KAWASUSO, A., (JAERI)

- **Primary Bragg Reflection**
- **Total Reflection**

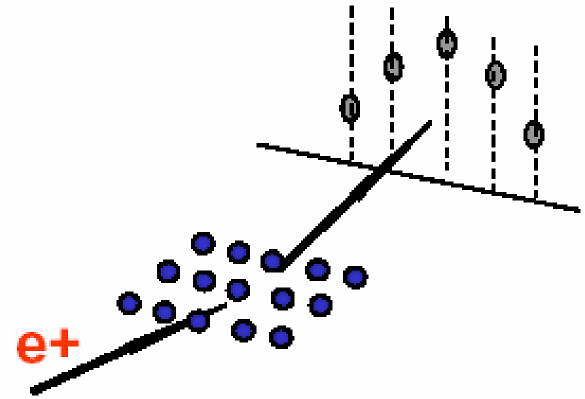

Negative Inner Potential

Positive Inner Potential

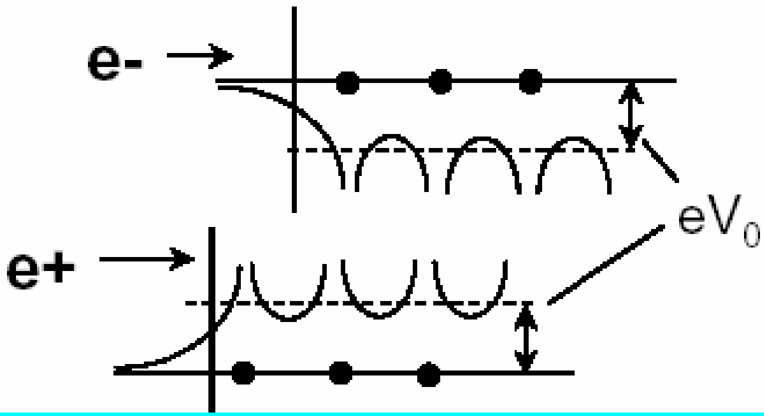

Bragg condition: $E\sin^2\theta = 37.5\, n^2/d^2 + eV_0$

Primary Bragg peak

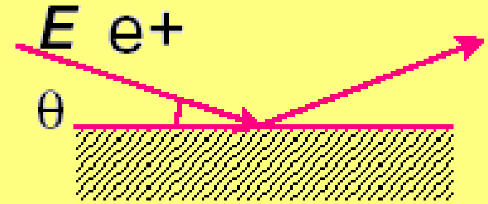

Si(111) ▪ : d=3.14 A

$eV_0 = \begin{cases} -12 \text{ eV for } e^- \\ +12 \text{ eV for } \mathbf{e^+} \end{cases}$ $\quad E\sin^2\theta \begin{cases} <0 \\ \mathbf{>0} \end{cases}$ for n=1

Total reflection

E. ($E\sin^2\theta$) < eV_0

⬇

$\theta = \sin^{-1}[eV_0 / E]^{1/2}$

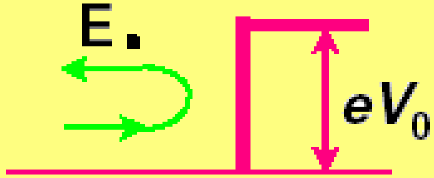

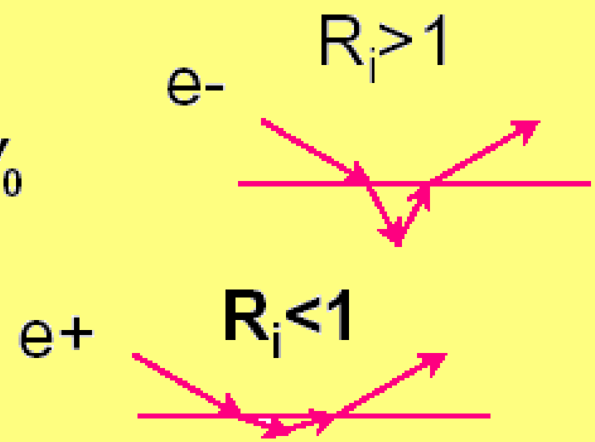

Possible Application of RHEPD

Diffraction pattern
Rocking curve
(+Dynamical theory)

- •Adsorbed layer
- •Surface roughness
- •Surface Debye temperature
- •Surface dipole barrier of metals

Potential of adsorbed atom

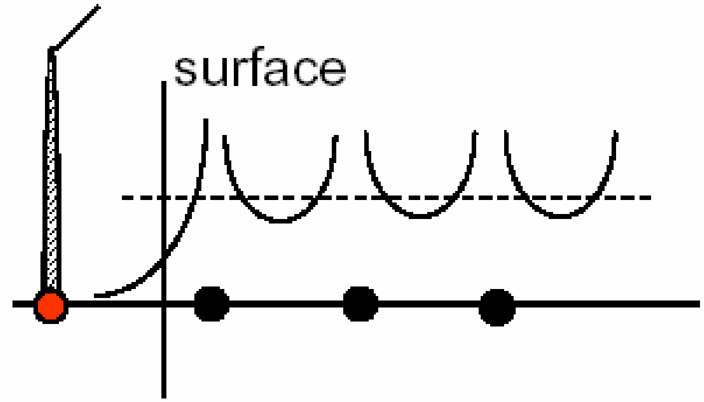

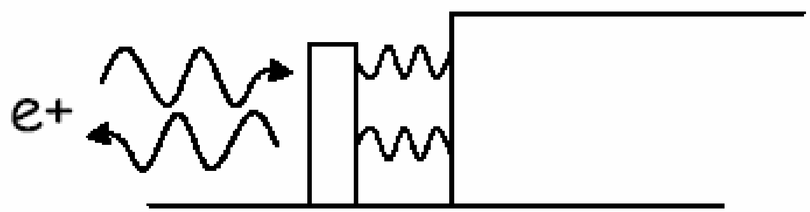

Flat surface

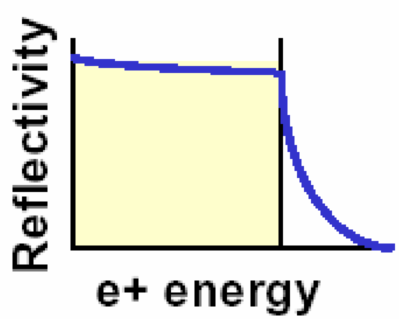

Irregular surface

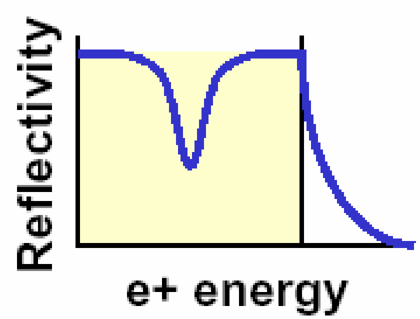

Present RHEPD apparatus at JAERI

Key elements
- Positron beam 10 -20 keV
- Low angular divergence <1°
- Small beam diameter <1mm

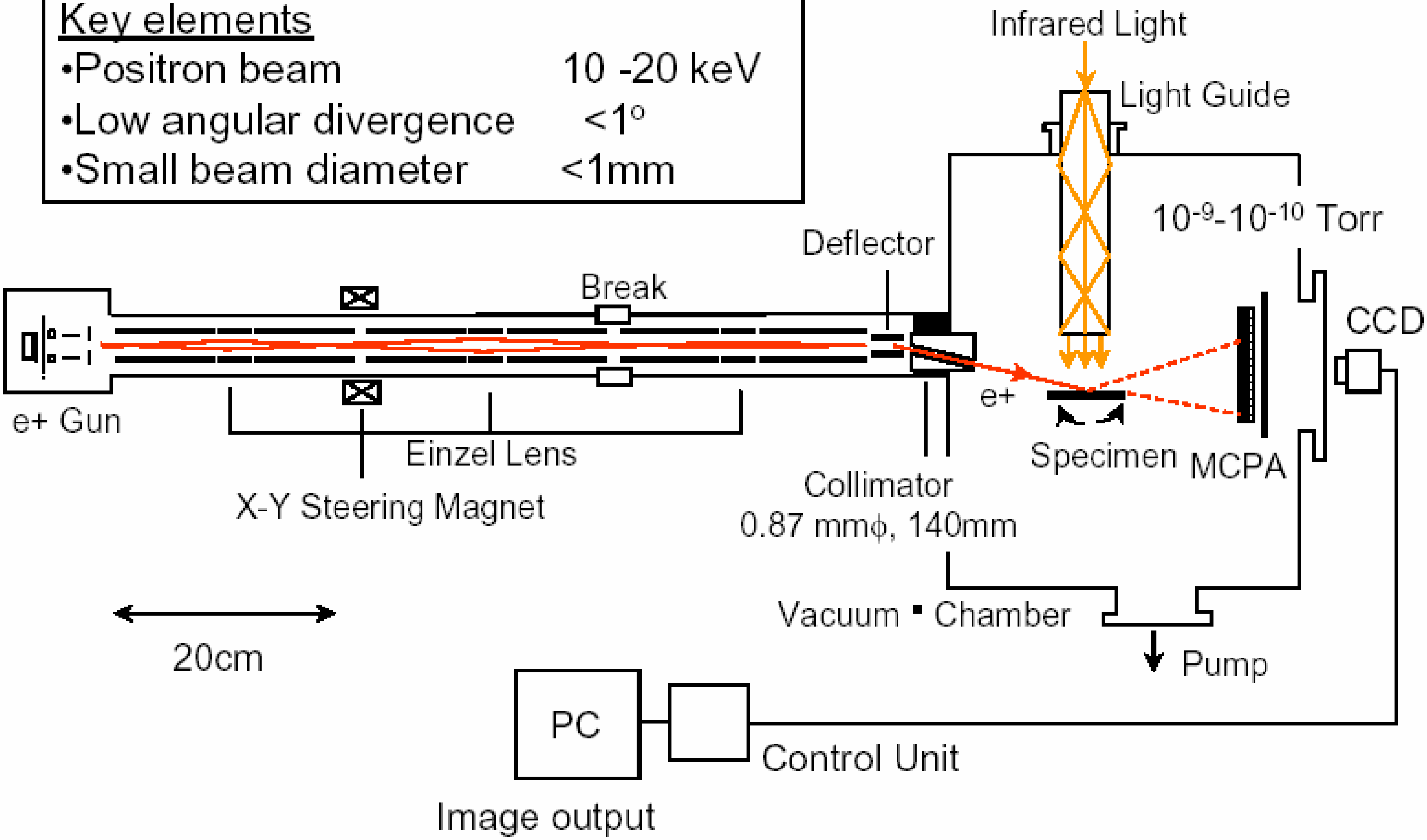

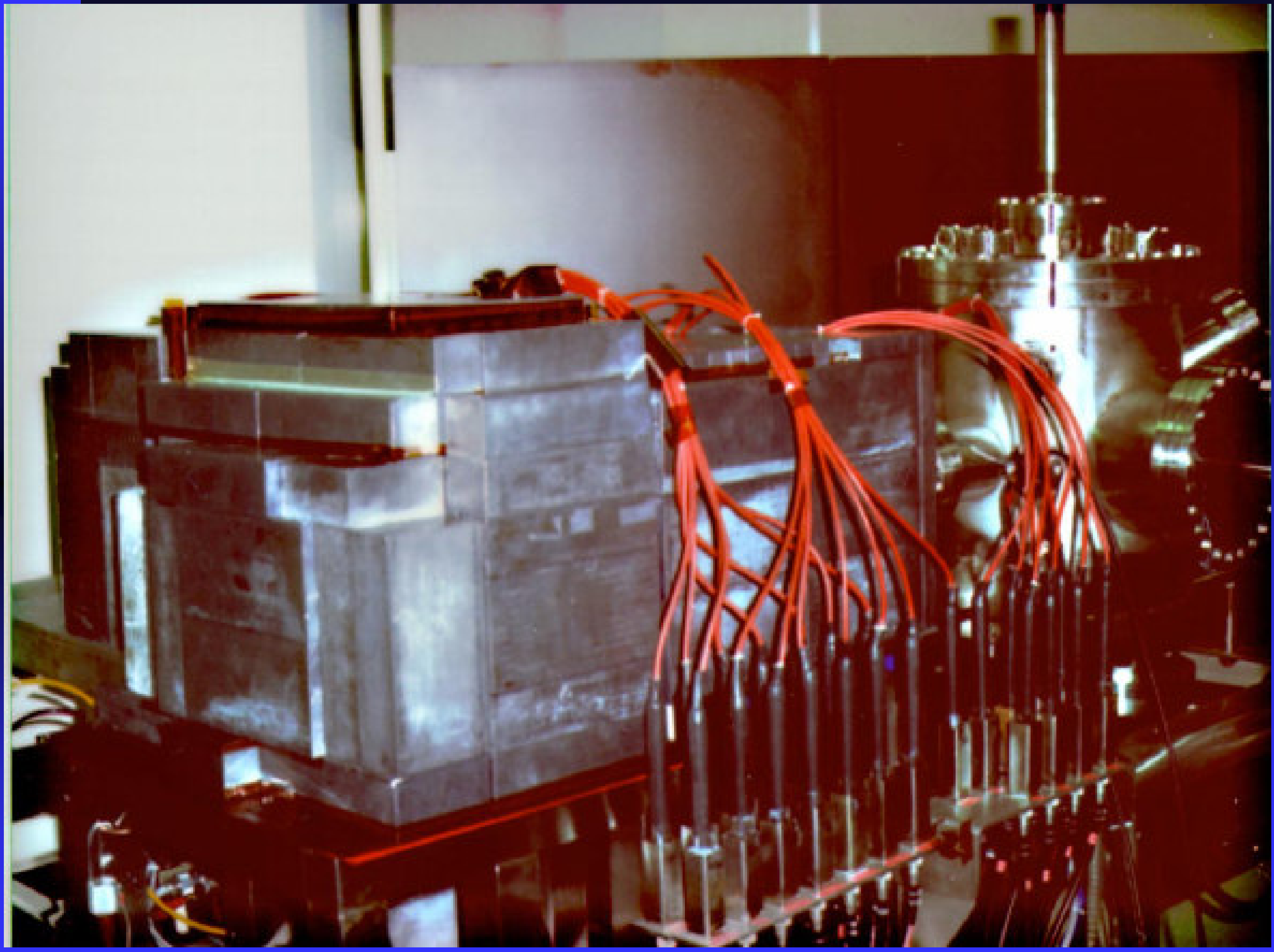

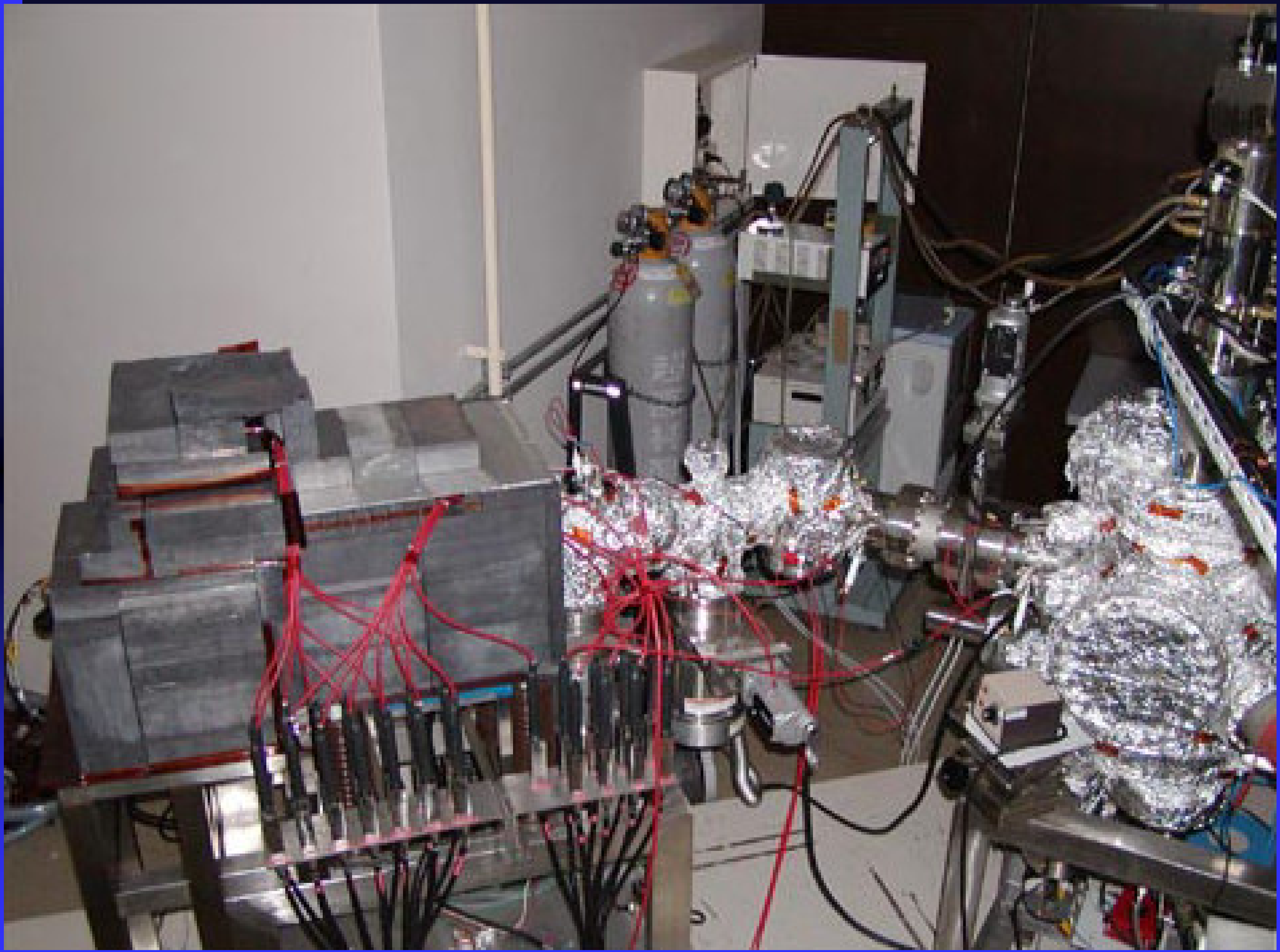

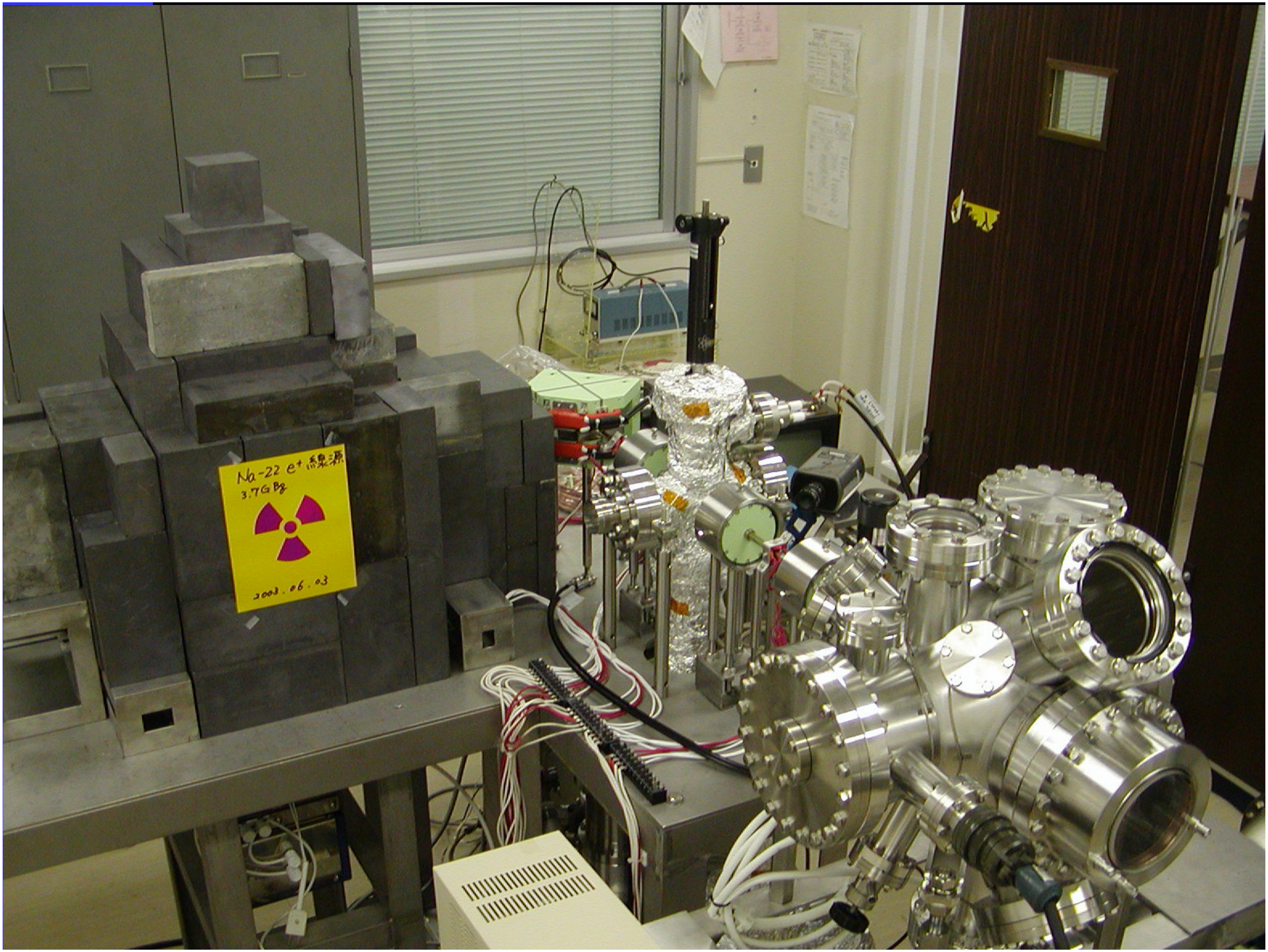
Na-22 e+ 線源
3.7GBq
2003.06.03

Characteristics of Positron Beam

Beam Energy	20 keV fixed
Final e+ flux	▪ 3000 e+/sec
Beam diameter	0.9 mm
Angular divergence	< 1 deg.

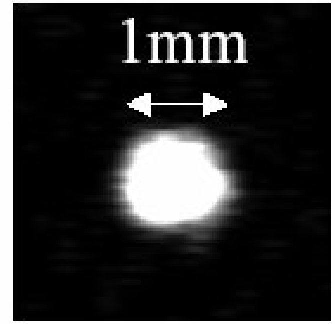

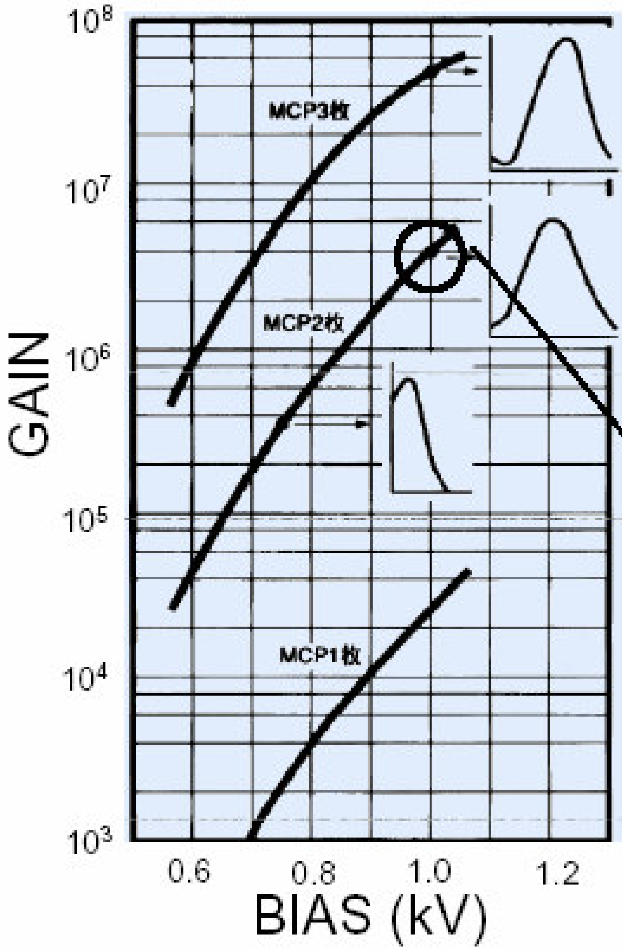

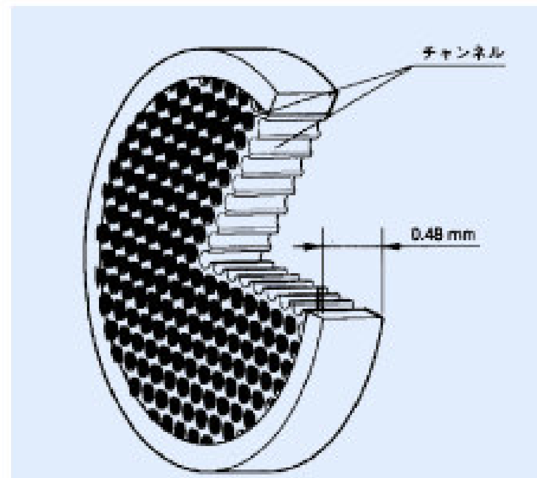

Max gain $4x10^6$

One RHEPD pattern :1-10 hrs.

First RHEPD pattern from Si(111)H

[11$\bar{2}$] incidence | [1$\bar{1}$0] incidence

RHEPD

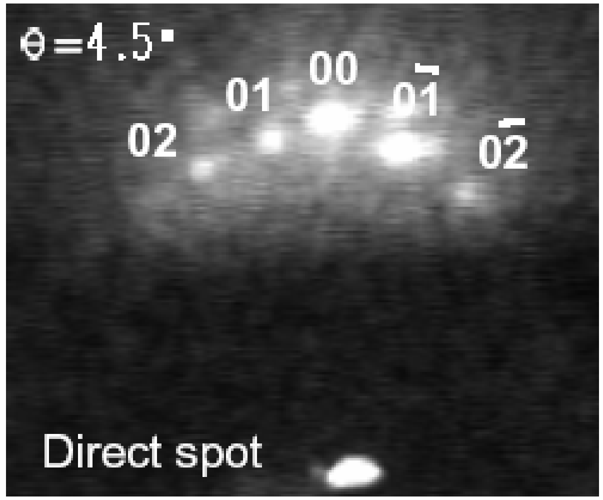

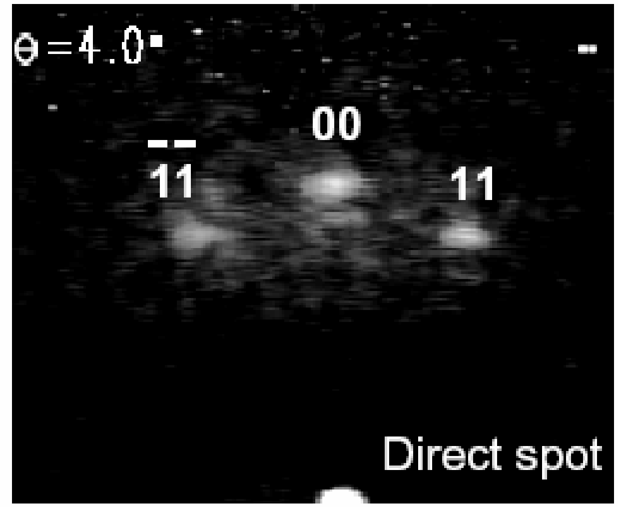

RHEED

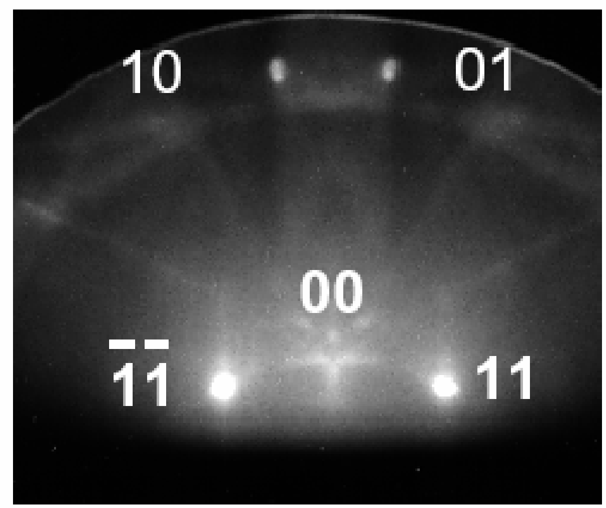

8. PAES

Weiss等人在1988年首先发展了正电子湮没诱发的俄歇电子谱仪（PAES），该技术的主要优点有：

（1）对表面灵敏，可以分析最表面的原子层；

（2）在非常低的能量损失下 （大约比电子俄歇谱EAES的能量损失低 5个量级 ）得到PAES谱；

（3）可以大大消除的二次电子本底 。因而PAES技术特别适宜于俄歇线型分析。

俄歇电子发射的基本原理是：低能正电子注入固体表面时，相当一部分扩散回到表面，被近表面或表面态捕获，一部分被捕获的正电子与芯电子湮没，产生芯空位，因而产生俄歇电子发射

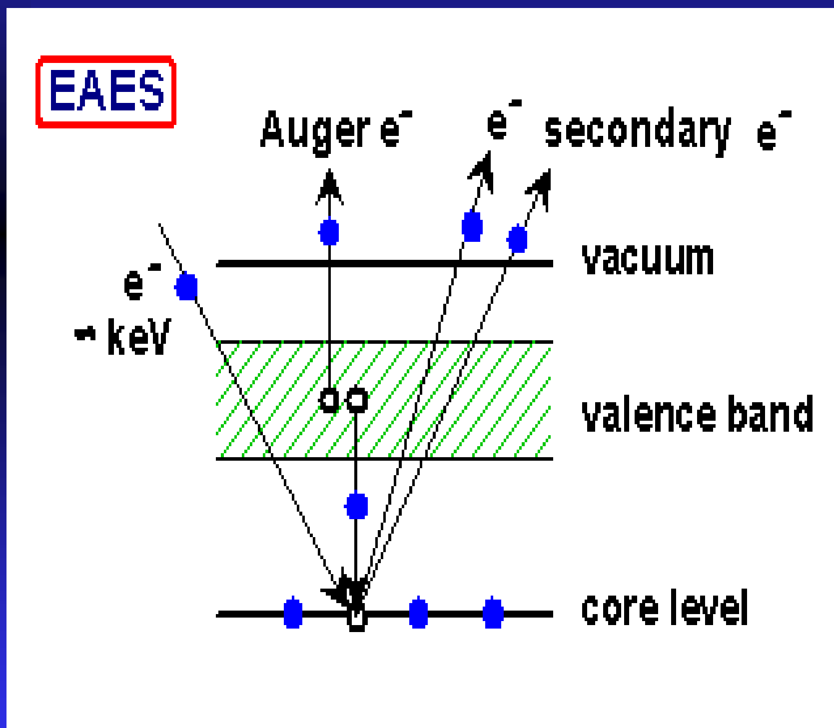

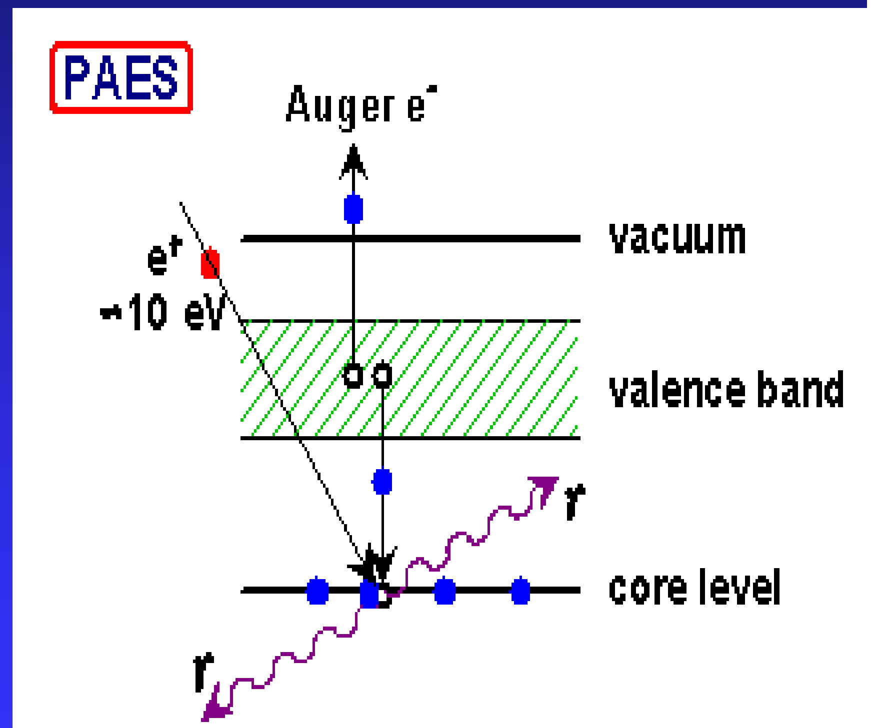

(a) Electron induced AES (EAES)

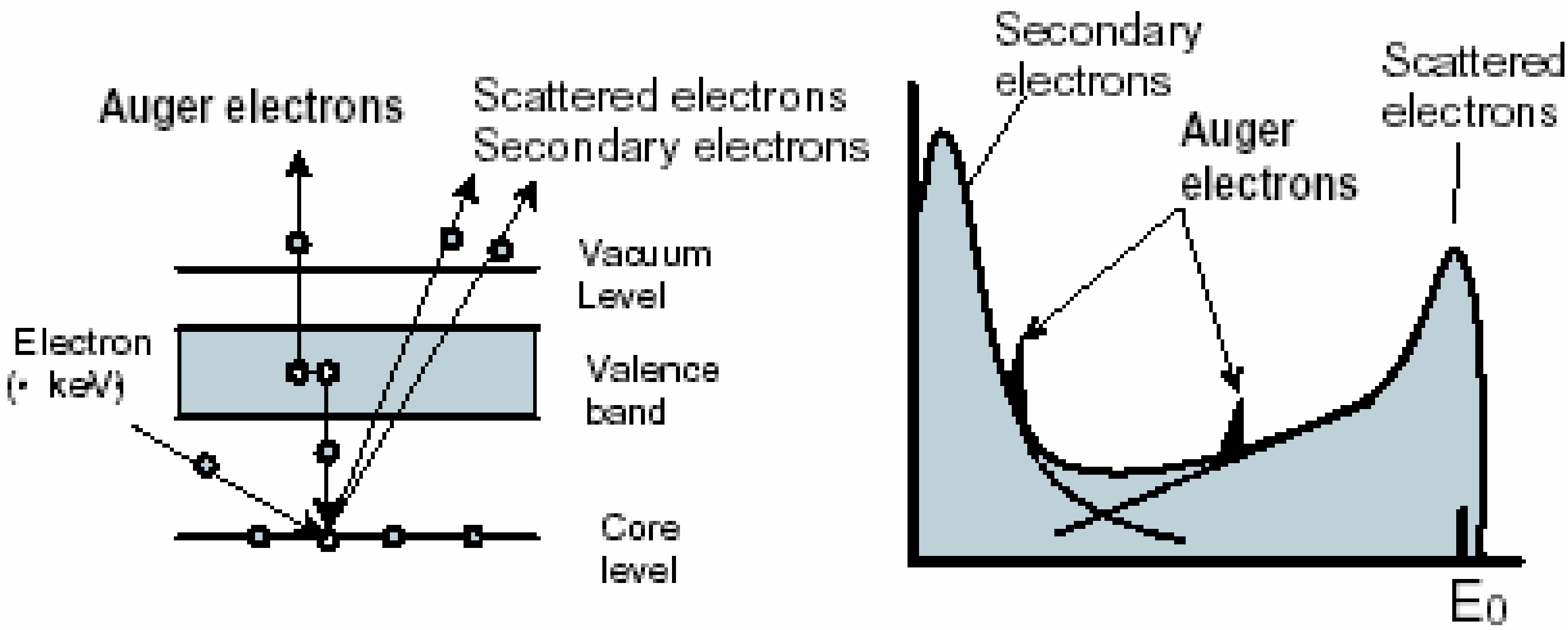

Positron-annihilation induced AES (PAES)

Core holes are created by annihilation of the core electrons with positrons trapped by the surface state.

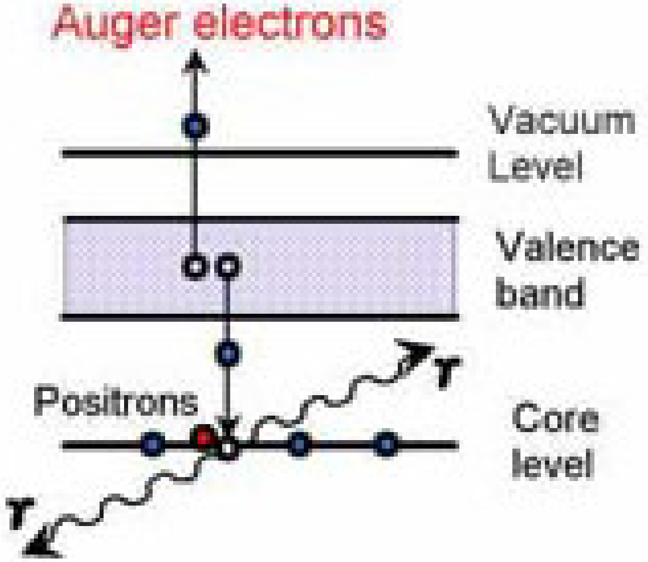

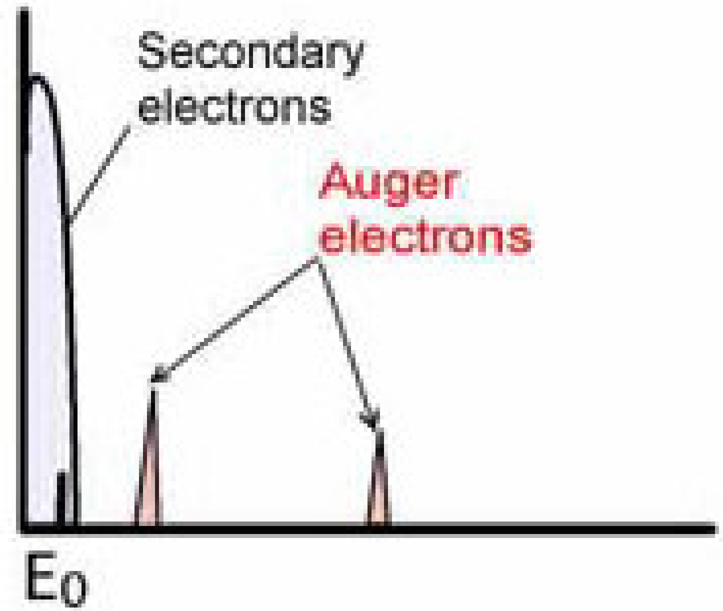

PAES 谱仪

- 日本AIST
- 美国University of Texas
- 美国Brookhaven National Laboratory
- 英国UEA

TOF-PAES

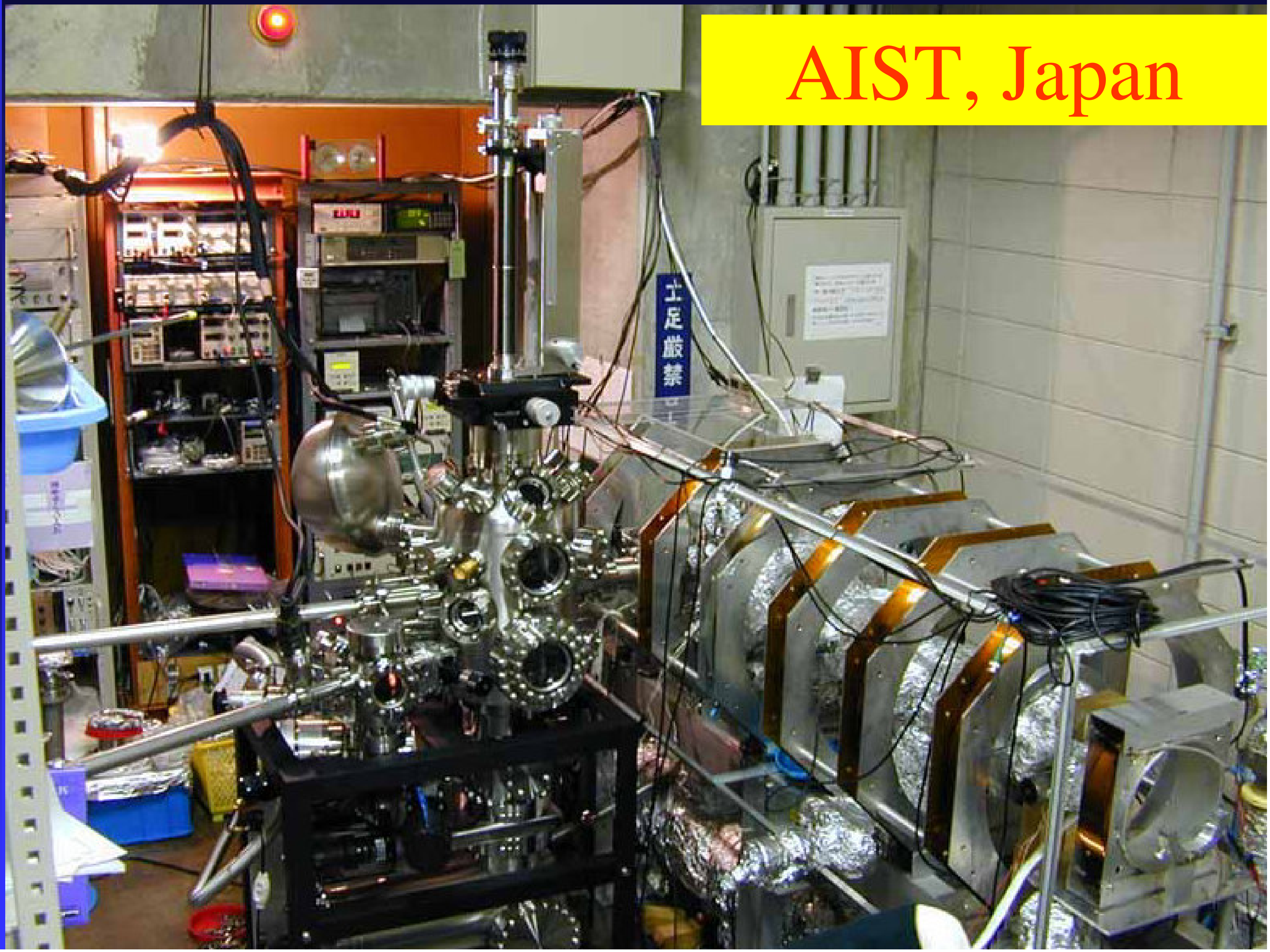

AIST, Japan

TOF-PAES apparatus

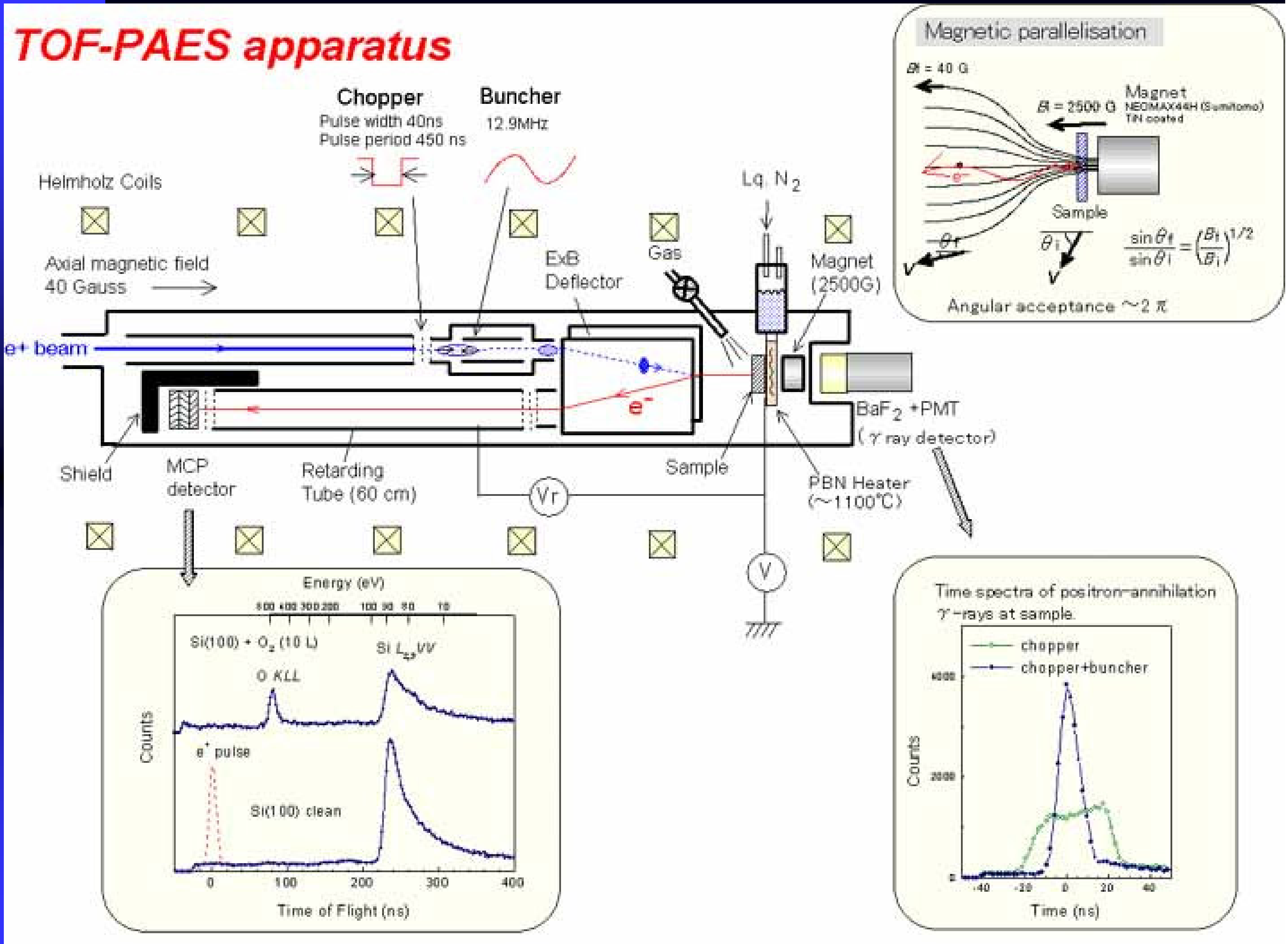

Applied Surface Science 149 (1999) 260–263

Time-of-flight positron-annihilation induced Auger electron spectroscopy studies of adsorption of oxygen on Si(100)

Toshiyuki Ohdaira *, Ryoichi Suzuki, Tomohisa Mikado

Electrotechnical Laboratory, 1-1-4 Umezono, Tsukuba, Ibaraki 305-8568, Japan

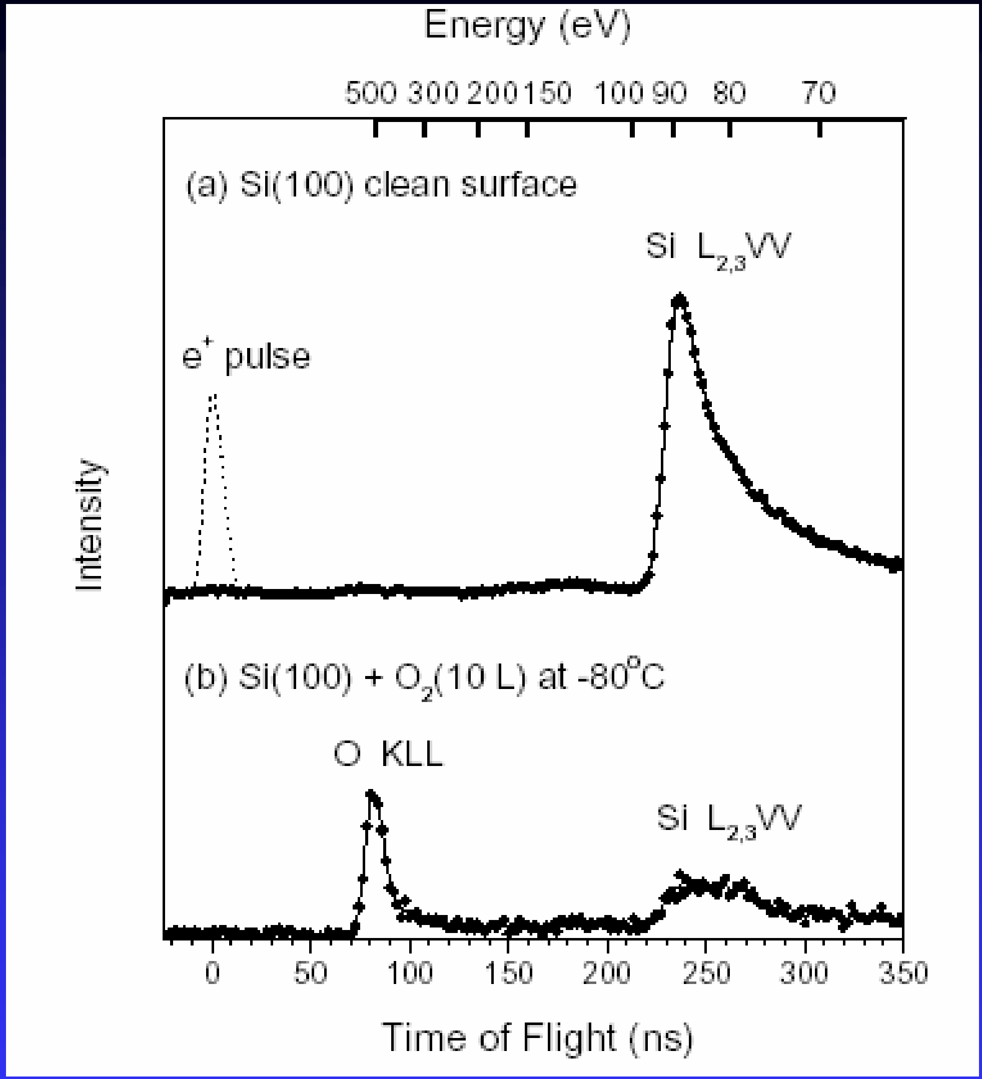

(1 L = 10^{-6} Torr·sec)

TOF-PAES spectra for clean and 10-Langmuir O_2 exposed Si(100) surfaces. The exposure was done at a substrate temperature of –80° C

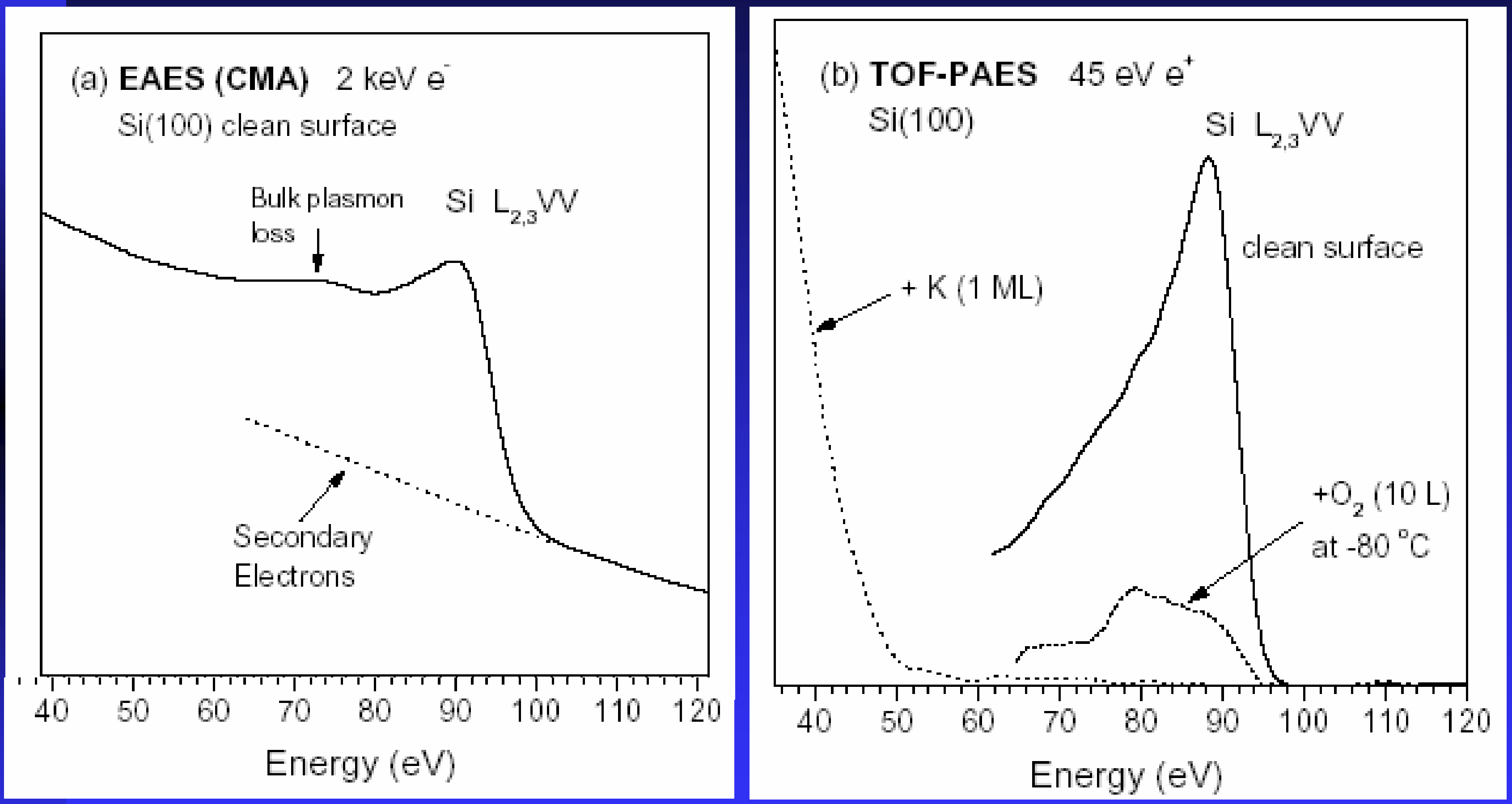

(a) **EAES (CMA)** 2 keV e⁻
Si(100) clean surface
Bulk plasmon loss
Si $L_{2,3}VV$
Secondary Electrons
40 50 60 70 80 90 100 110 120
Energy (eV)
(b) **TOF-PAES** 45 eV e⁺
Si(100)
Si $L_{2,3}VV$
clean surface
+ K (1 ML)
$+O_2$ (10 L) at -80 °C
40 50 60 70 80 90 100 110 120
Energy (eV)

Applied Surface Science 194 (2002) 291–295

Surface analysis of a well-aligned carbon nanotube film by positron-annihilation induced Auger-electron spectroscopy

T. Ohdaira[a,*], R. Suzuki[a], Y. Kobayashi[a], T. Akahane[b], L. Dai[c]

[a]*National Institute of Advanced Industrial Science and Technology (AIST), 1-1-1 Umezono, Tsukuba, Ibaraki 305-8568, Japan*
[b]*National Institute for Materials Science, Advanced Materials Laboratory, 1-1 Namiki, Tsukuba, Ibaraki 305-0044, Japan*
[c]*CSIRO Molecular Science, Bag 10, Clayton South, Vic. 3169, Australia*

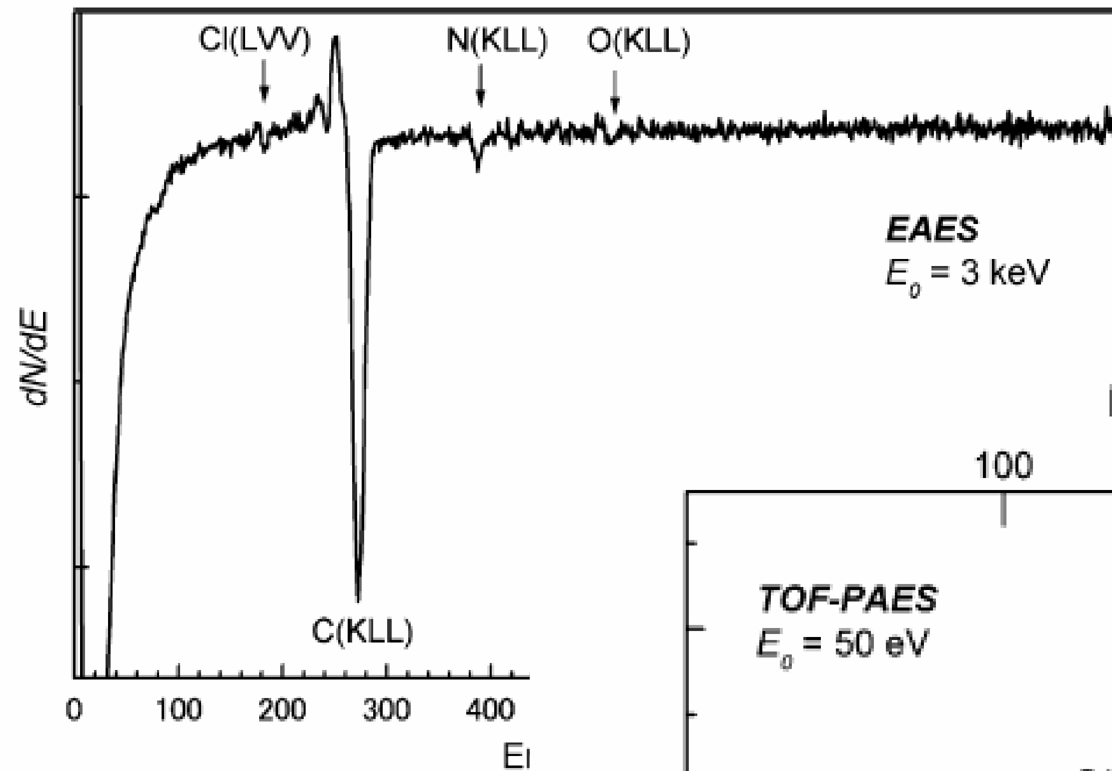

3 keV EAES measured for the surface of the wel

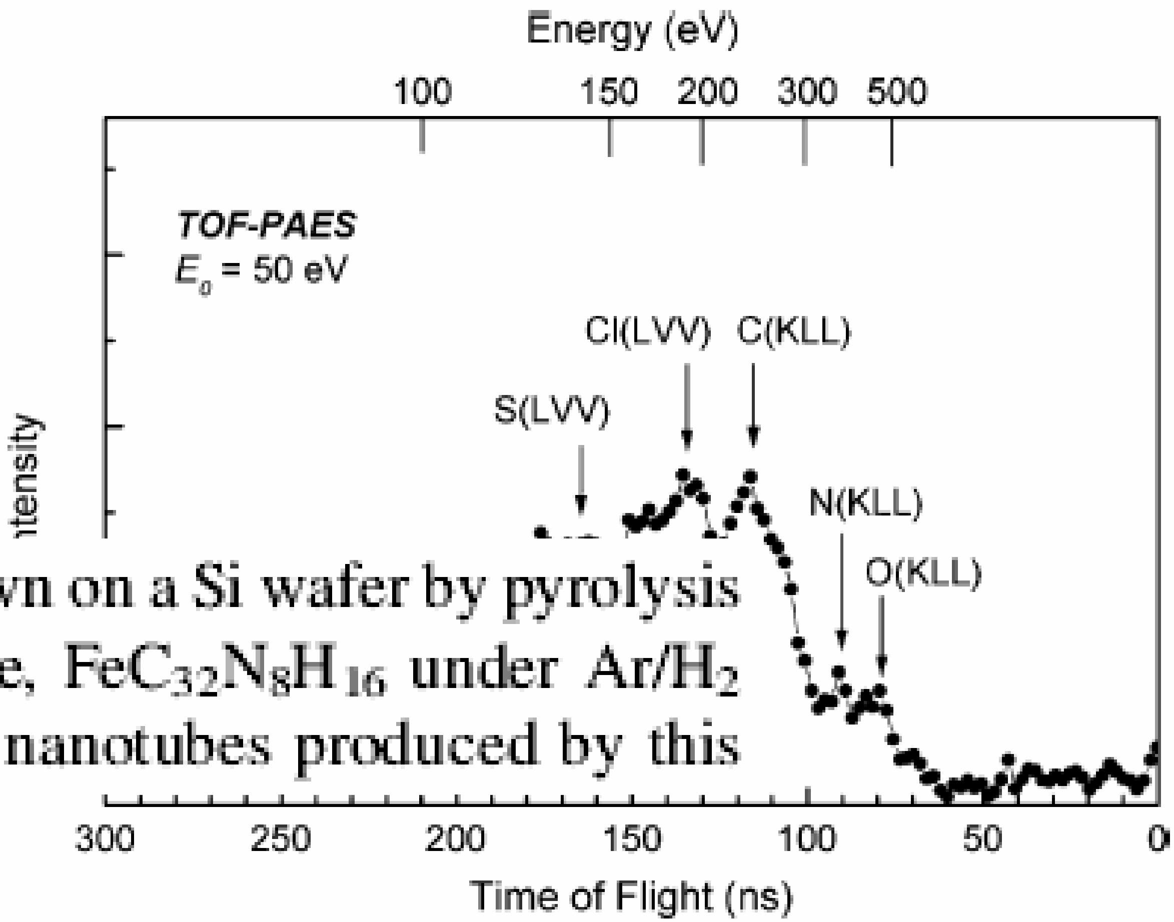

The CNT film was grown on a Si wafer by pyrolysis of iron(II) phthalocyanine, $FeC_{32}N_8H_{16}$ under Ar/H_2 at 800–1100 °C [9]. The nanotubes produced by this

Fig. 2. TOF–PAES spectrum measured for the surface of well-aligned CNT film.

美国德克萨斯大学PAES

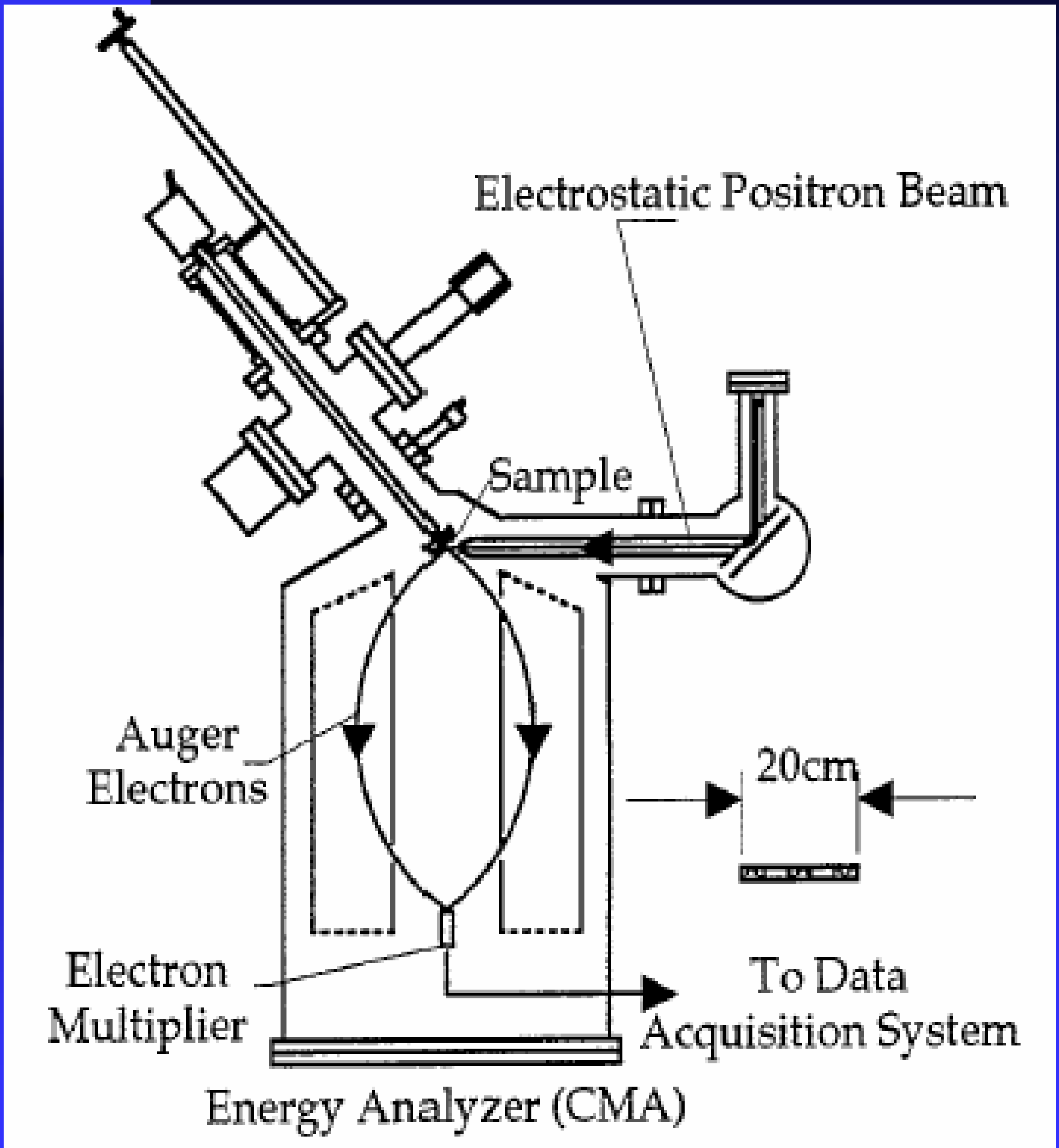

美国Texas大学Arlington分校的Weiss在1995年建立了一台能量分辨为2%的高分辨PAES谱仪，由一低能静电正电子束（10eV）、一个大型圆柱形能量分析器和一个超高真空样品室组成，配备60mCi的^{22}Na，可获得~8×10^{4} e^{+}/s束流强度，由于芯空位是由正负电子湮没产生而不是通过碰撞电离产生，因而入射的正电子束能量可以比发射的俄歇电子能量还要小。

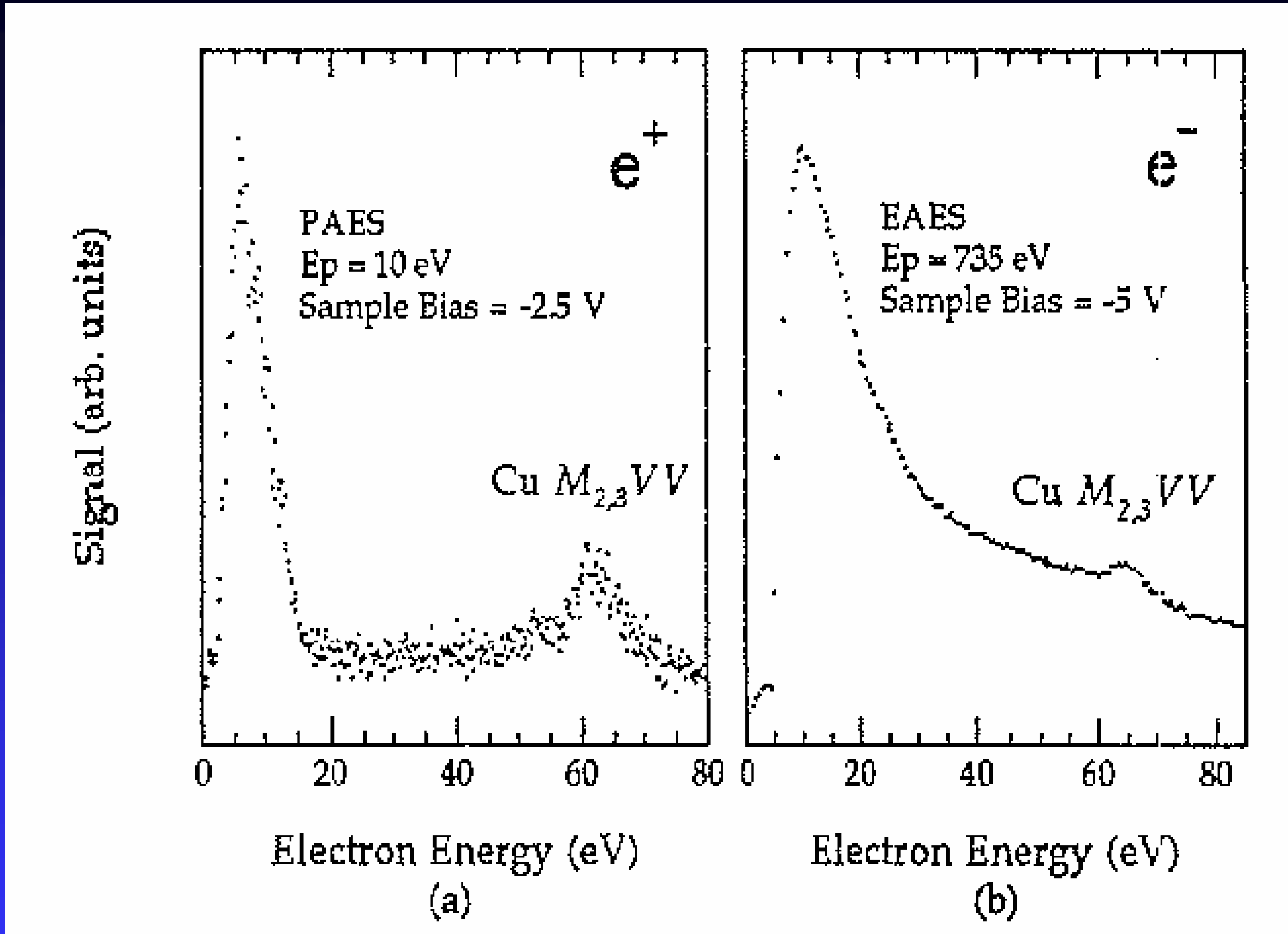

正电子和电子在多晶铜表面引起的俄歇电子发射。

（a）正电子能量10eV，（b）电子能量735eV。

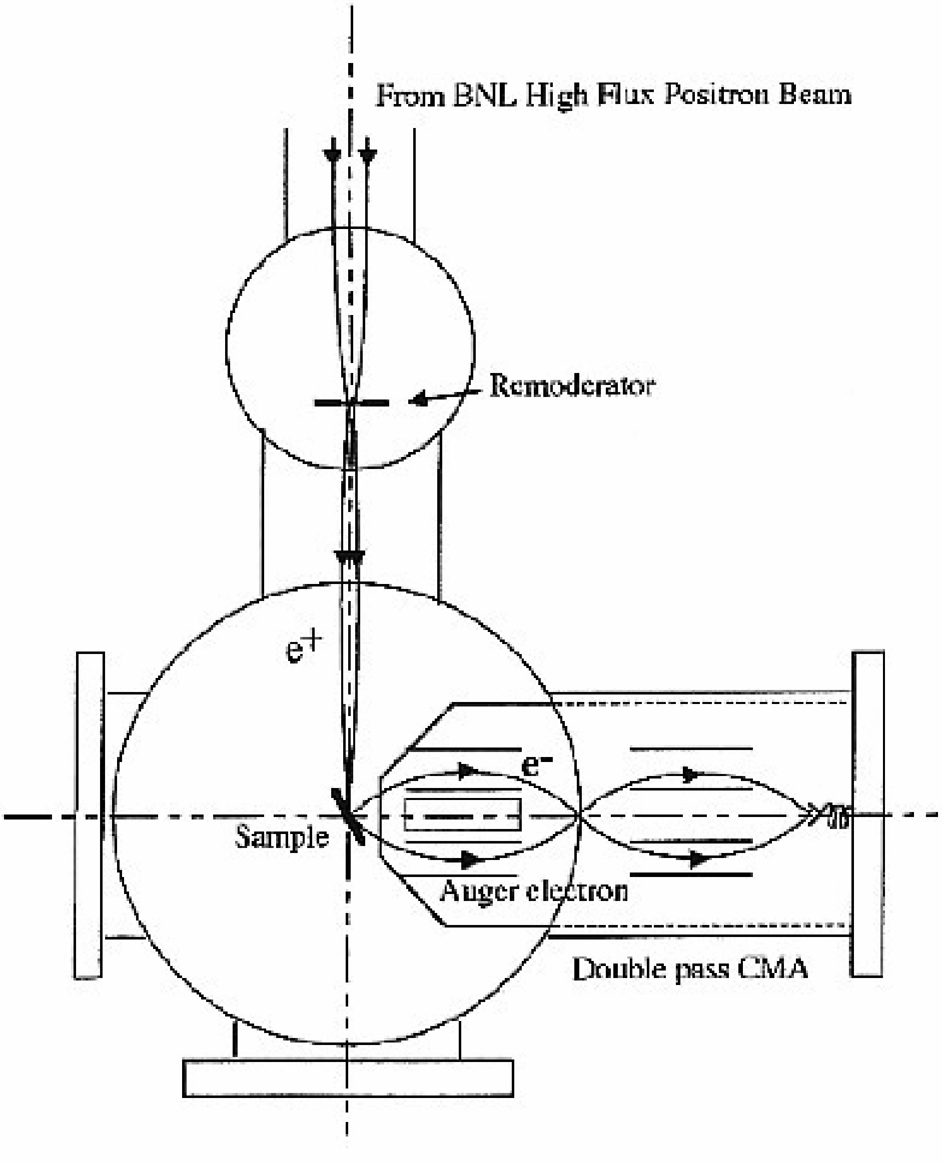

PAES Beamline at the BNL High Flux Positron Beam

Brookhaven National Lab.
PAES

这个装置可产生比通常的**PAES**要大100倍的正电子束流强度，这样可以使测量时间从原来的几小时减少到几分钟，因此可用来对薄膜生长动力学和不稳定的多成份表层系统进行高分辨测量研究。

PHYSICAL REVIEW LETTERS

Measurement of the Energy Spectrum of Secondary Electrons Ejected from Solids by Positron Impact

N. Overton and P. G. Coleman

School of Physics, University of East Anglia, Norwich NR4 7TJ, United Kingdom

(Received 15 August 1996; revised manuscript received 17 April 1997)

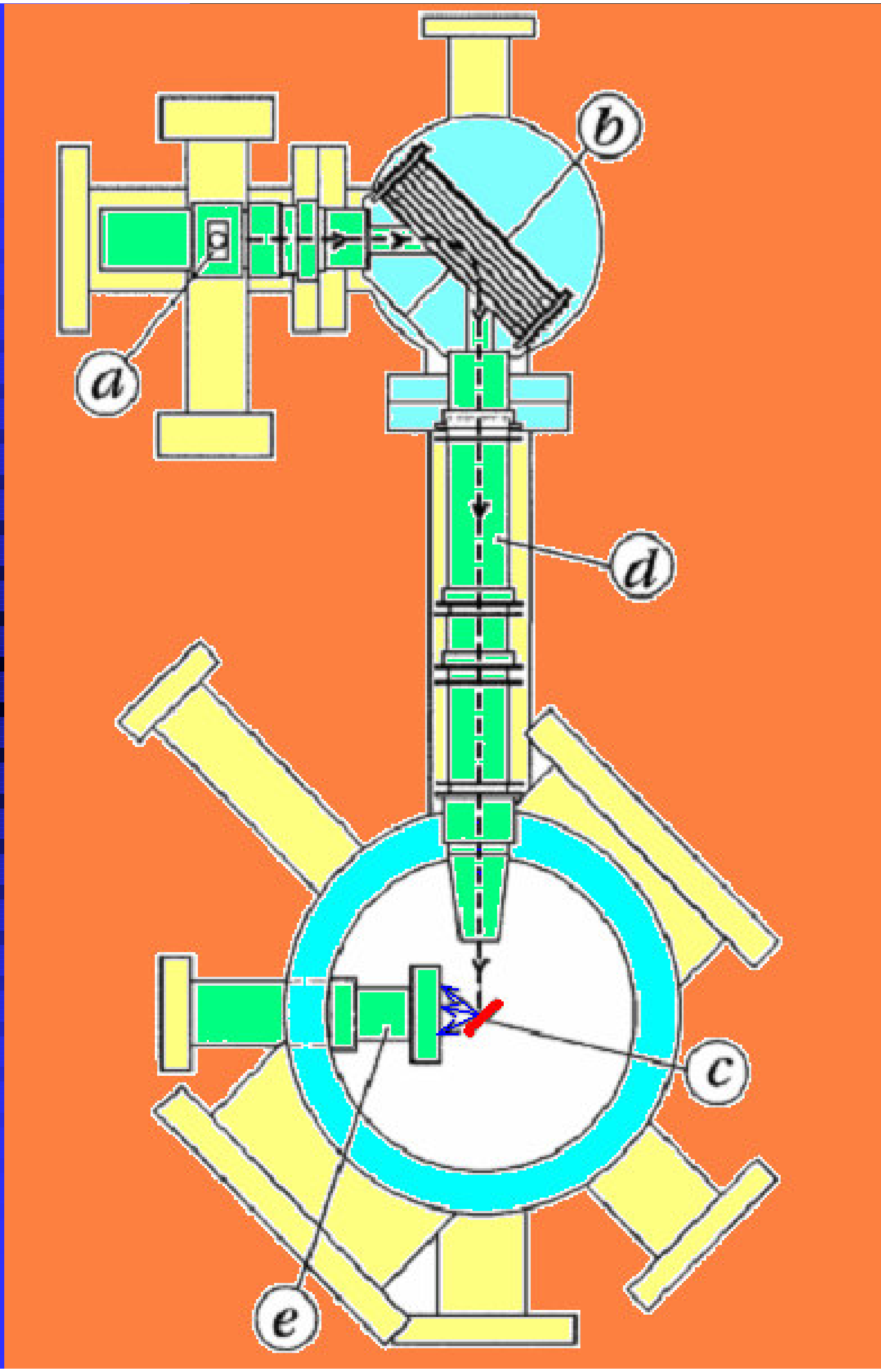

Schematic of the UEA electrostatic beam system:

(a) source,

(b) electrostatic reflector,

(c) sample,

(d) electrostatic lense,

(e) microchannel plate detector/RFA assembly.

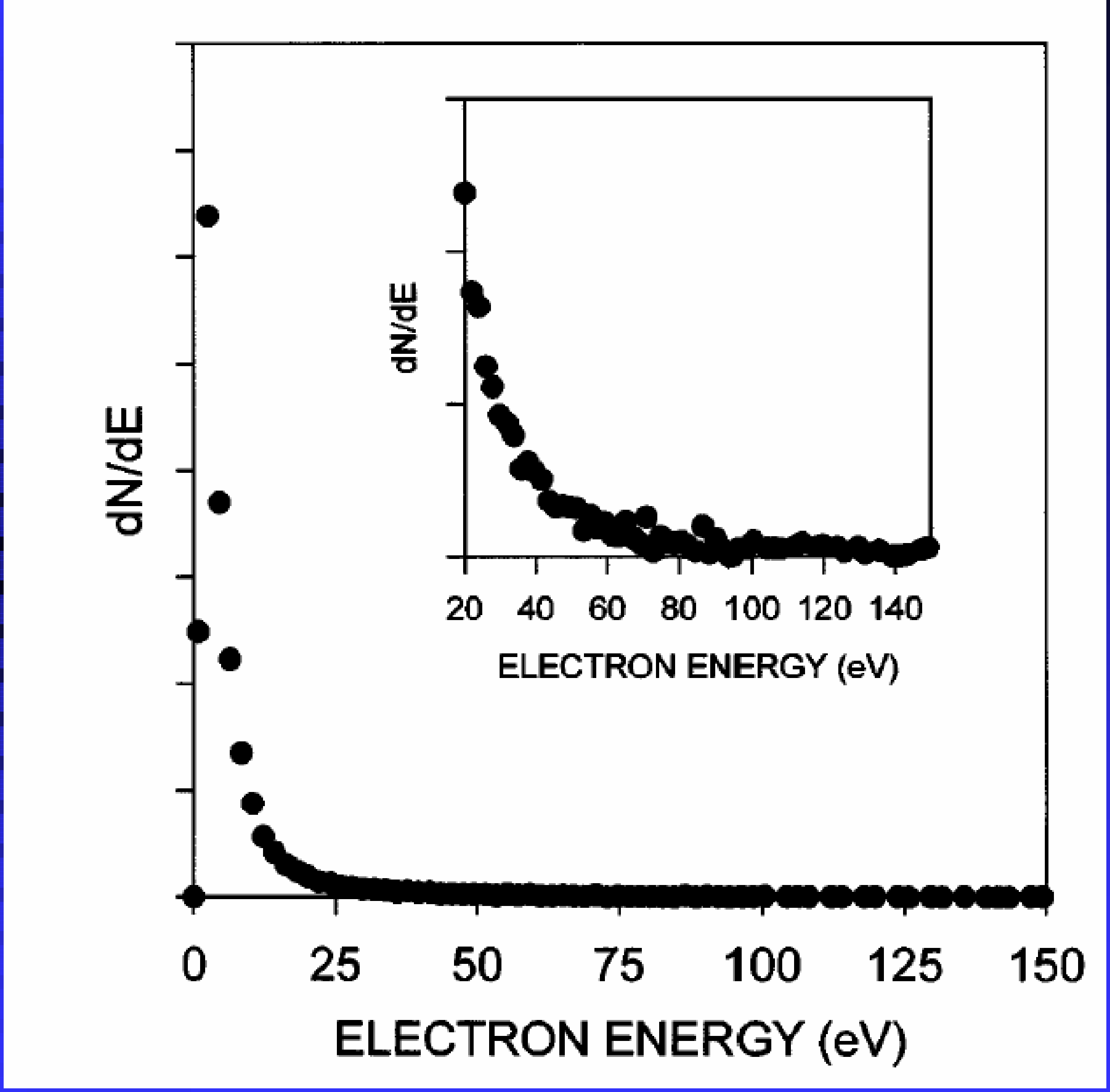

Differential energy spectra of secondary electrons ejected by 300 eV positron impact on Cu.

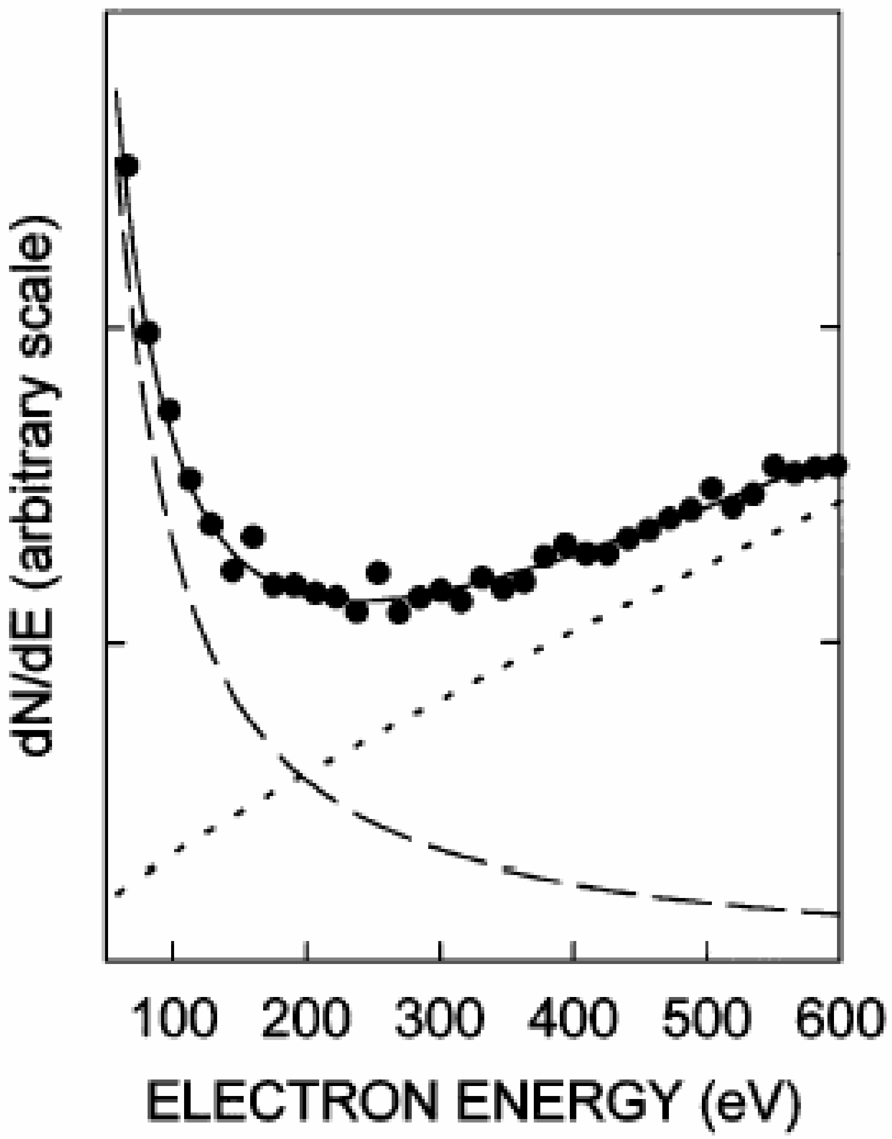

FIG. 5. Differential energy spectra of electrons leaving a Cu surface bombarded by 2 keV electrons (full circles). Solid line: fit to the form $AE^{-m} + BE^{n}$. Broken line: AE^{-m} (secondaries). Dotted line: BE^{n} (backscattered).

9. 微束与正电子显微技术

- 微束技术
- 显微技术

微　束

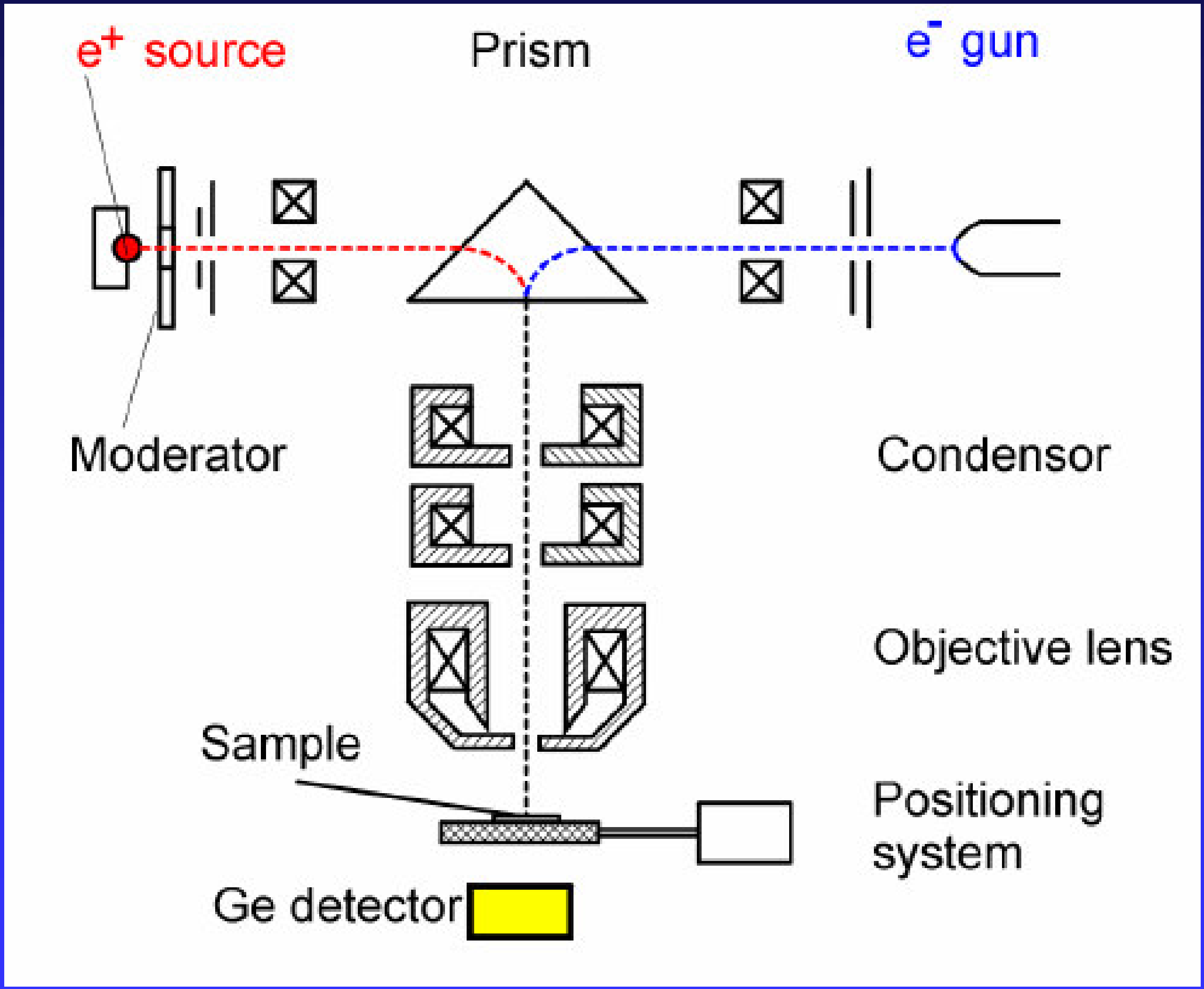

The Positron Microscope at Bonn University

1995, Netherlands

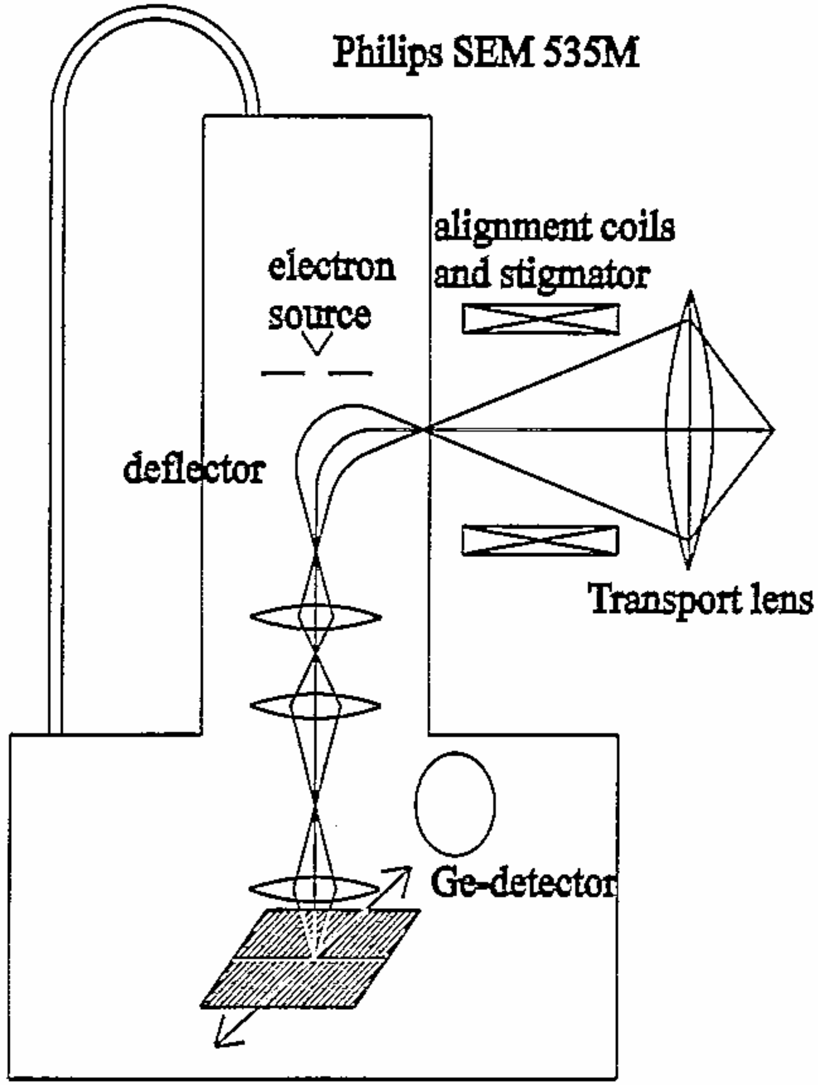

Fig. 1. Schematic design of the setup of the positron microbeam with the 90° deflector, the transport optics consisting of a magnetic lens, alignment coils, and a stigmator and the SEM.

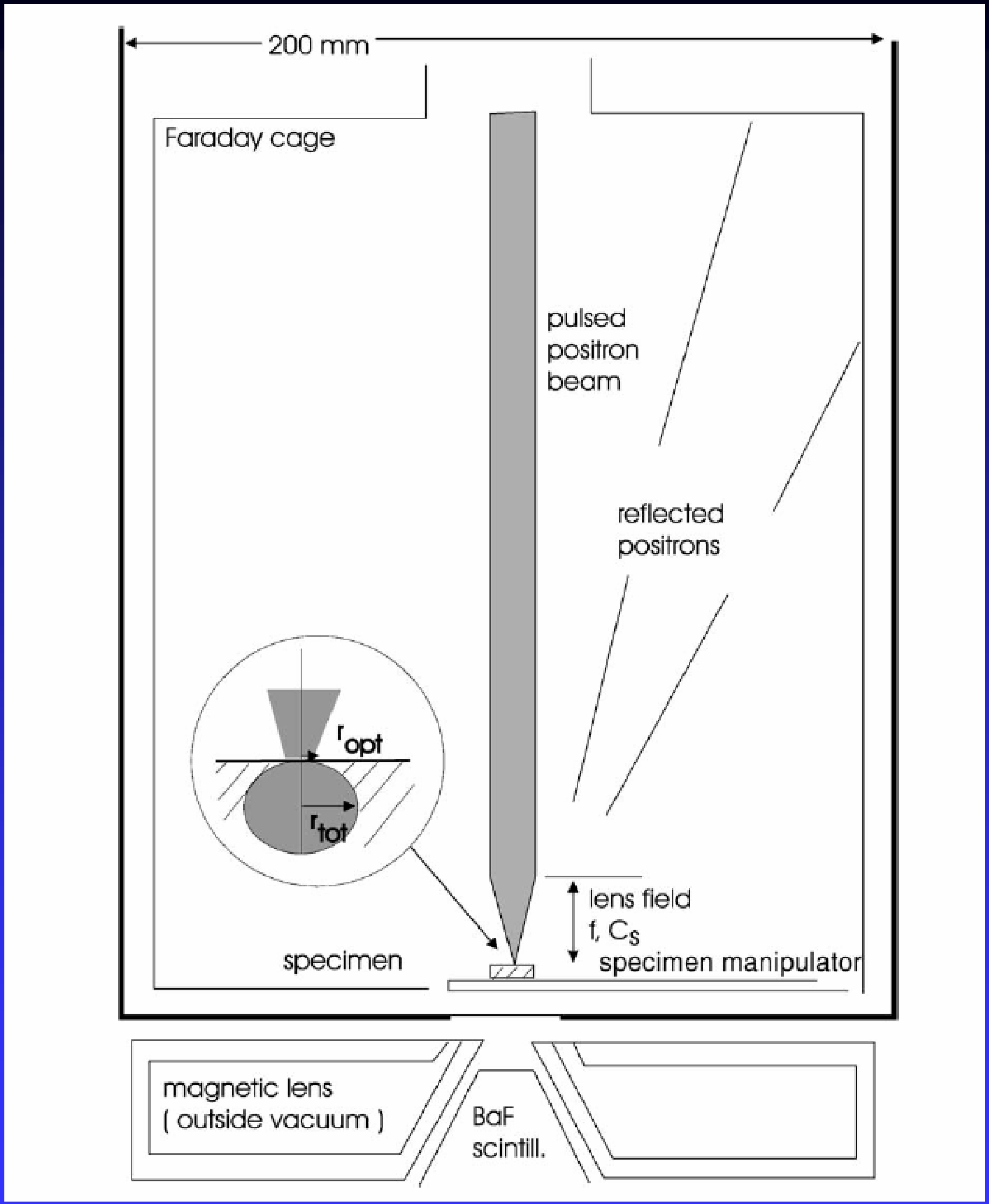

Specimen chamber of the München SPM.

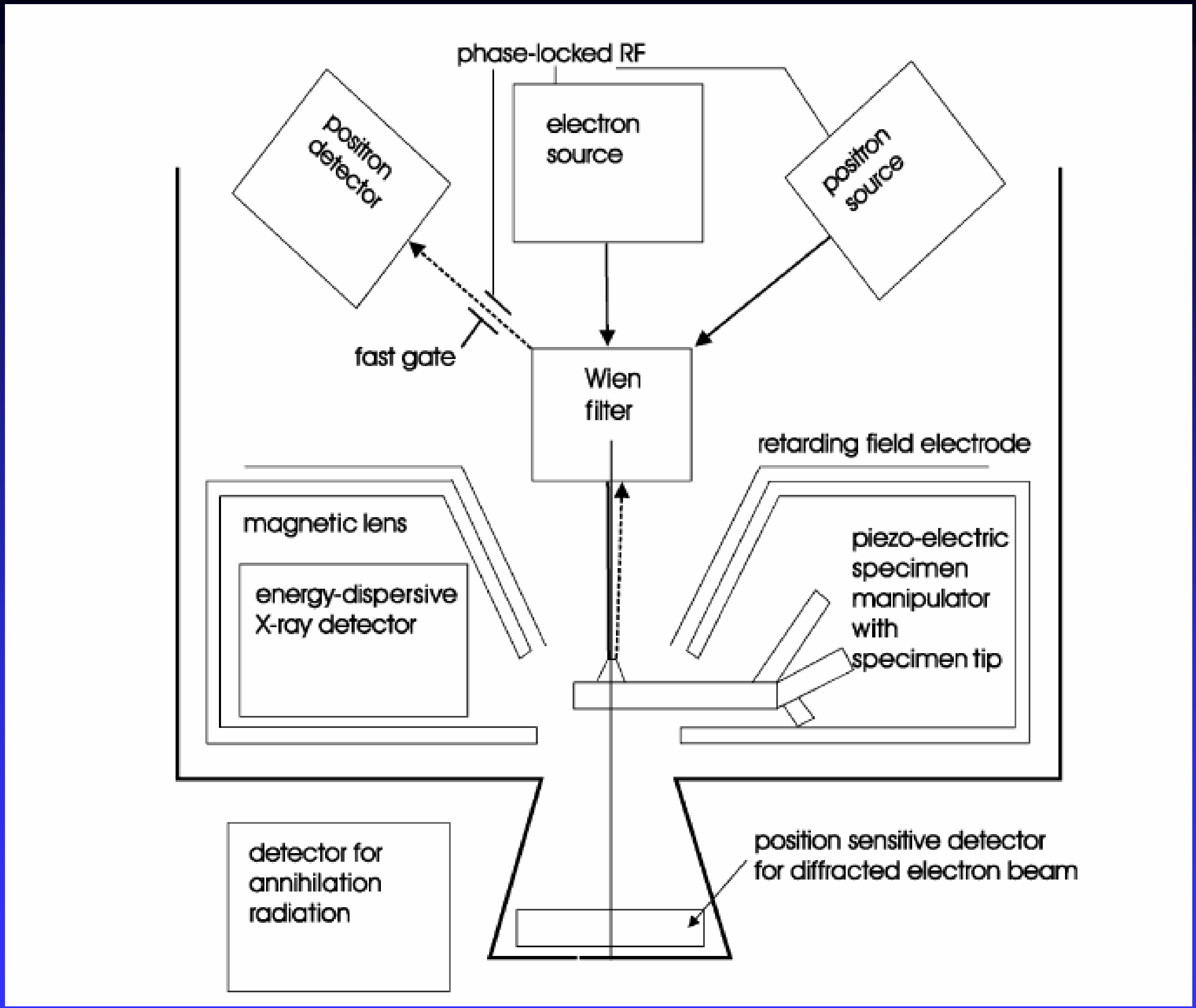

Schematics of a dual beam microscope for defect imaging at nanometer resolution.

正电子显微镜

- 1983年Hulett等人根据Mueller发展的场发射电子显微镜(FEEM)提出了正电子再发射显微镜(PRM)，它具有比FEEM更多的优点。
- PRM可以研究增强亮度膜本身的结构，因为通过正电子捕获和湮没，可以对膜的空位和位错进行显像。
- PRM可以以单原子态的区域显像空位，这是其它方法不可比拟的；
- 其次，由于正电子发射的能量与空位电位在相同的量值，PRM图像可以突出显示化学差异，如样品的不同区域化学成分的不同，导致Ps形成截面不同，Ps形成大的区域其显像图象强度变弱。

正电子显微镜种类

- **Transmission electron microscope (TEM)**
- **Positron reemission microscope (PRM)**
- **Scanning positron microscope (SPM).**

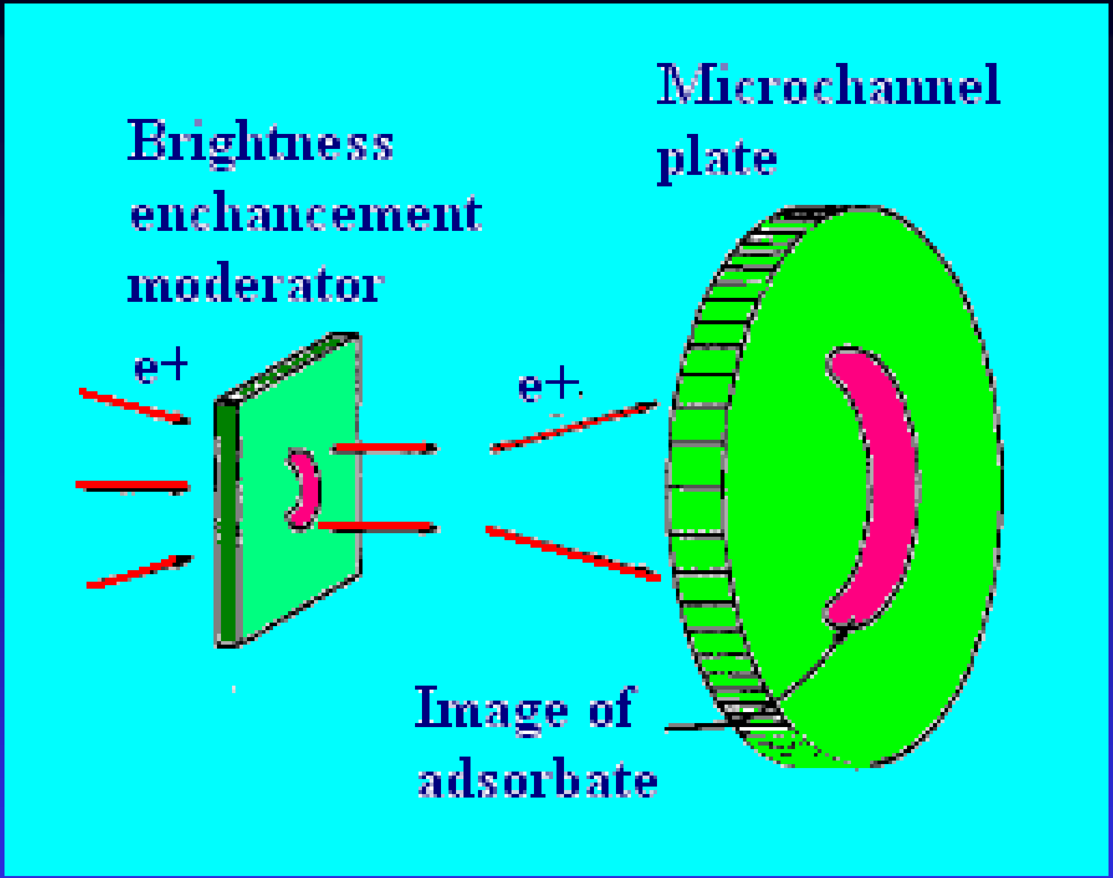

Schematic showing the positron re-emission microscope principle.A fraction of the positrons implanted in the sample thermalise, diffuse to the surface and are re-emitted, and a magnified image is formed. Contours of adsorbates on the surface will also be imaged by the low-energy positrons.

First Results of a Positron Microscope

James Van House and Arthur Rich
University of Michigan, Department of Physics, Ann Arbor, Michigan 48109
(Received 14 July 1987)

TEM

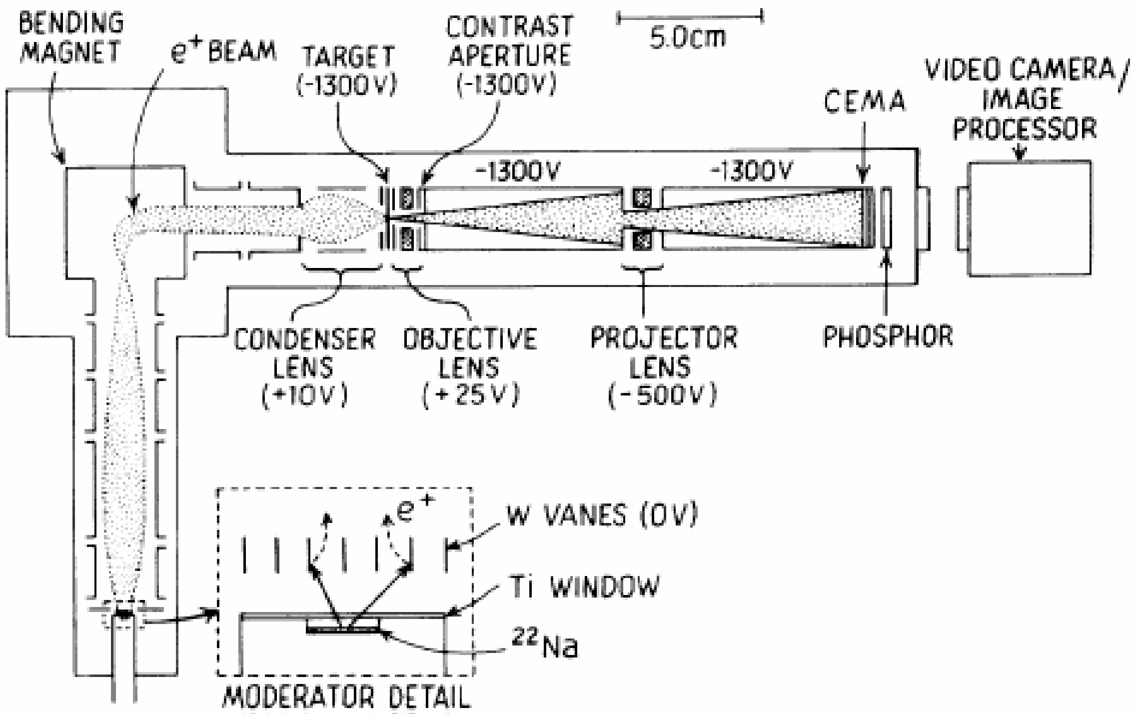

FIG. 1. The transmission positron microscope. Positrons (e^+) from a ^{22}Na source are incident on a W vane moderator. The reemitted slow e^+ are focused into a beam which is transported to a bending magnet. The beam is subsequently incident on a low-aberration condenser lens which focuses it onto the target.

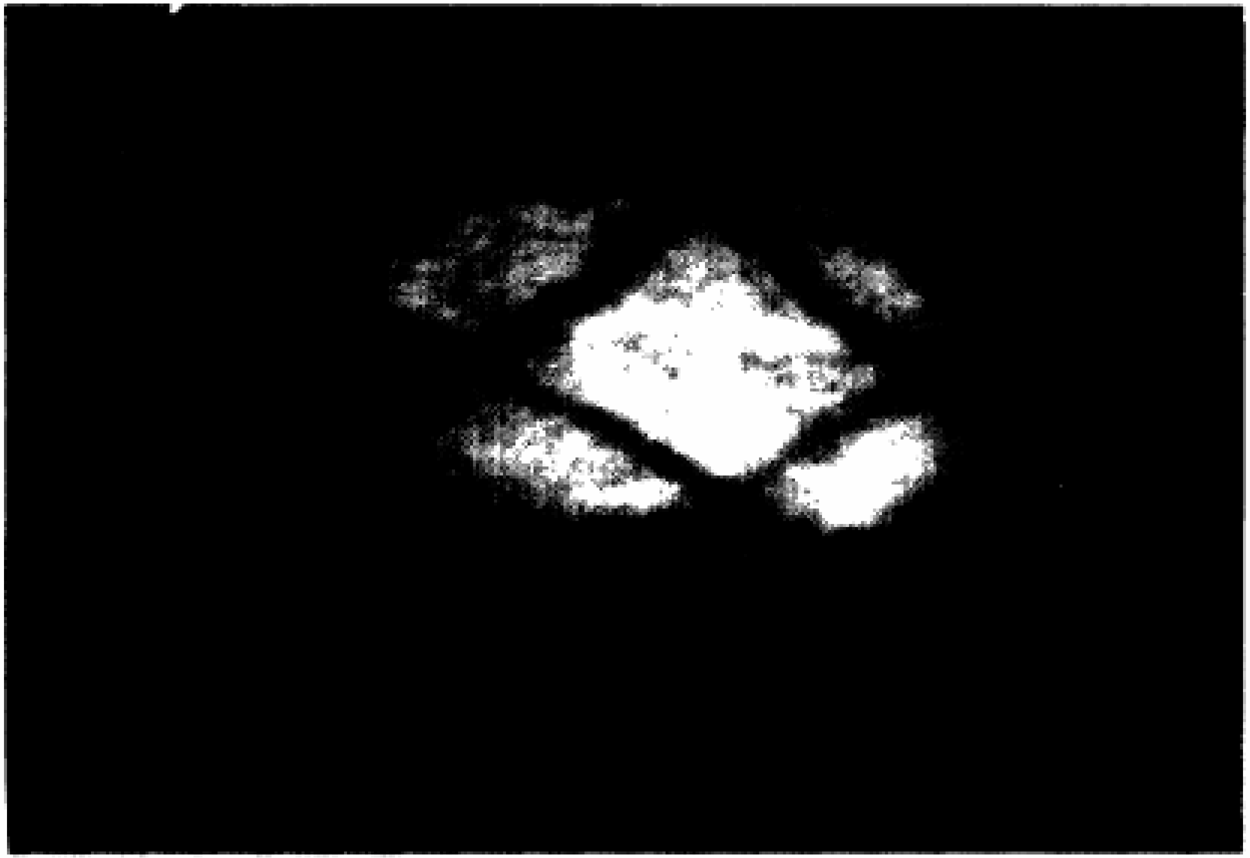

FIG. 3. The first TPM picture. The photograph is a VYNS film, taken at 55 times magnification. The image was obtained after adjustment of the objective lens voltage until the filamentary structure of the unbroken areas of the foil between the grid wires (spacing 250 μm) was in focus. The brightest areas are tears in the fragile VYNS film.

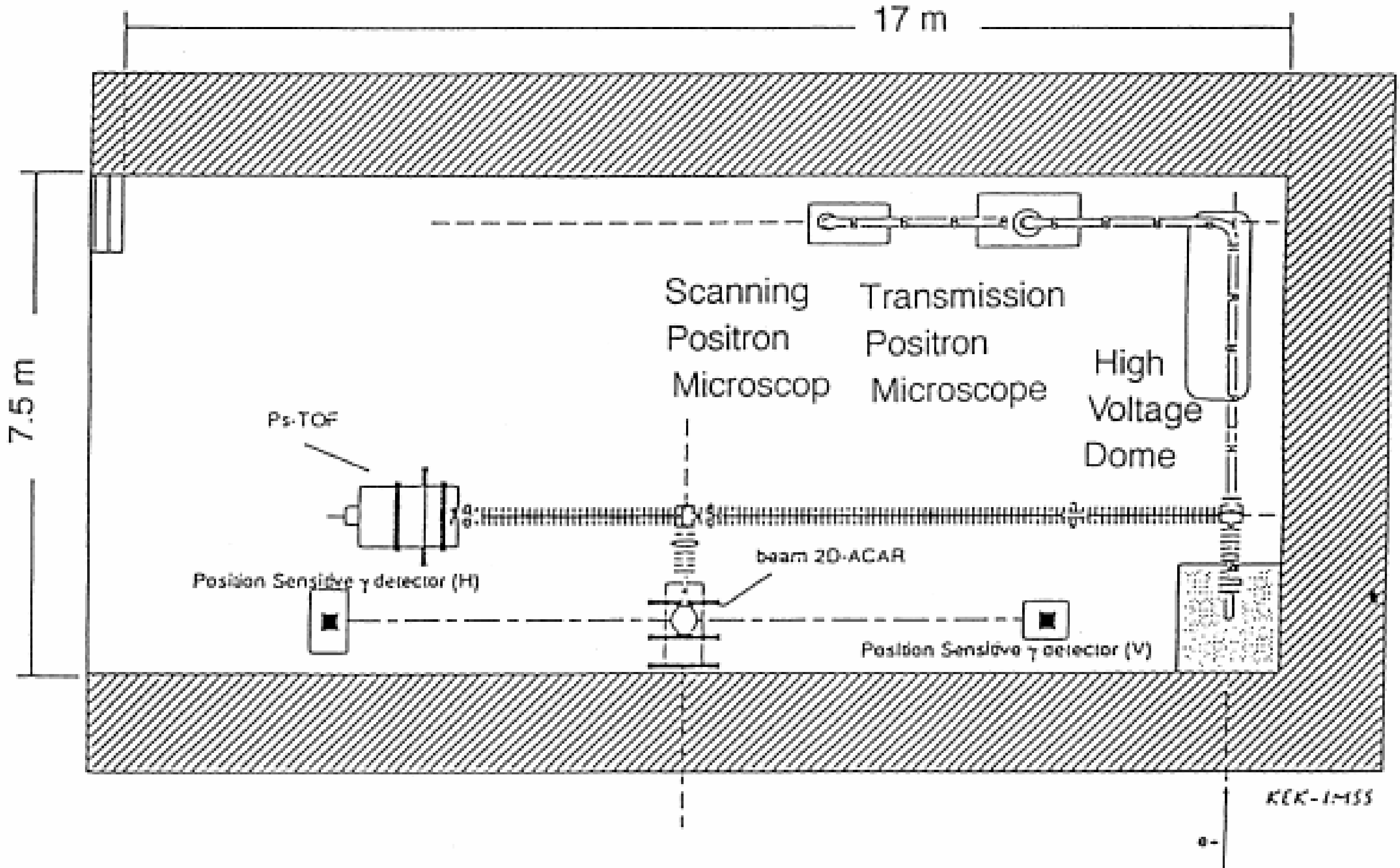

Fig. 1. Layout of transmission positron microscope and scanning positron microscope at KEK.

PRM

The positron reemission microscope

The PRM offers potential resolutions below 10 angstroms, and should be particularly useful in studies of surfaces and thin overlayers, as well as in biological applications

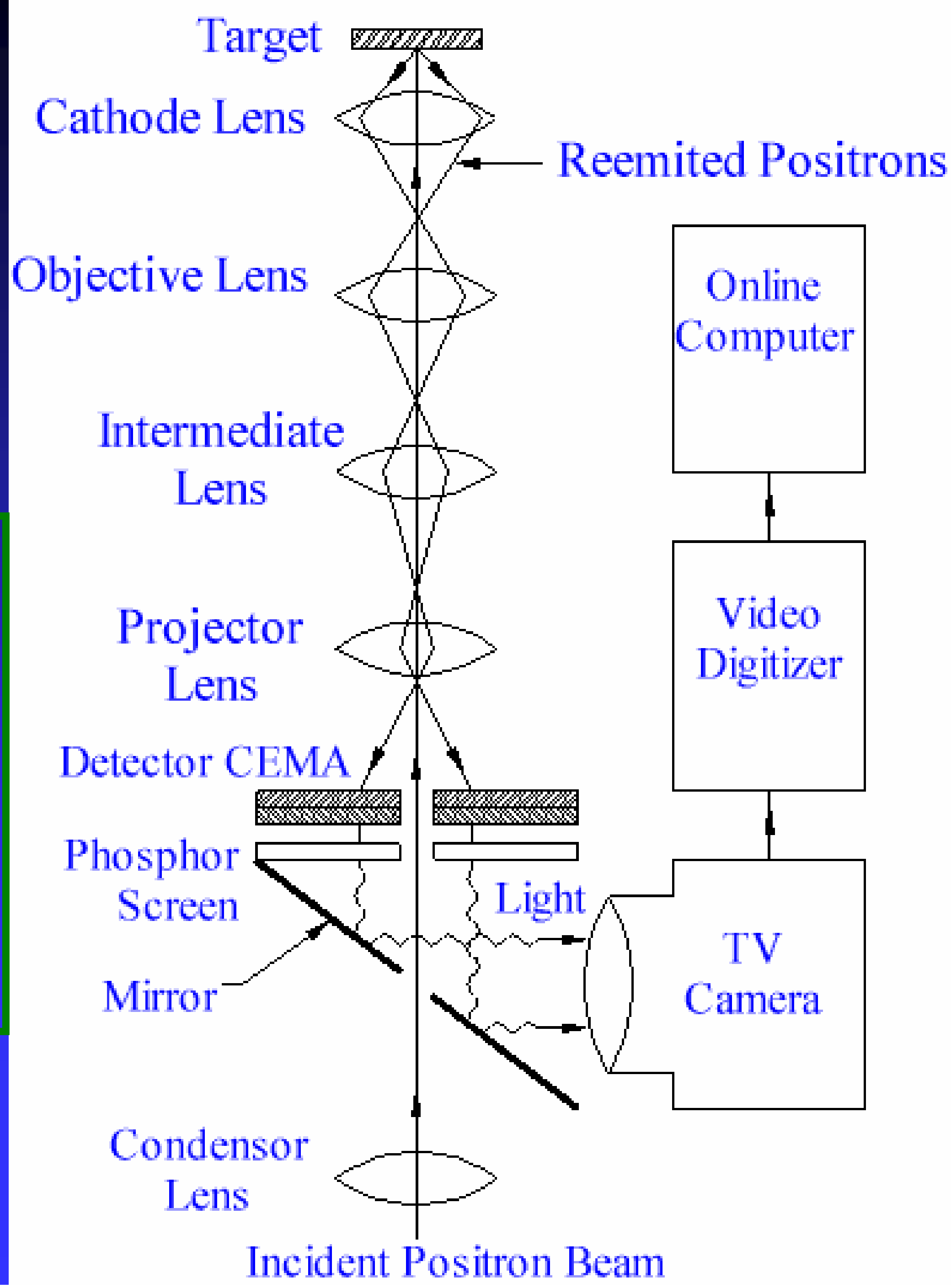

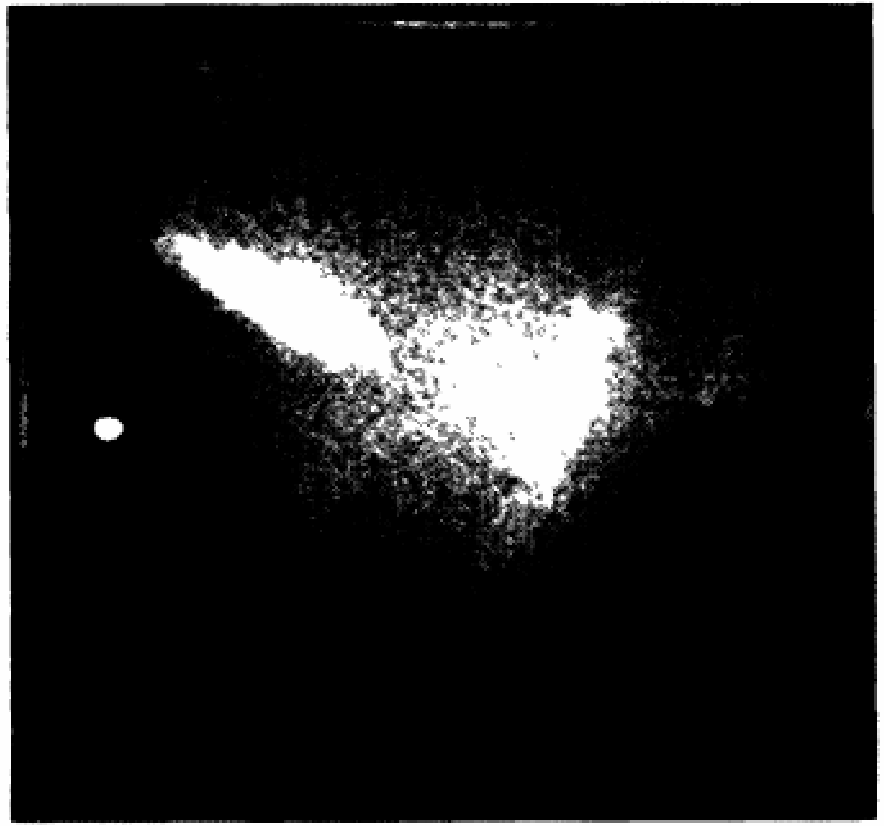

(b)

FIG. 2. (a) 1150× PRM image of the region of interest outlined in Fig. 1. Arrows indicate the path of integration used (see Fig. 3) to determine the sharpness of the edges of some of the features. (b) The same region following 5 min of electron bombardment from behind. In both cases, the images were obtained over a 14-h period with the whitest areas representing 40 counts/pixel in (a) and 65 counts/pixel in (b).

- **Brandes**等人对**PRM**成像进行了细致的研究．他测量**Ni**膜在未退火和退火后的显像，发现未退火显像中灰度较深区（即来自近表面缺陷）在退火后的显像中已消失。他们获得的分辨为**300±100nm**．为了提高分辨率，除需提高场强外，微道板斑点上正电子计数需达到7×10^{9}个，这就需要提高束流的强度。

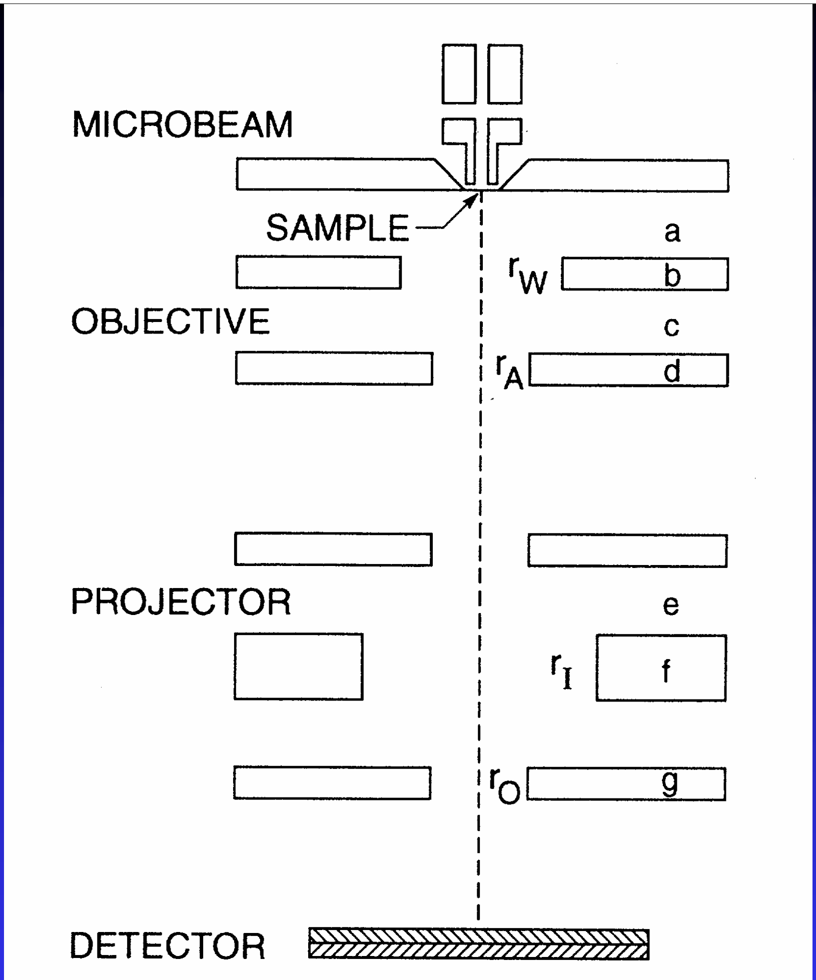

FIG. 1. PRM schematic showing lens configuration and detector. 1-keV positrons from the brightness-enhanced positron beam are focused by the microbeam lens onto the sample. A magnified real image of the reemitted, thermal energy positrons is formed by the microscope objective and projector at the surface of the detector. The dimensions of the objective lens are

- 反射型PRM可用来研究较厚样品的表面结构。Michigen大学研究组建立了一台放大倍数56，位置分辨为2.3μm的反射型PRM。这种类型的PRM还可研究薄膜在生长过程中的动力学，显像膜生长区的图象，并用再发射正电子能谱确定其成分。
- 透射型PRM的图象与透射电子显微镜类似，其优点是可以确定晶体晶格位置的不纯原子是否被替换或形成空隙，而透射电子显微镜却做不到这一点。

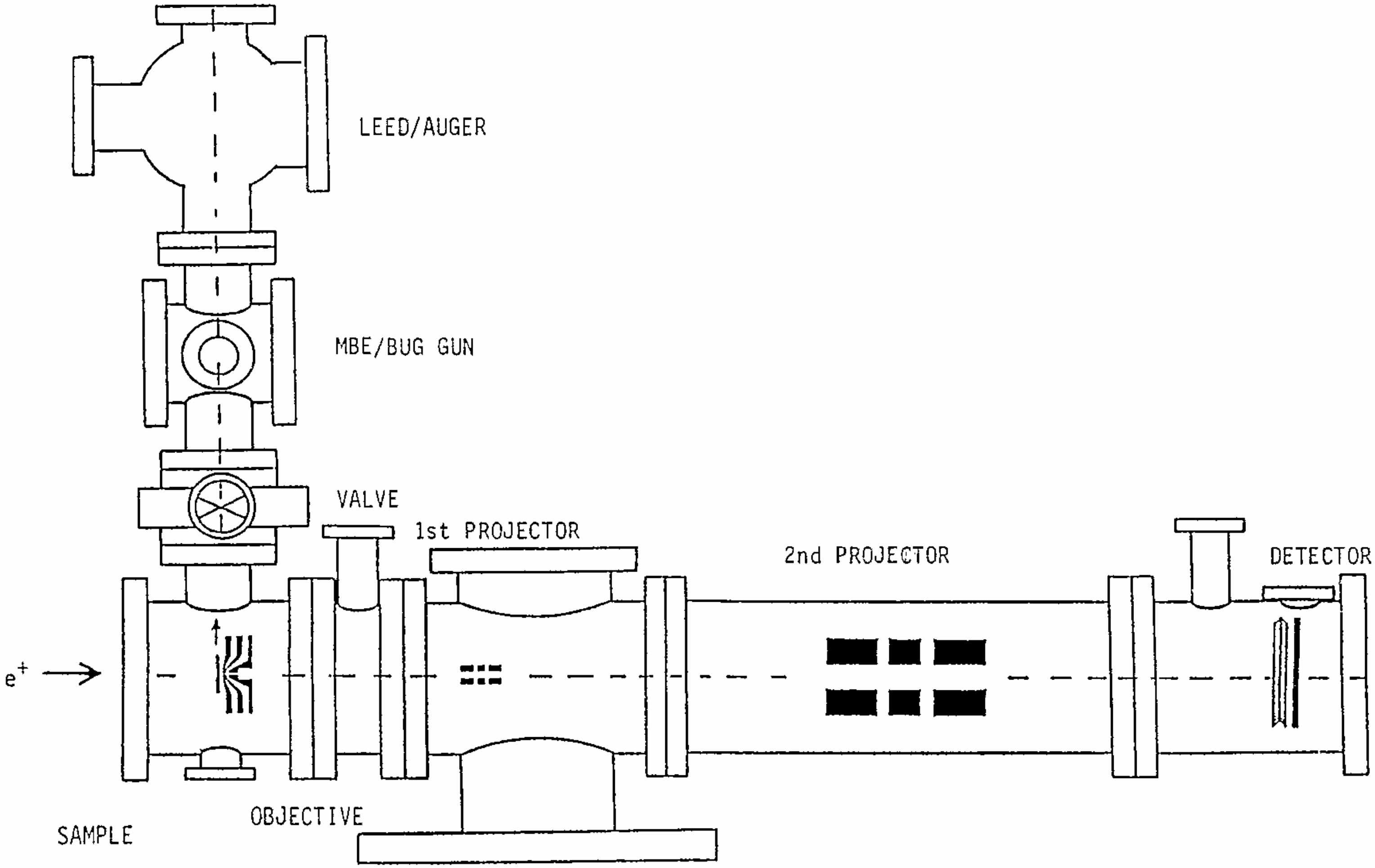

Fig. 1. Brandeis second generation PRM. In addition to the PRM optical components (objective, 1st and 2nd projector lenses, and MCP detector), some of the in situ sample diagnostic and preparation tools are also shown. The ''bug gun'' is for electrospray deposition of small biological structures.

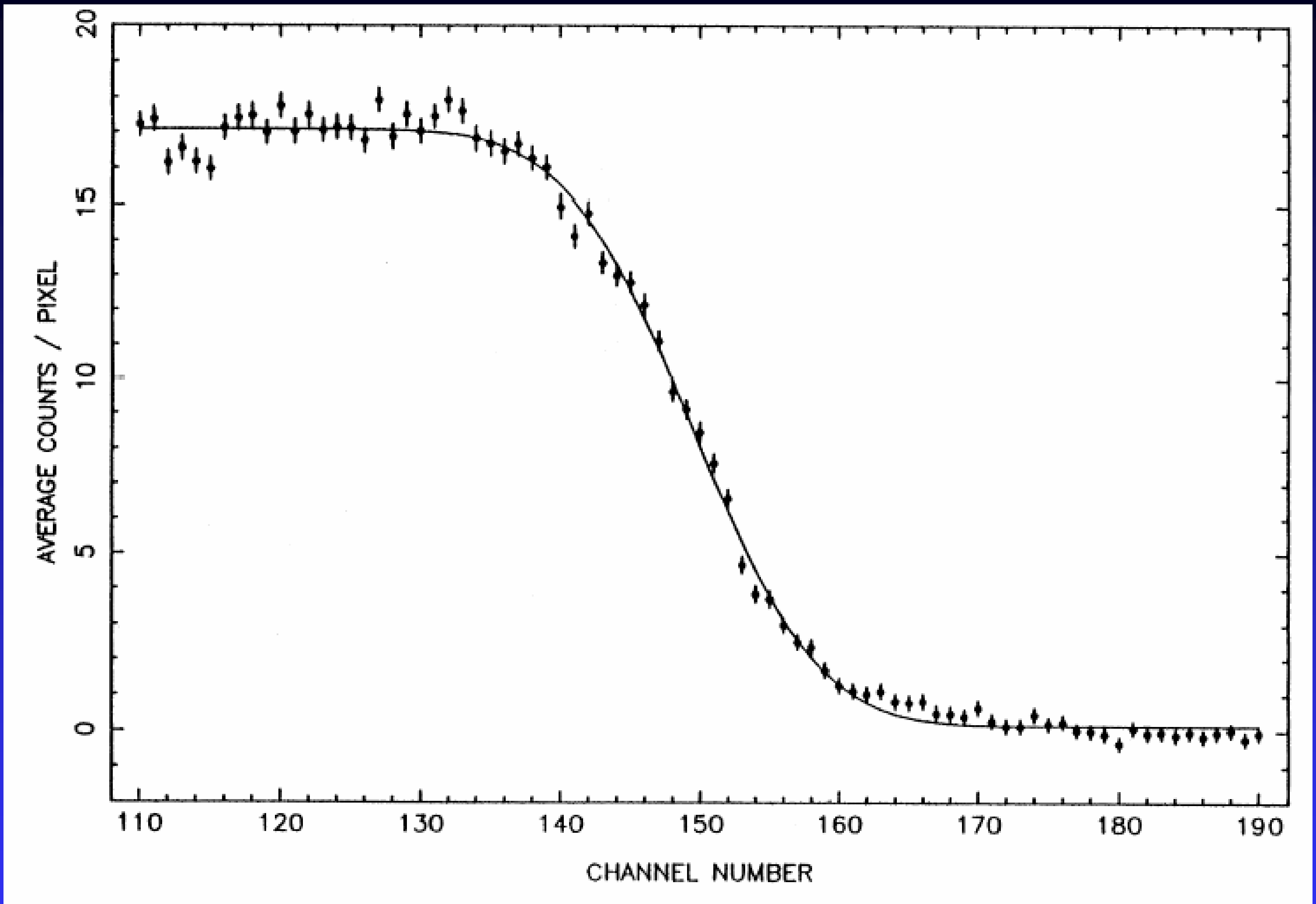

FIG. 5. A 100 pixel wide cut through the magnified (4400×) PRM image of the compound sample shown in Fig. 4(b). The solid line is the emission profile generated by fitting Eq. (5) to the data [$C_1=0.1(3)$, $C_2=0.95(2)$, $x'=149(1)$, $\sigma=7.1(2)$, and $\chi^2/\nu=176/77$]. One channel equals 355 Å.

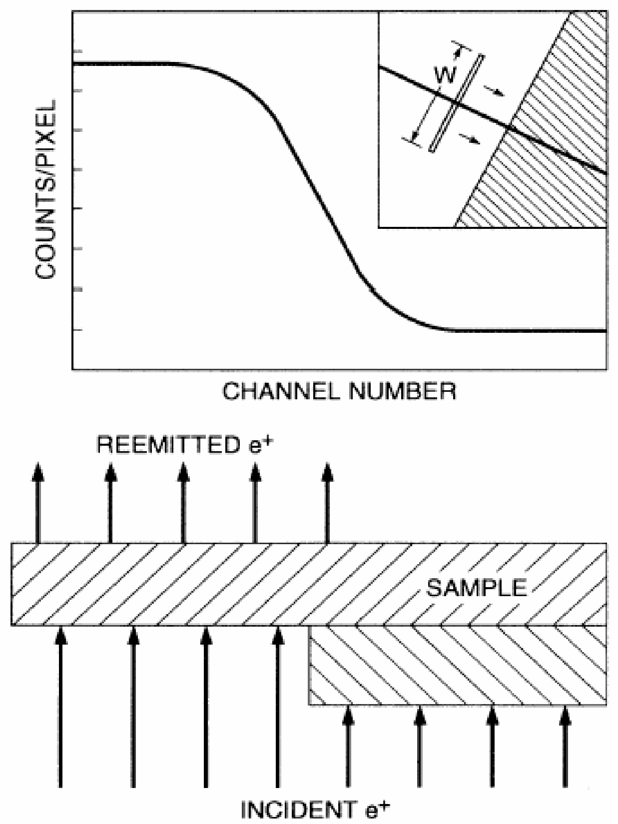

FIG. 3. Schematic of double-layer sample used to investigate the positron implantation and diffusion process. Positrons implanted in the underlying right half of the sample have twice as far to diffuse and will be trapped at the interface if they diffuse that far. An example of a positron emission curve for this double-layer sample is shown above the sample drawing. The inset schematically shows the cutting procedure; the width of the cuts w is indicated.

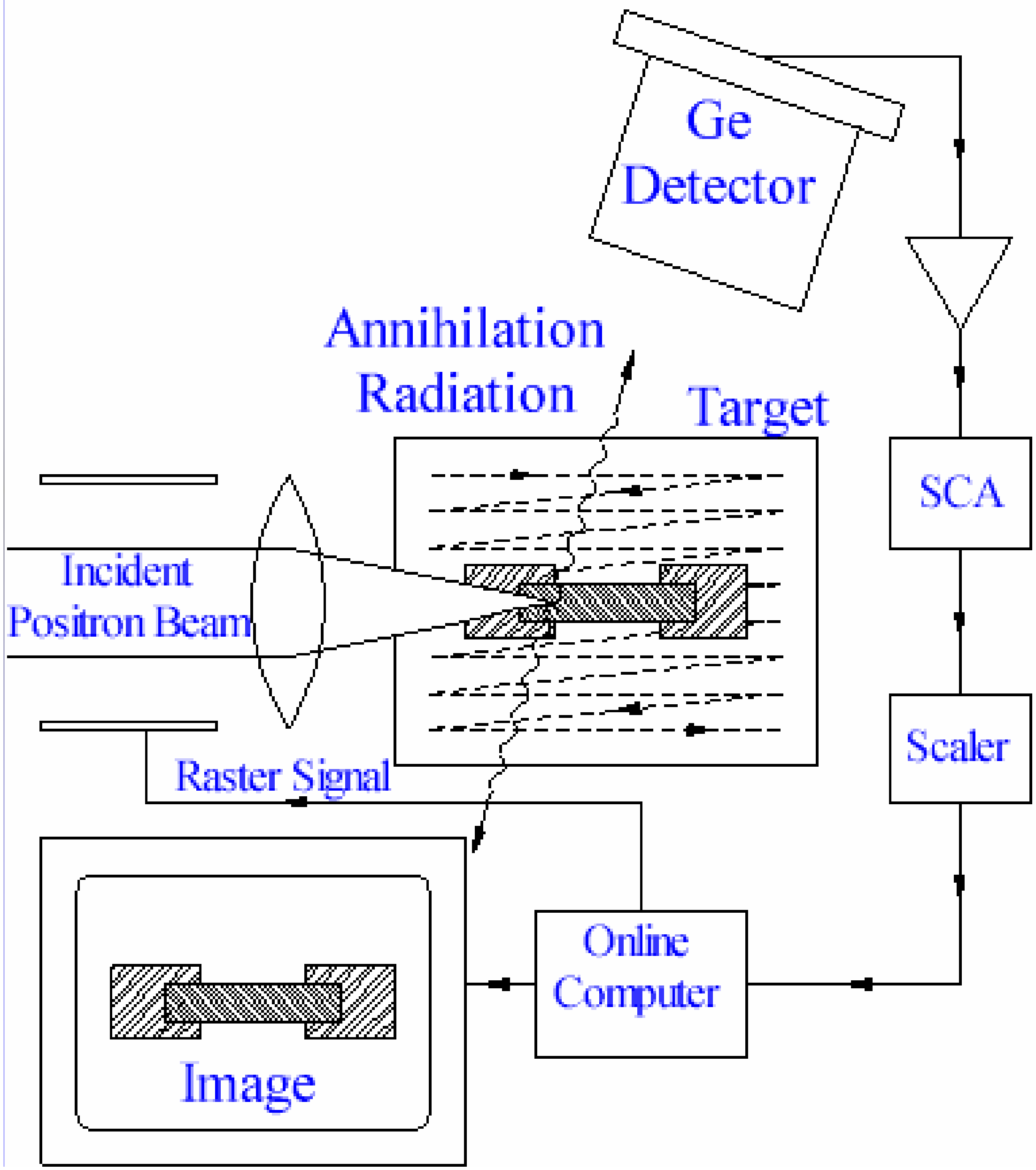

SPM

- The advantages of the SPM are the wide variety of signals available and the ability to examine target properties at various depths from the surface.

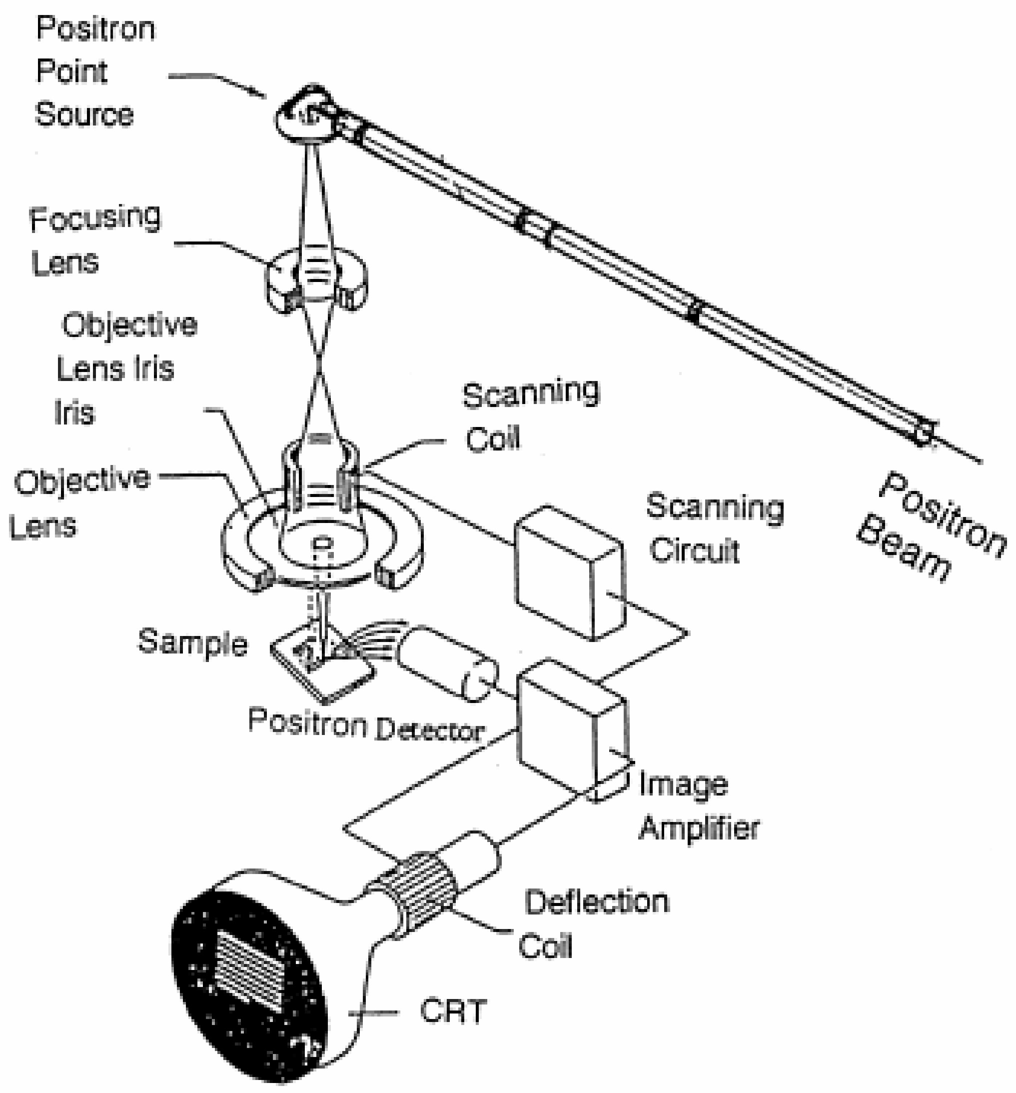

Fig. 5. Scanning positron microscope.

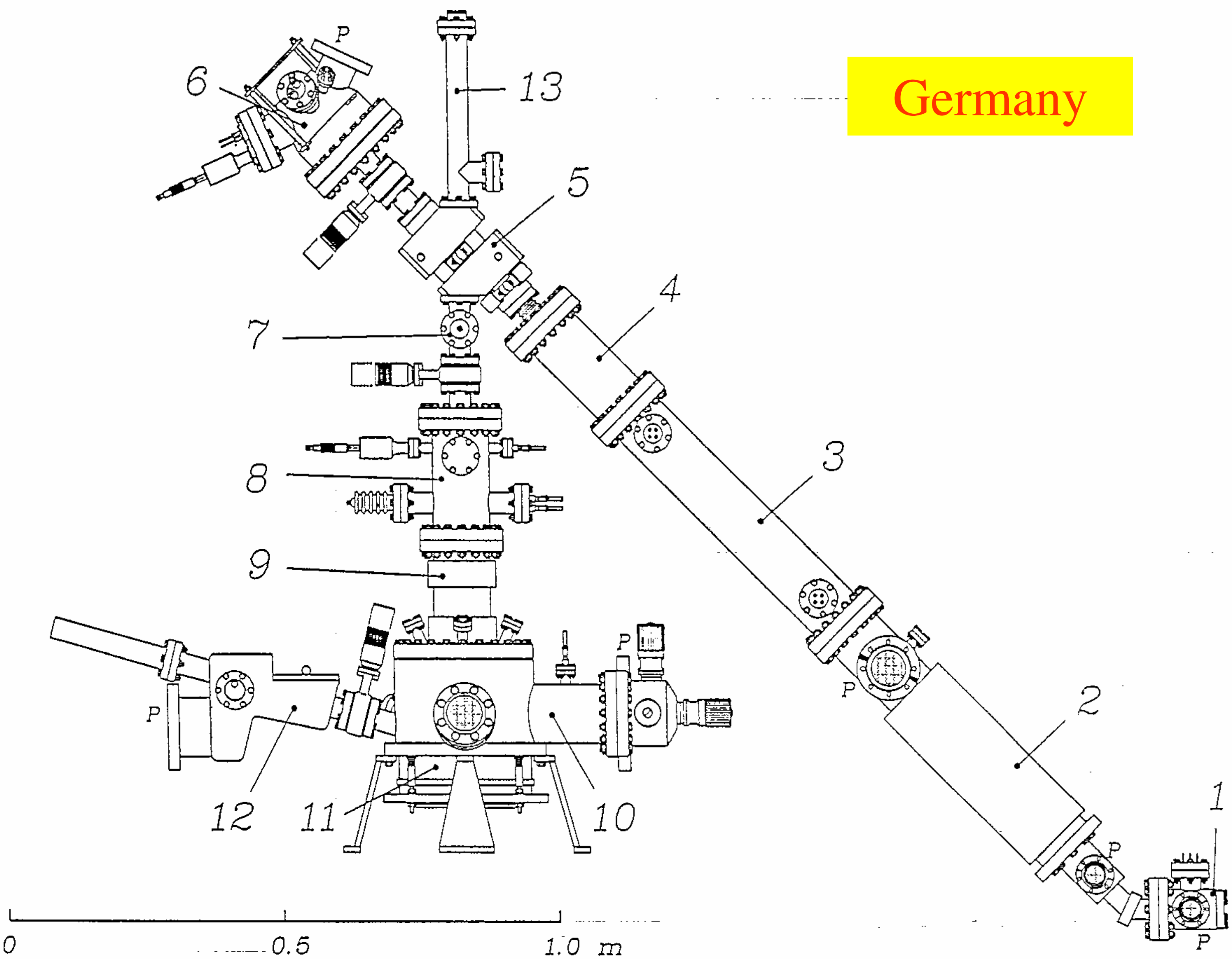

Fig. 1. Setup of the Scanning Positron Microscope: (1) radioactive source and moderator; (2) drift tube for pulse forming (sawtooth); (3) first buncher; (4) accelerator; (5) beam switch; (6) remoderator unit; (7) second buncher; (8) main accelerator (0.5–30 keV); (9) scanning coils; (10) specimen chamber with manipulator; (11) probe forming lens with detector in the central bore; (12) load lock; (13) electron gun; P: pumping ports. (Some components are rotated into the plane of the drawing).

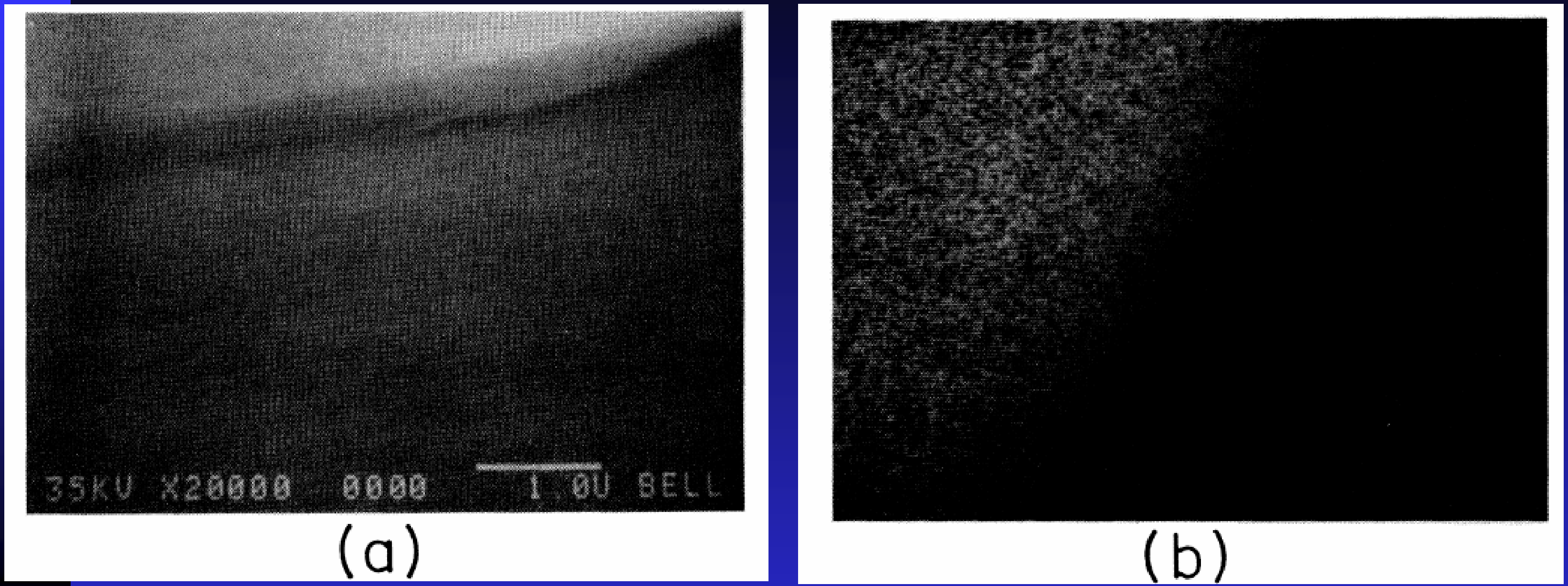

FIG. 4. Scanning-electron-microscope image of the compound sample. The image shows a region where the two foils appear to be in good contact and a region where they are separated. The white bar in the bottom right of the image is 1 μm in length. (b) PRM image ($M = 4400\times$) of the compound sample boundary. The positron microbeam ($E = 5$ keV) has been shifted to straddle the boundary. The image acquisition time was 24.6 h.

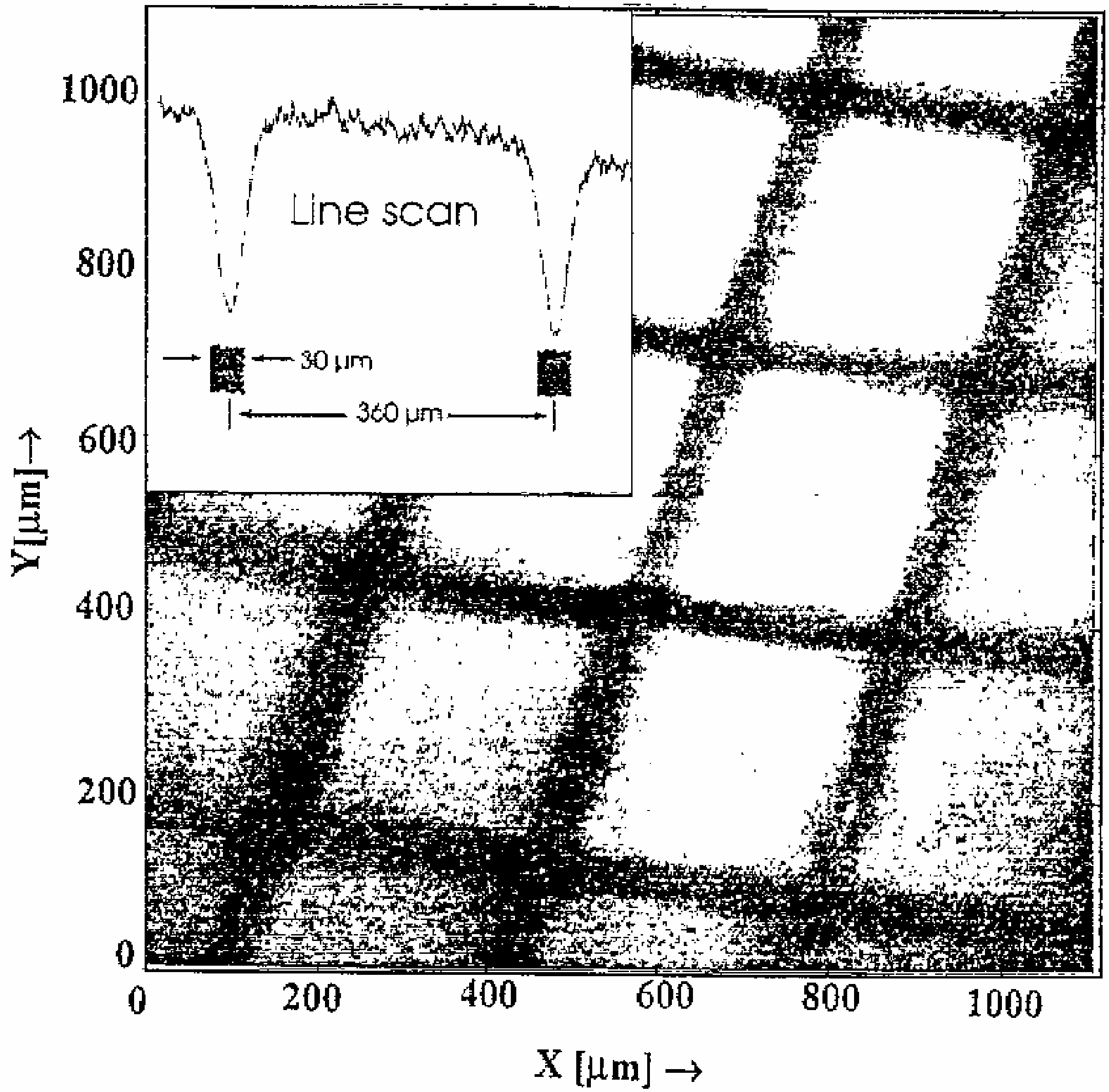

Fig. 3. Positron image of a gold mesh of 360 µm spacing and 30 µm bar width, placed at the remoderator position, obtained with the primary beam.

Depth defect profiling with positron microbeam

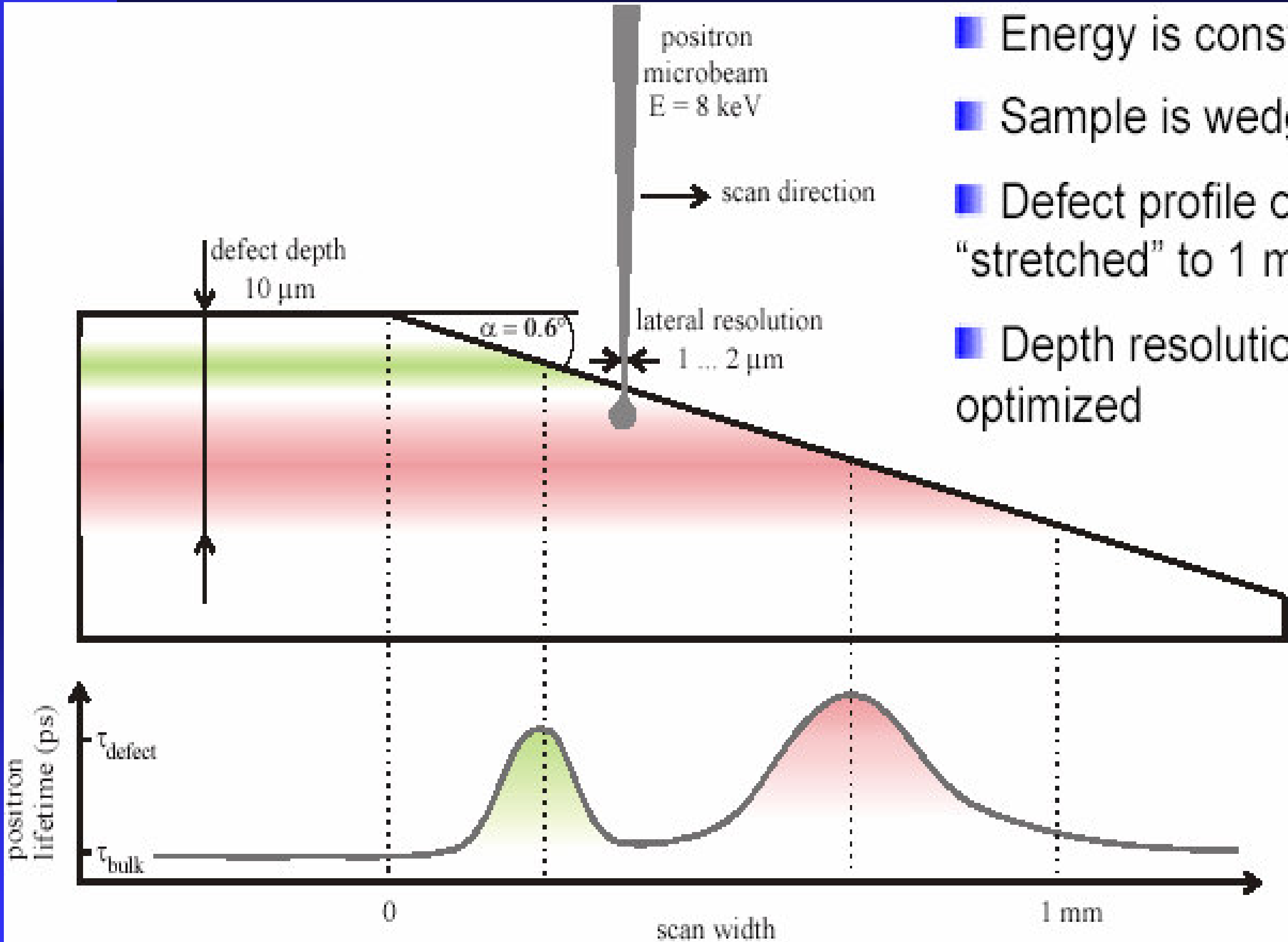

- Energy is constant at 8 keV
- Sample is wedged at 0.6°
- Defect profile of 10 µm is "stretched" to 1 mm
- Depth resolution can be optimized

- First time used to study Rp/2 effect in Si after self-implantation

Defects in high-energy self-implanted Si – The $R_p/2$ effect

- after high-energy (3.5 MeV) self-implantation of Si (5×10^{15} cm^{-2}) and RTA annealing (900°C, 30s): two new gettering zones appear at R_p an $R_p/2$ (R_p – projected range of Si^+)
- visible by SIMS profiling after intentional Cu contamination

TEM image by P. Werner, MPI Halle

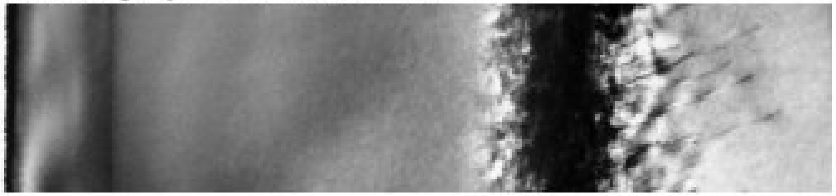

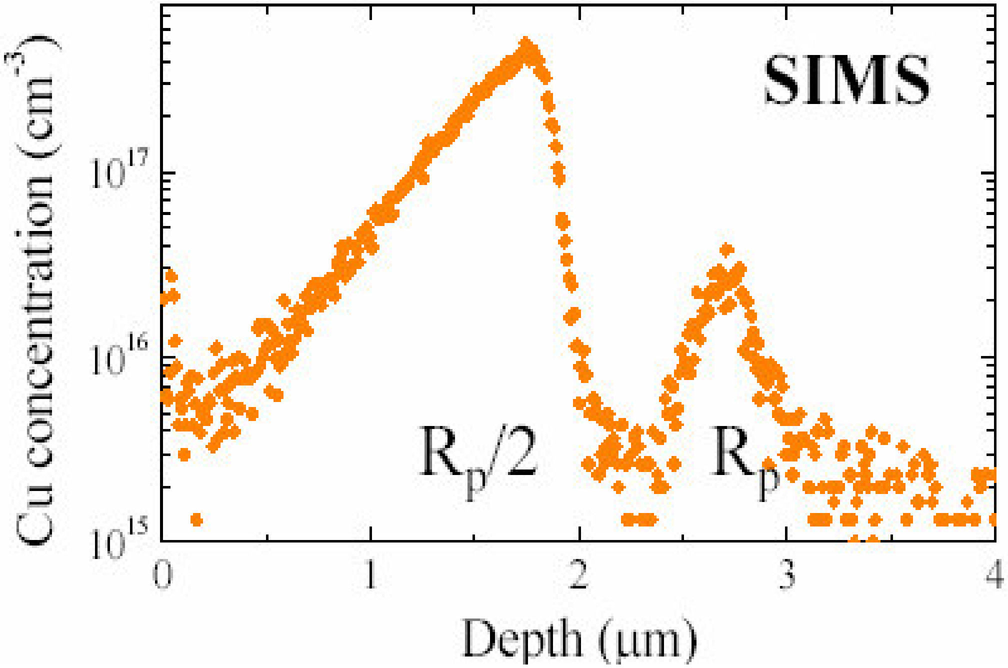

- at R_p: gettering by interstitial-type dislocation loops (formed by excess interstitials during RTA)
- no defects visible by TEM at $R_p/2$
- **What type are these defects?**

Interstitial type [3,4]

Vacancy type [1,2]

[1] R. A. Brown, et al., J. Appl. Phys. **84** (1998) 2459
[2] J. Xu, et al., Appl. Phys. Lett. **74** (1999) 997
[3] R. Kögler, et al., Appl. Phys. Lett. **75** (1999) 1279
[4] A. Peeva, et al., NIM B **161** (2000) 1090

$R_p/2$ effect investigation

- Both defect regions are gut visible
  - vacancy clusters with increasing concentration up to 2 μm ($R_p/2$)
  - in R_p region: lifetime τ_2=320 ps; open volume corresponds to di-vacancy; defects are stabilized by dislocation loops
- very good agreement with the SIMS profile of in-diffused Cu

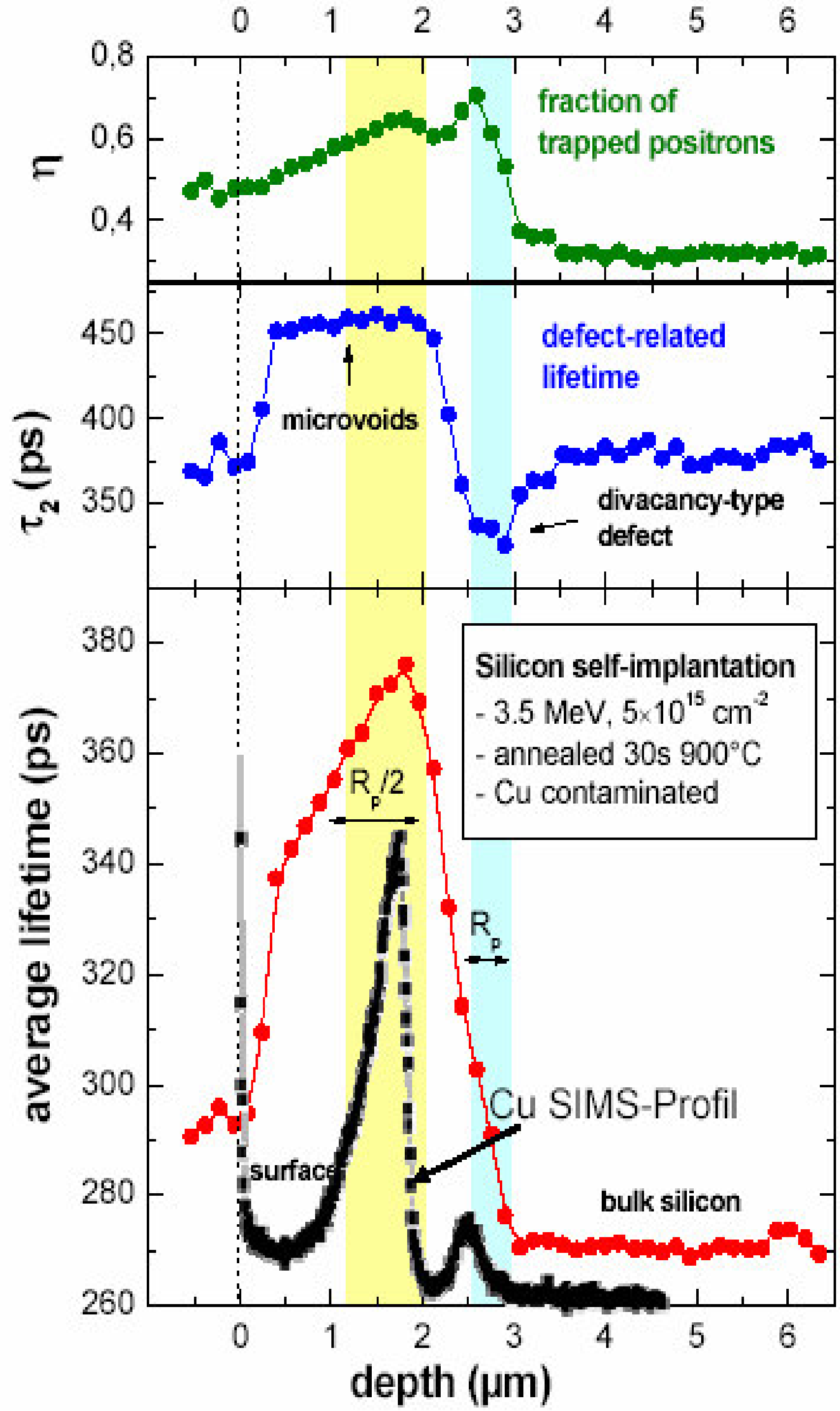

Positron lifetime image of fatigue crack with SPM

The Munchen scanning positron microscope (SPM)

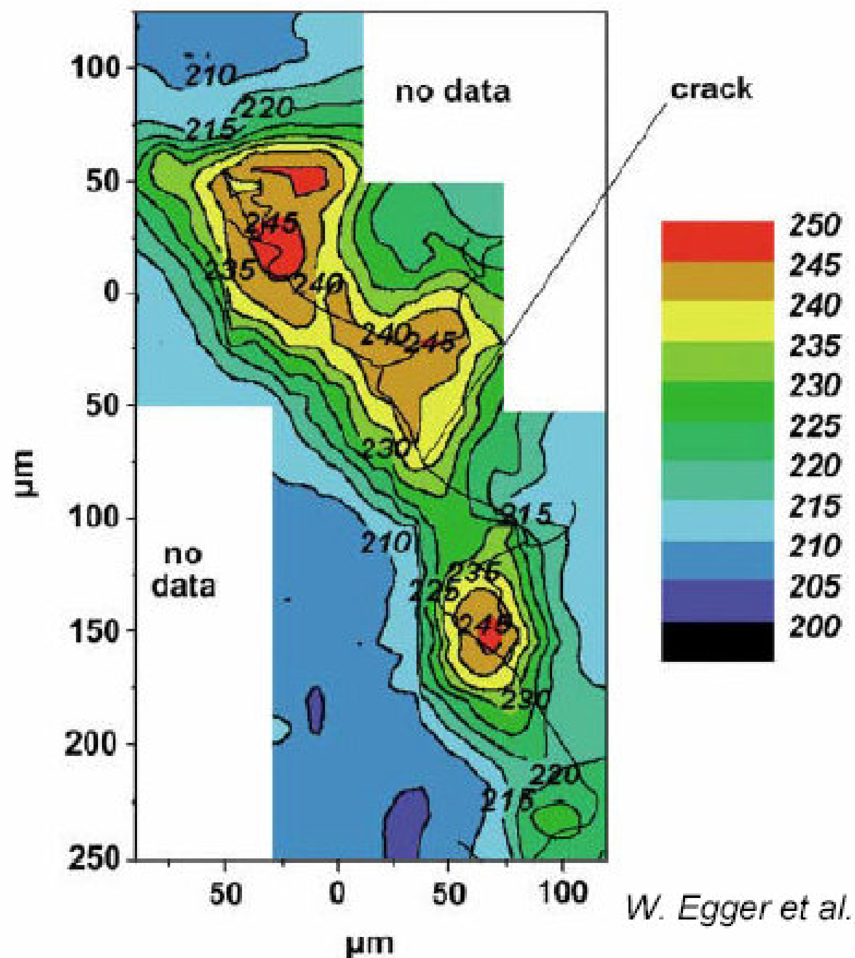

- Lifetime measurements around a fatigue crack created in technical copper was measured
- e^+ Energy = 16 keV
- spatial resolution about 5 μm
- two lifetimes were observed:
  - 190 ps – dislocations
  - 360-420 ps – within 40 μm from the crack – vacancy clusters

↓

have been for the first time microscopically observed

W. Egger et al., Applied Surface Sci. 194 (2002)

Fig. 1. Fatigue crack in copper and map of mean positron lifetime[ps] at 16 keV positron implantation energy.

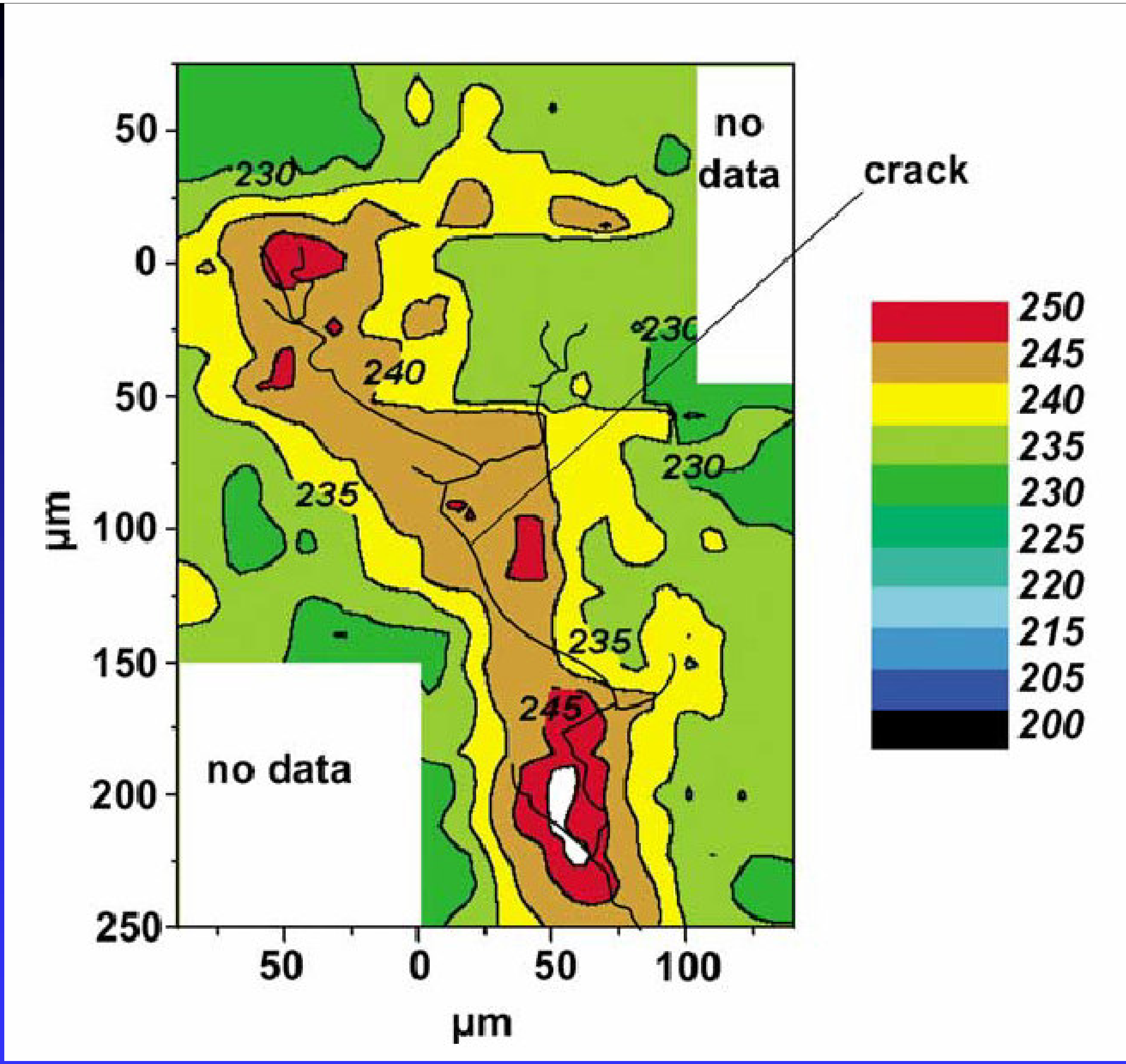

Fig. 2. Fatigue crack in copper and map of mean positron lifetime [ps] at 5 keV positron implantation energy.

VOLUME 87, NUMBER 6 PHYSICAL REVIEW LETTERS 6 AUGUST 2001

Lifetime Measurements with a Scanning Positron Microscope

A. David, G. Kögel, P. Sperr, and W. Triftshäuser
Institut für Nukleare Festkörperphysik, Universität der Bundeswehr München, 85577 Neubiberg, Germany
(Received 26 February 2001; published 19 July 2001)

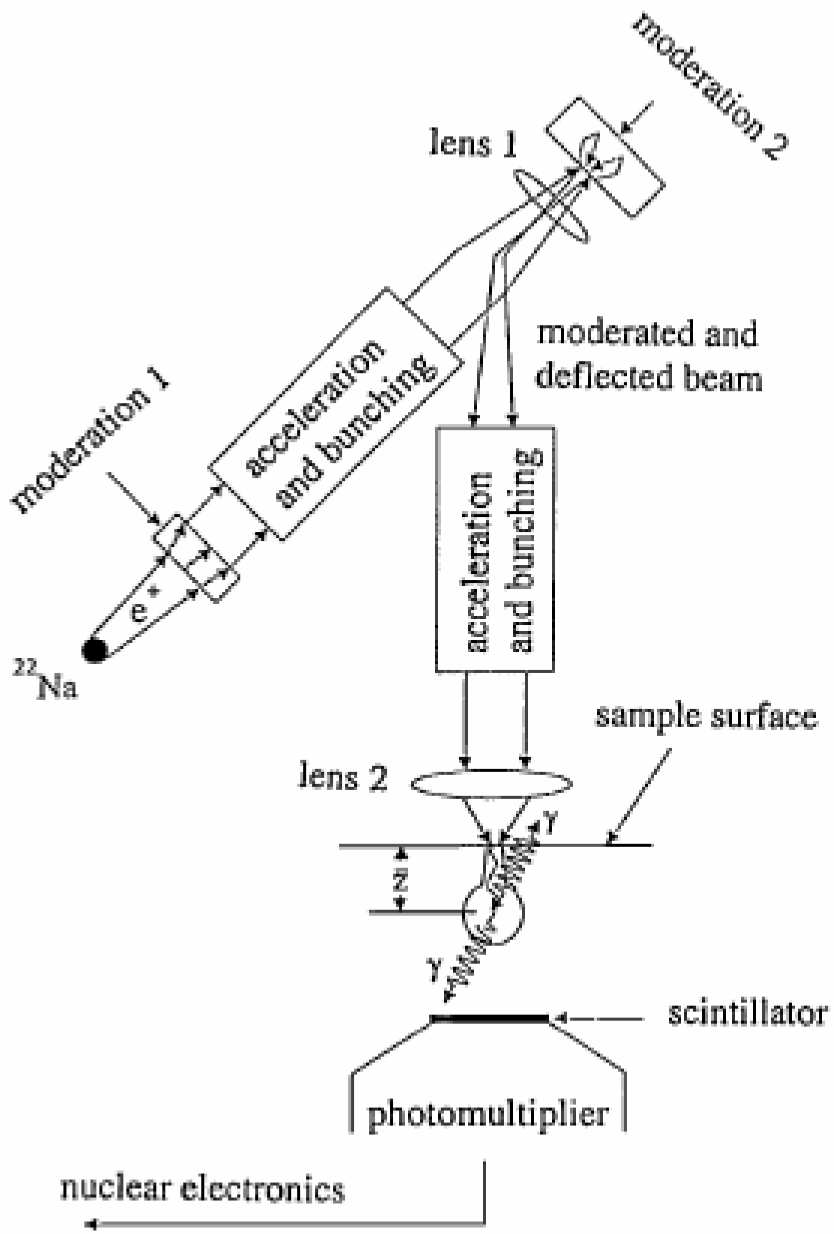

components of the scanning positron microscope

Positron spot size is less than 20 mm the positrons are reemitted with a measured efficiency of 23 6 2%.

Scanning positron microscope

- Variable energy micro-beam of monoenergetic positrons
- Lateral resolution of 2 μm is achieved
- Lifetime measurements at different beam energies are possible

↓

- Principle disadvantage: broad positron implantation profile at high energies

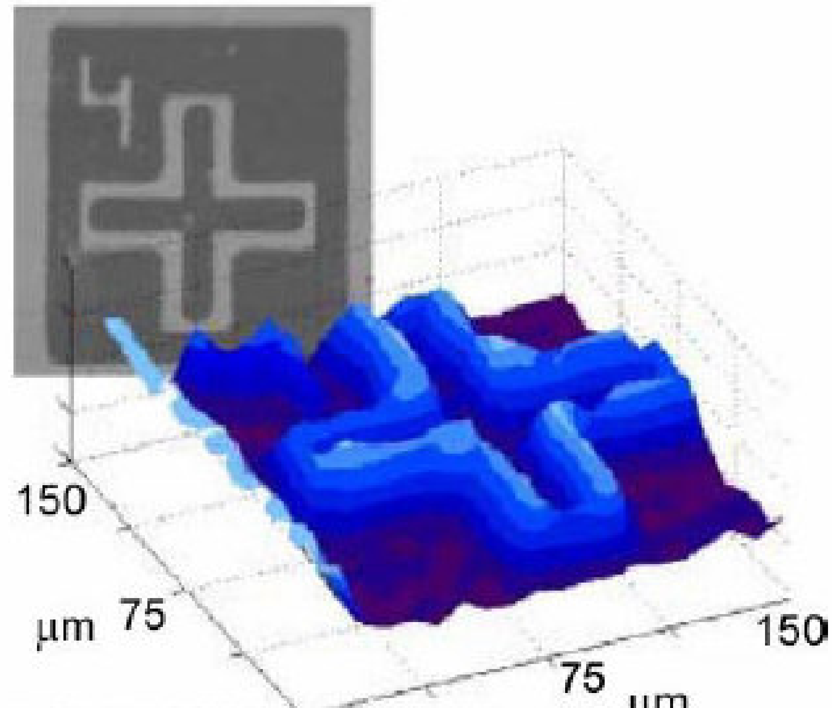

Phys. Rev. Lett. 87, 067402 (2001)

Electron and positron beam image of the surface of a test chip. Light area is SiO_2, dark area is platinum

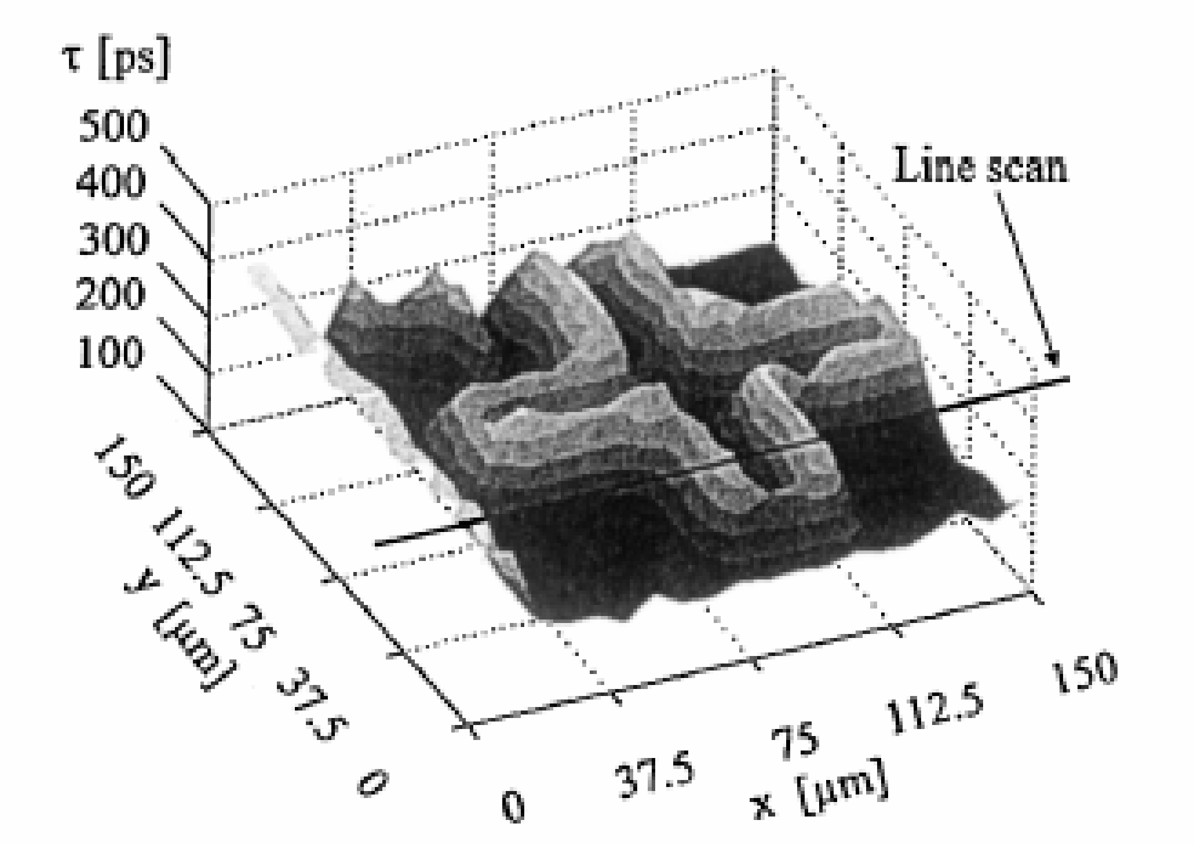

Positron beam image of the same test chip as of Fig. 2. The mean positron lifetime is plotted as a function of the *x* and *y* dimensions. The coordinates of the line scan are indicated. The positron energy is 8 keV.

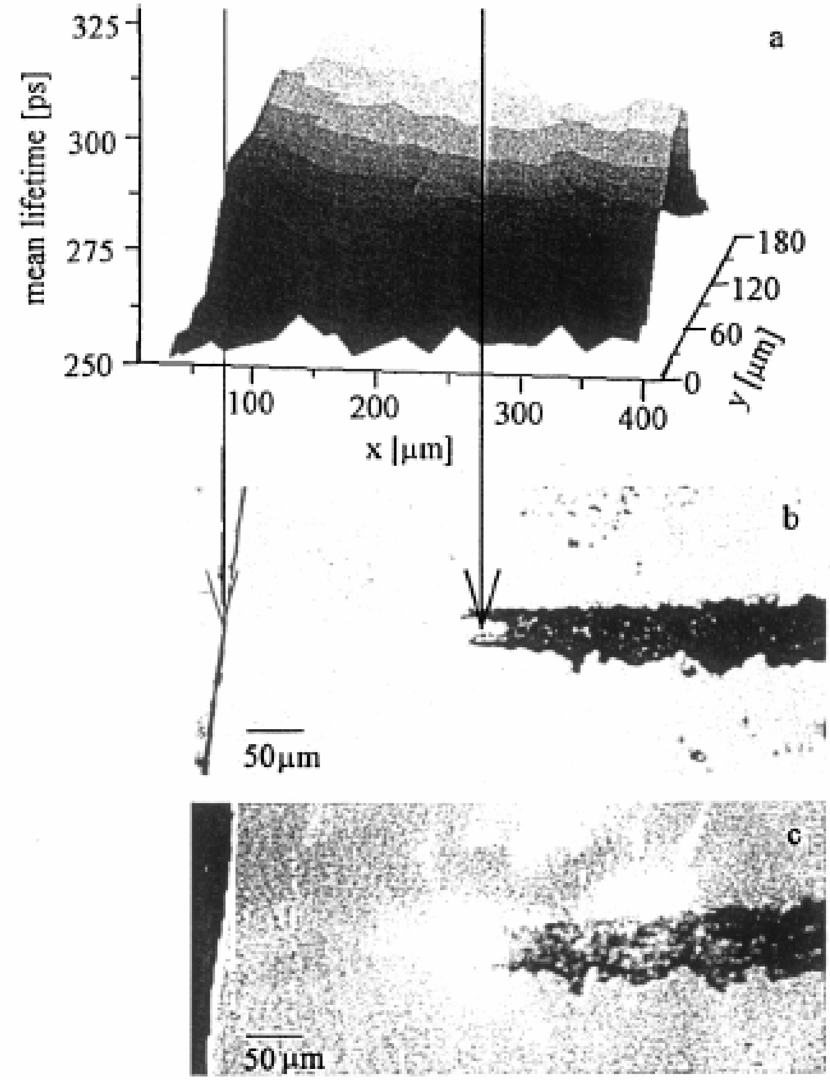

FIG. 4. Image of the GaAs wafer (scratched and unscratched area) as obtained with a light microscope (b), with the electron microbeam (c), and from the lifetime results of the positron microbeam (a). Incident energies of the electron and positron beam are 12 and 17 keV, respectively. The frames are aligned by means of the edge of a Pt foil which can be identified in all three images (left arrow). The right arrow points to the tip of the scratch.

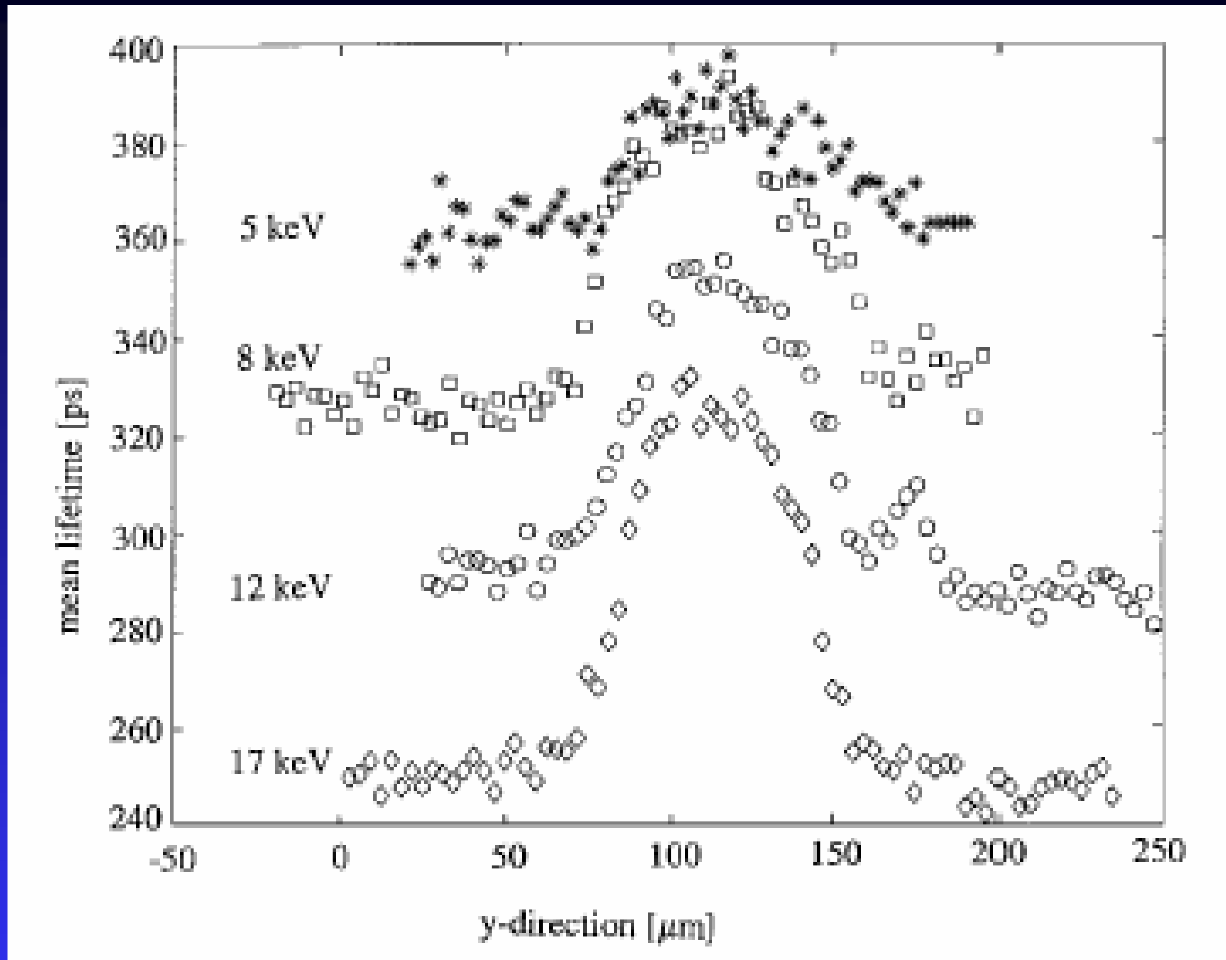

Line scans of the positron microbeam, perpendicular to the scratch, are shown for different incident positron energies. The mean positron lifetime is plotted as a function of position and of positron energy.

3D-pulsed positron microbeam

Lawrence Livermore National Laboratory

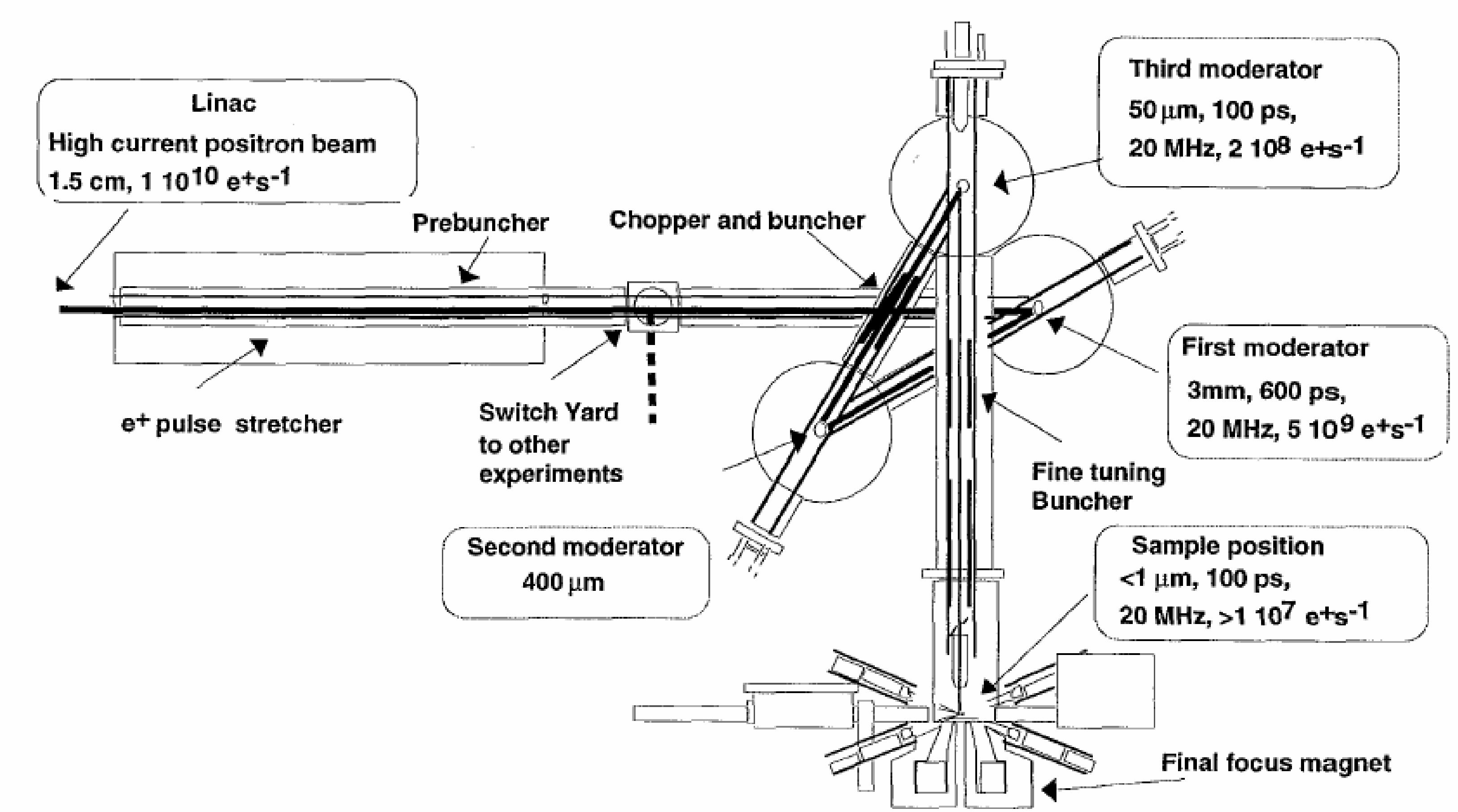

10^7e+/s, beam size: ϕ<1µm, E+: 1-50keV

10. Polarized positron

The spin polarized slow positron beam and the reemitted polarized slow positron spectroscopy

Terunobu Nakajyo [a,*], Mutsumi Tashiro [a], Tomoya Koizumi [a], Ikuzo Kanazawa [a]
Fumio Komori [b], Yasuo Ito [c]

[a] *Department of Physics, Tokyo Gakugei University, Koganeishi, Tokyo 184, Japan*
[b] *Institute for Solid State Physics, University of Tokyo, Minatoku, Tokyo 106, Japan*
[c] *Research Center for Nuclear Science and Technology, University of Tokyo, Tokai, Ibaraki 319-11, Japan*

Received 2 June 1996; accepted 15 July 1996

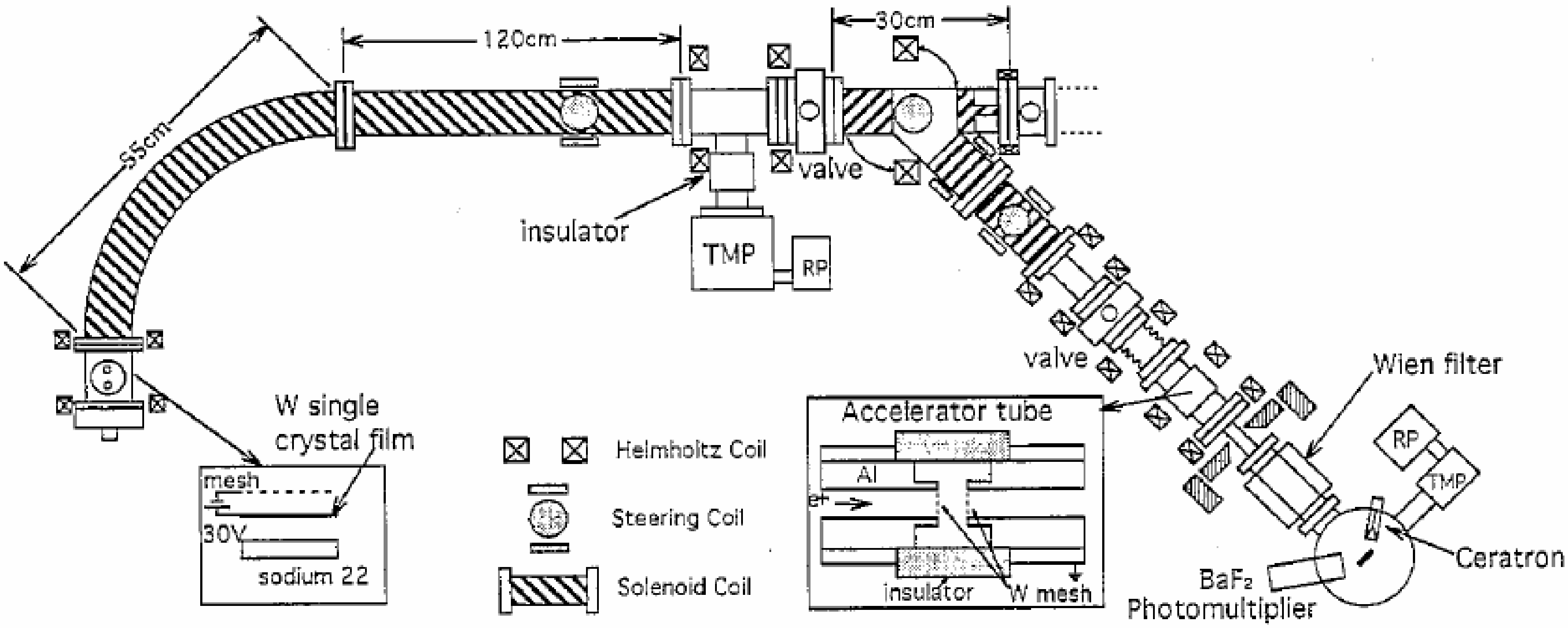

Fig. 1. The apparatus of the spin polarized slow positron beam.

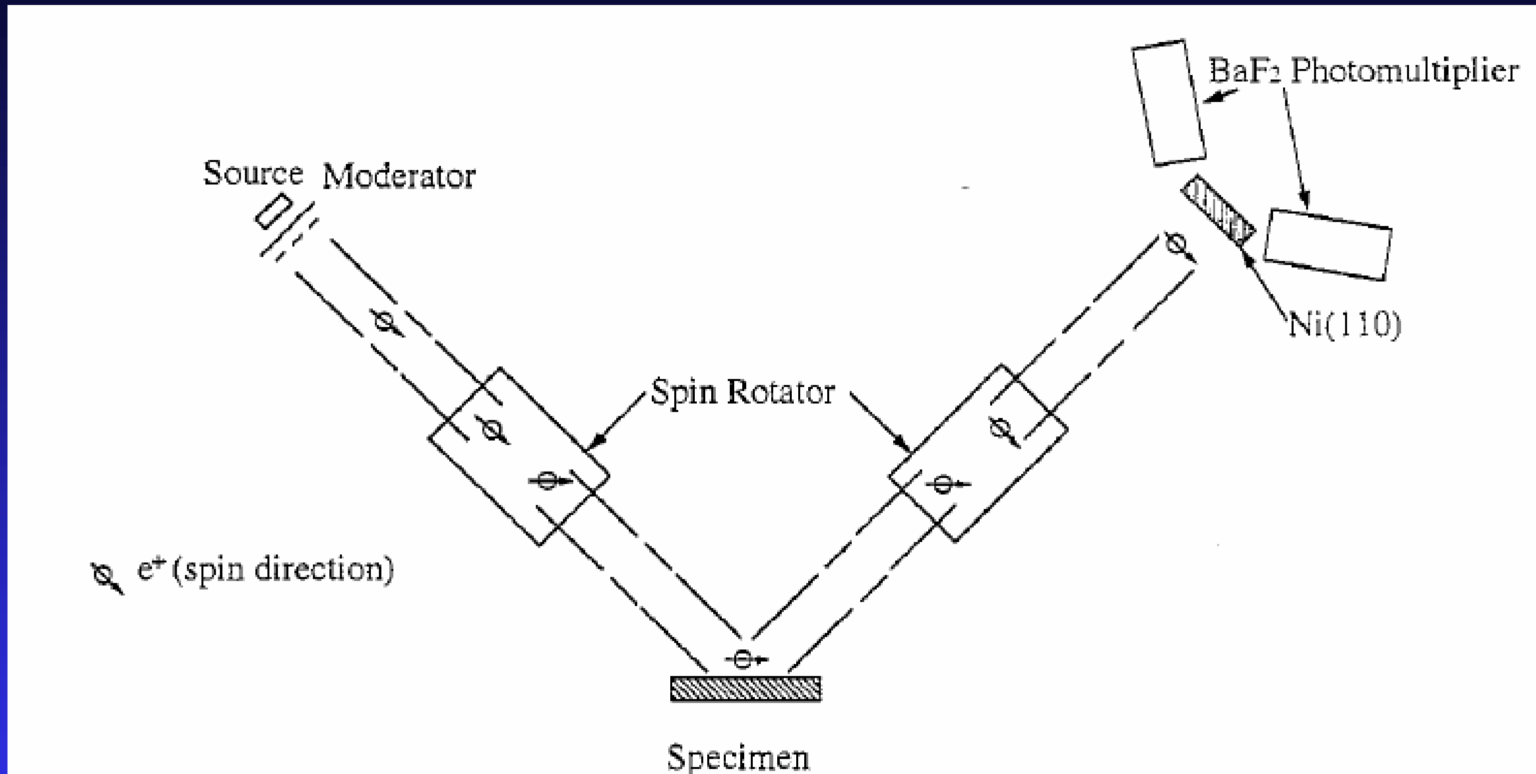

Fig. 4. The schematic system for the reemitted spin-polarized slow-positron spectrometer. Using the first-spin rotator (the Wien filter), the spin direction of incident slow positrons is variable.

JLC

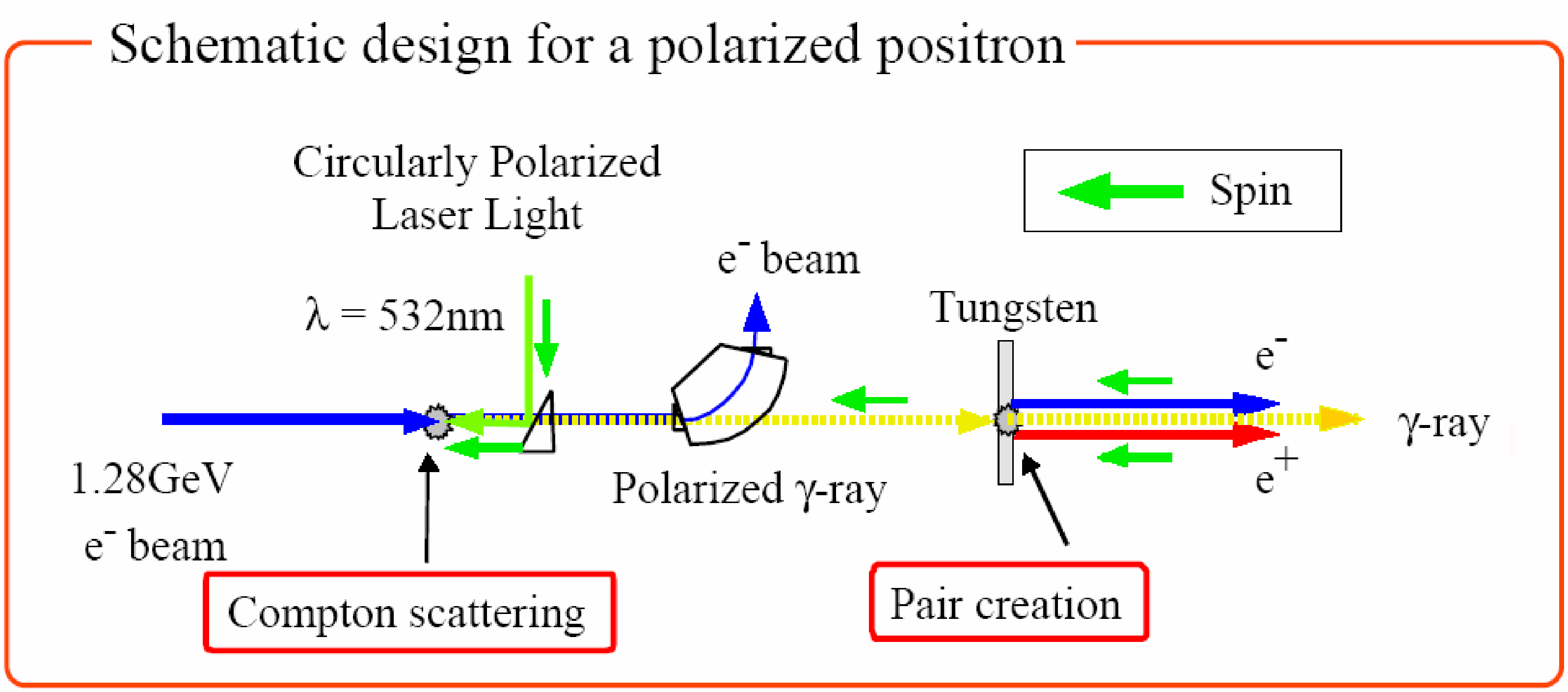
Schematic design for a polarized positron
Circularly Polarized
Laser Light
λ = 532nm
e⁻ beam
Spin
Tungsten
e⁻
γ-ray
e+
1.28GeV
e⁻ beam
Polarized γ-ray
Compton scattering
Pair creation

In high energy region, g-rays and positrons are highly polarized.

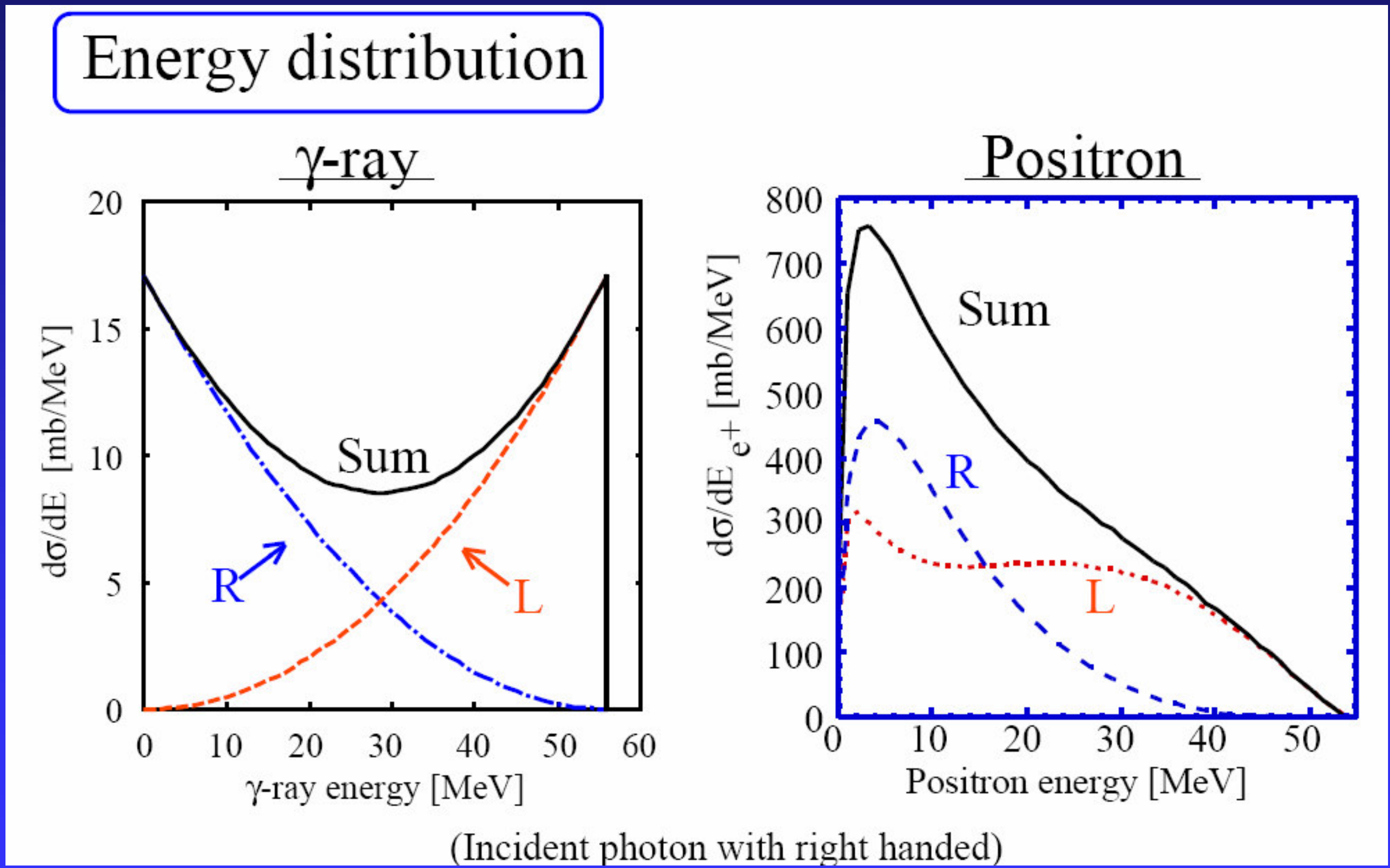

Schematic design for positron polarization measurement

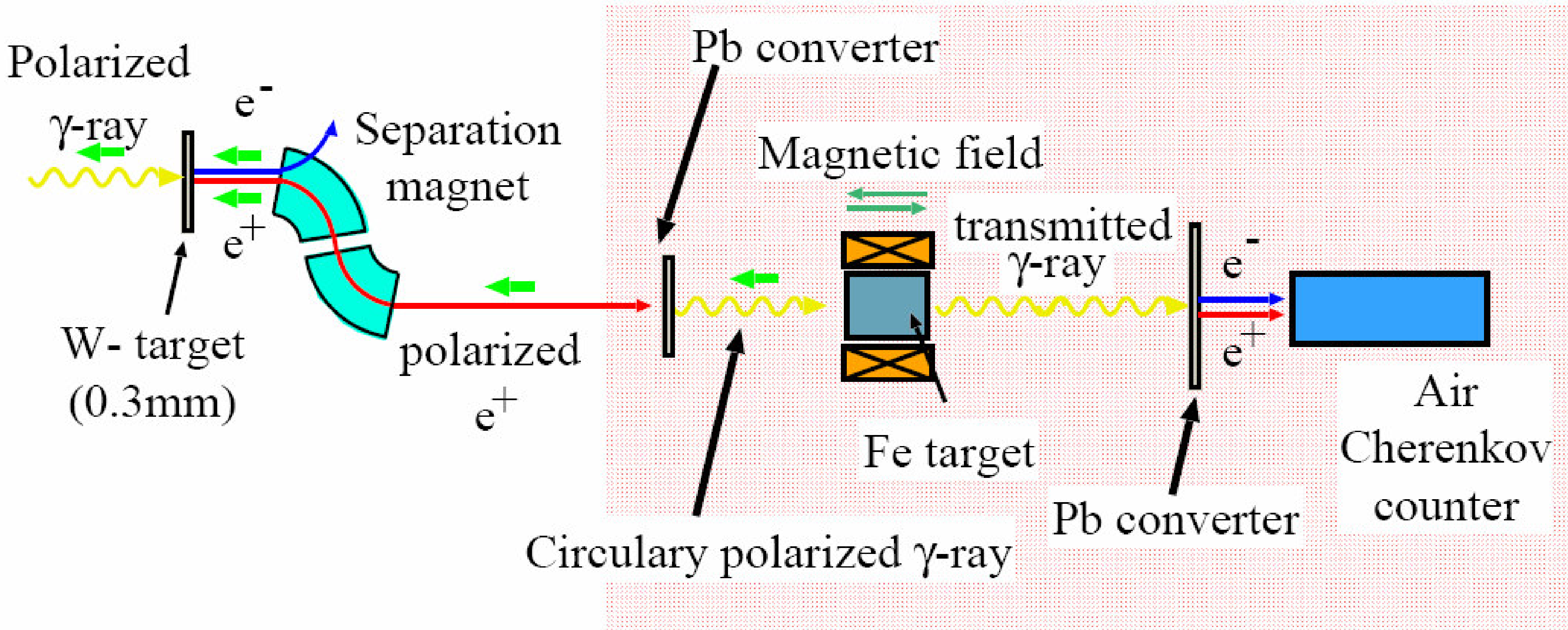

Positron beam polarimeter

Thank you!